FACULTY
OF MECHANICAL
ENGINEERING
CTU IN PRAGUE

Master's thesis

Design and Cold-air Tests of a Single-stage Axial Micro Turboexpander for an ORC Power System

Bc. Jan Špale

Department of Energy Engineering
Supervisor: Ing. Václav Novotný

December 14, 2020

ZADÁNÍ DIPLOMOVÉ PRÁCE

I. OSOBNÍ A STUDIJNÍ ÚDAJE

Příjmení: **Špale** Jméno: **Jan** Osobní číslo: **459635**

Fakulta/ústav: **Fakulta strojní**

Zadávající katedra/ústav: **Ústav energetiky**

Studijní program: **Strojní inženýrství**

Studijní obor: **Energetika**

II. ÚDAJE K DIPLOMOVÉ PRÁCI

Název diplomové práce:

Návrh a vzduchové experimenty jednostupňového axiálního turboexpandéru pro ORC jednotku

Název diplomové práce anglicky:

Design and cold-air tests of a single-stage axial micro turboexpander for an ORC power system

Pokyny pro vypracování:

The overarching goal of the thesis is to design an ORC single-stage axial micro turboexpander in order to retrofit an existing volumetric expander in a microcogeneration system. The objective of the turboexpander application is to increase the isentropic efficiency of the expansion process and to increase the reliability of the expansion machine.
The thesis will consist of the following tasks:
1) Conduct a thorough literature research of the available micro scale ORC turboexpanders and their architectures.
2) Revise the possibilities of additive manufacturing technologies for manufacturing of micro scale turboexpanders.
3) Describe the target ORC system with the boundary conditions for the turboexpander.
4) Design the micro turboexpander from the standpoints of fluid dynamics as well as mechanical design.
5) Perform cold air tests with a preliminary proof of concept turbine assembly to verify the experimental methodology and the peculiarities of the additive manufacturing. Perform the tests for several different additive manufacturing methods.
6) Present the experimental results, discuss the achieved efficiency characteristics, especially with respect to manufacturing methods and geometrical variations. Discuss the results with respect to potential applicability for the future ORC expander.

Seznam doporučené literatury:

MACCHI, Ennio a Marco ASTOLFI. Organic Rankine Cycle (ORC) Power Systems: Technologies and Applications., Woodhead Publishing, 2016. ISBN 9780081005118

Jméno a pracoviště vedoucí(ho) diplomové práce:

Ing. Václav Novotný, ústav energetiky FS

Jméno a pracoviště druhé(ho) vedoucí(ho) nebo konzultanta(ky) diplomové práce:

Datum zadání diplomové práce: **19.10.2020** Termín odevzdání diplomové práce: **23.12.2020**

Platnost zadání diplomové práce: **30.06.2022**

Ing. Václav Novotný podpis vedoucí(ho) práce	podpis vedoucí(ho) ústavu/katedry	prof. Ing. Michael Valášek, DrSc. podpis děkana(ky)

III. PŘEVZETÍ ZADÁNÍ

Diplomant bere na vědomí, že je povinen vypracovat diplomovou práci samostatně, bez cizí pomoci, s výjimkou poskytnutých konzultací. Seznam použité literatury, jiných pramenů a jmen konzultantů je třeba uvést v diplomové práci.

29.10.2020
Datum převzetí zadání

Podpis studenta

MASTER'S THESIS ASSIGNMENT

I. Personal and study details

Student's name: **Špale Jan** Personal ID number: **459635**

Faculty / Institute: **Faculty of Mechanical Engineering**

Department / Institute: **Department of Energy Engineering**

Study program: **Mechanical Engineering**

Branch of study: **Energetics**

II. Master's thesis details

Master's thesis title in English:

Design and cold-air tests of a single-stage axial micro turboexpander for an ORC power system

Master's thesis title in Czech:

Návrh a vzduchové experimenty jednostupňového axiálního turboexpandéru pro ORC jednotku

Guidelines:

The overarching goal of the thesis is to design an ORC single-stage axial micro turboexpander in order to retrofit an existing volumetric expander in a microcogeneration system. The objective of the turboexpander application is to increase the isentropic efficiency of the expansion process and to increase the reliability of the expansion machine.
The thesis will consist of the following tasks:
1) Conduct a thorough literature research of the available micro scale ORC turboexpanders and their architectures.
2) Revise the possibilities of additive manufacturing technologies for manufacturing of micro scale turboexpanders.
3) Describe the target ORC system with the boundary conditions for the turboexpander.
4) Design the micro turboexpander from the standpoints of fluid dynamics as well as mechanical design.
5) Perform cold air tests with a preliminary proof of concept turbine assembly to verify the experimental methodology and the peculiarities of the additive manufacturing. Perform the tests for several different additive manufacturing methods.
6) Present the experimental results, discuss the achieved efficiency characteristics, especially with respect to manufacturing methods and geometrical variations. Discuss the results with respect to potential applicability for the future ORC expander.

Bibliography / sources:

MACCHI, Ennio a Marco ASTOLFI. Organic Rankine Cycle (ORC) Power Systems: Technologies and Applications., Woodhead Publishing, 2016. ISBN 9780081005118

Name and workplace of master's thesis supervisor:

Ing. Václav Novotný, Department of Energy Engineering, FME

Name and workplace of second master's thesis supervisor or consultant:

Date of master's thesis assignment: **19.10.2020** Deadline for master's thesis submission: **23.12.2020**

Assignment valid until: **30.06.2022**

Ing. Václav Novotný
Supervisor's signature

Head of department's signature

prof. Ing. Michael Valášek, DrSc.
Dean's signature

III. Assignment receipt

The student acknowledges that the master's thesis is an individual work. The student must produce his thesis without the assistance of others, with the exception of provided consultations. Within the master's thesis, the author must state the names of consultants and include a list of references.

29.10.2020
Date of assignment receipt

Student's signature

Acknowledgements

A great acknowledgement goes to my supervisor, colleague and friend – Ing. Václav Novotný for his immense support which he provided me during my studies and especially during the preparation of the thesis. His dedication for the topic is incredible and I truly honour his passion for scientific research.

I would like also to point out special acknowledgement for Prof. Dr.-Ing. Andreas P. Weiß for his willingness as the research partner, for his patient guidance on many aspects of turbomachinery and mostly for the positive energy he sparks while explaining or speaking about turbomachines in general.

I also want to acknowledge my colleagues from Laboratory of Organic Rankine Cycles and its Applications (LORCA) of the University Centre for Energy Efficient Buildings (UCEEB) CTU, many of whom were my tutors at my professional work. Many thanks especially to Ing. Jakub Maščuch, Ph.D. for all the mentoring from the position of the leader of the research group.

Thanks to everyone who directly participated on the test rig setup, turboexpander measurement or data evaluation. Namely, Ing. Jan Novotný for designing the instrumentation and control for the power load, Tobias Popp M.Eng., Dipl.-Ing. (FH) Harald Wirth and Philipp Streit M.Eng. for the much-needed support during the long days at the laboratory performing measurements, and once again my supervisor Ing. Václav Novotný for all the effort he put into the measurement sessions and test rig preparations together with me.

Last but not least, to everyone who supported me during the preparation of this thesis – to my significant other, to my parents and family, to my friends – thank you for all the much-appreciated support.

This work was also more or less directly supported by the following funding bodies and projects:

- Bavarian-Czech Academic Agency

– grant no. BTHA-JC-2018-56, also 8E188012, Low cost turboexpanders for decentralized energy applications – possibilities of 3-D print manufacturing from modern plastic materials

– grant no. BTHA-MOB-2020-1: "Research mobility focused on micro turboexpander design for Organic Rankine cycles and experimental work at Drucklufttechnik laboratory at OTH, 13.1.-7.2.2020"

- Technology Agency of the Czech Republic

  – project no. TJ01000090 Research of additive manufacturing (3-D print) possibilities for manufacturing of expanders for low-temperature decentralized energy applications

  – project no. TO01000160 Optimised expanders for small-scale distributed energy systems

I am deeply grateful to the above-mentioned institutions for the granted financial support to accomplish this thesis.

Preface

"We should not expect ever to utilize in practice all the motive power of combustibles. The attempts made to attain this result would be far more hurtful than useful if they caused other important considerations to be neglected. The economy of the combustible is only one of the conditions to be fulfilled in heat engines. In many cases it is in fact only secondary. It should often give precedence to safety, to strength, to the durability of the engine, to the small space which it must occupy, to small cost of installation, etc. To know how to appreciate in each case, at their true value, the considerations of convenience and economy which may present themselves; to know how to discern the more important of those which are only accessories; to balance them properly against each other in order to attain the best results by the simplest means: such should be the leading characteristics of the man called to direct, to coordinate among themselves the labour of his comrades, to make them cooperate towards one useful end of whatsoever sort it may be."

Nicolas Léonard Sadi Carnot - Reflexions sur la puissance motrice du feu. (Reflections on the Motive Power of Fire), 1824. Translated to English by Sir William Thompson, Lord Kelvin in 1897

Declaration

I hereby declare that the presented thesis is my own work and that I have cited all sources of information in accordance with the Guideline for adhering to ethical principles when elaborating an academic final thesis.

I acknowledge that my thesis is subject to the rights and obligations stipulated by the Act No. 121/2000 Coll., the Copyright Act, as amended, in particular that the Czech Technical University in Prague has the right to conclude a license agreement on the utilization of this thesis as a school work under the provisions of Article 60 (1) of the Act.

In Prague on December 14, 2020 . . . . . .

Czech Technical University in Prague
Faculty of Mechanical Engineering

Citation of this thesis

Špale, Jan. *Design and Cold-air Tests of a Single-stage Axial Micro Turboexpander for an ORC Power System*. Master's thesis. Czech Technical University in Prague, Faculty of Mechanical Engineering, 2020.

Abstrakt

Hlavním cílem této diplomové práce je navrhnout mikro turboexpandér pro biomasovou kogenerační jednotku pracující s organickým Rankinovým cyklem. V úvodu této práce je proveden zevrubný rozbor aktuálního stavu poznání v této oblasti. Dále jsou diskutovány dostupné a možné konfigurace a architektury turboexpandérů pro ORC systémy nízkých výkonů. Specifika spjatá s návrhem takovýchto strojů jsou shrnuta na závěr rešeršní části.

Samostatná kapitola je věnována přehledu technologií 3-D tisku a aditivní výroby ve vztahu k výrobě, prototypování a celkovému potenciálu těchto technologií pro turboexpandéry nízkých výkonů. Rešerše dostupné literatury odhalila značný potenciál pro použití této výrobní metody pro výrobu prototypů turbostrojů, ten nicméně nebyl doposavad podložen experimentálně a referencí je poskrovnu.

Kapitola návrhu ORC mikro turboexpandéru seznamuje čtenáře s metodologií návrhu stroje a prezentuje výsledky návrhu hlavních komponent turboexpandéru pomocí sestaveného modelu. Dále navazuje kapitola věnující se experimentálním pracem na 3-D tištěných turboexpandérech pomocí různých aditivních výrobních technologií. Experimenty byly provedeny na trati se stlačeným vzduchem s účelem získat účinnostní charakteristiky těchto sestav turbín. Byl zkoumán zejména vliv kvality tisku, drsnosti povrhu a dokončovacích operací na výslednou isentropickou účinnost stroje. Závěr přináší doporučení ohledně možností využití aditiviních technologií pro turboexpandéry nízkých výkonů na základě poznatků nabytých z experimentů a také prezentuje předpokládané budoucí práce autora v tomto tématu.

Klíčová slova turboexpandér, turbosoustrojí, organický Rankinův cyklus, aditivní výroba, 3-D tisk, experimentální vývoj, kombinovaná výroba elektřiny a tepla

Abstract

Main goal of the thesis is to design a micro scale turboexpander for biomass combined heat and power plant (CHP) operating with Organic Rankine Cycle (ORC). In the beginning of the thesis, a research summary of small-scale ORC turboexpanders is presented. Several turbine architectures for ORCs and the peculiarities and specifics of designing an ORC turbomachine are discussed.

A single chapter is devoted to additive manufacturing technologies and their specifics with respect to small scale turbomachinery. The reason is the vast potential of additive manufacturing for turboexpanders design. A literature review of experimental work is followed by general recommendations for applying these novel technologies.

The methodology of the ORC micro turboexpander design is described thoroughly in Chapter 4 as well as the design calculation itself. A standalone Chapter 5 is dedicated to the experimental investigation of the prototypes of additively manufactured turbine assemblies. Cold-air tests were performed on a test rig built in-house for this specific purpose. The measurement devices and the experimental method to obtain isentropic efficiency of the machine are described as well. The final results of the experiments are discussed, for instance the differences in isentropic efficiency of the turbines manufactured by different technologies, the effect of surface roughness on the profile loss or the ventilation loss model validation. Finally, recommendations towards utilization of additive manufacturing methods for prototypes for cold air tests are given based on the experience gained during the experiments. The future works are proposed towards expander application in ORC test-rigs with aim towards future commercialization.

Keywords turboexpander, turbomachinery, Organic Rankine Cycle, additive manufacturing, experimental investigation, combined heat and power

Contents

Chapter 1

Introduction

Distributed energy systems are playing an increasingly important role in modern power generation. This is due to environmental reasons, such as exploiting local renewable resources, avoiding grid transmission loss, economic reasons, as the fuel may be very cheap by-product (biomass, waste heat), strategic reasons - grid independence, resilience of virtual power plants and much more. Systems with small power output also bring the possibility of energy production to a wide range of potential customers. Many technologies considered for these systems require an expander as the key and crucial component to transform heat into mechanical energy with an indisputable effect on both the cost and performance of the energy system. [1] Examples of these technologies include micro or small Rankine cycles, *Organic Rankine Cycles* (ORC) and other novel thermodynamic cycles for biomass combustion and waste heat recovery [2], [3], [4], micro solar plants and reversible heat pumps [1], [5], [6], small compressed air energy storage or pressure recovery in gas and steam lines instead of throttling.

For medium and large-scale ORC power systems, a *turbine* is the state of the art and a conventional expansion machine. For the small to micro scale systems though, *volumetric expanders* dominate the market. Main reason for that is the possibility to derive the design of a small volumetric expander from an off-the-shelf volumetric compressor, common machine in refrigeration and compressed air technology, connected with low investment costs. Turboexpanders for small scale ORC plants are nowadays rather scarce and seldom used. Other reason for that may be that volumetric machines are able to operate in a wide range of conditions with decent efficiency compared to narrow design points of turboexpanders. Apart from that, volumetric machines are bringing mostly drawbacks in an increased complexity of the system – additional lubrication system is usually needed, wear occurs on the contact surfaces and the sealing is rather complicated.

Designing a turbine for an already existing small-scale ORC CHP plant, currently in operation with a volumetric expander, promises not only an in-

crease in efficiency of the expansion process but maybe even more importantly an increase in reliability of the operation of the expander by omitting any contact surfaces between the stator and rotor. As no wear on these surfaces occurs, an increase in the lifespan of the machine is expected as well. All of these results are the key turning points for a turboexpander development.

It is a long-time attitude that turboexpanders are connected with an additional cost compared to volumetric expander due to added engineering work with customization of the turbine and also a complicated manufacturing process. In this work, the author dares to prove the opposite. Creating a simple design tool for the preliminary design of the turboexpander and utilizing *additive manufacturing* (AM) technologies, one can reduce the additional costs and lead production time of customized micro turboexpanders for ORC power systems. There has been an enormous advance in research and development of AM technologies in the past decade and the potential of these methods for turbomachinery has not yet been completely investigated.

A simple mean line one dimensional design tool for axial impulse single stage ORC micro turboexpanders is created based on existing tools and correlations with an intention to further refine it in the future. An ultimate objective is to create a tool which would automatically perform the design procedure from the preliminary simulation to blade shape optimization using *computational fluid dynamics* (CFD) and which would run parametrically only with a single input of the boundary conditions and preferences of the intended application.

The approach adopted in the design procedure in this work is a bit different to the conventional one though. A simple 1-D design methodology which aims specifically at the development of an impulse single stage axial turbine with partial admission is adopted within this thesis as it appears from previous experience as a very elegant method for a customizable design of an ORC micro scale turboexpander for given boundary conditions without a long design procedure. These would standardly include several intermediate steps which typically consist of a CFD optimization of the flow components and a lot of time and effort with only little added improvement in terms of isentropic efficiency. This ORC turbine design will already be a third generation of micro turboexpanders developed by the research team at CTU and it is not experimentally verified by cold aerodynamic tests within the scope of the thesis.

Also, as a consequence of finding a low-cost customizable turbine package, this work also investigates possibilities and aspects of additive manufacturing for turbomachinery applications, both theoretically in a literature research, and also experimentally by performing cold air trials with customized 3-D printed proof-of-concept turboexpanders. The *experimental investigation* was performed with the first two generations of turboexpanders at a single purpose test rig at Ostbayerische Technische Hochschule Amberg-Weiden (OTH-AW).

The author himself conducted the cold aerodynamic tests, evaluated the

data and presents the results of the experimental campaign in this thesis. The development and the set up of the test rig (from the mechanical and electronic standpoint) and the design of the previous two generations of turboexpanders though are a work of the collective of research engineers from CTU and OTH-AW, which the author was a part of, but not necessarily contributed to all of the previous research activities. The review is a mix of author's work and a work of wider research collective in which the author participated.

Chapter 2

State-of-the-art Small Scale ORC Power Systems

ORC power systems became an unrivalled technical solution and an industrial standard in several applications, such as low temperature heat utilization in geothermal systems, combined heat and power (CHP) systems in the scale of several MWs down to hundreds of kW or waste heat recovery (WHR) power systems down to dozens of kilowatts. ORC systems in small to micro scale domestic CHPs are still though very scarce and face mainly economical barriers with economy-of-scale and large cost per installed kilowatt in micro scale units. [7]

> *"The state of the art of ORC power systems are larger scale applications for power production in the industrial sector. Small scale systems have not been economically favourable due to the lack of turbines in this size range with adequate efficiencies (particularly when having to cope with high expansion ratios and variable operating conditions) and high specific costs associated with low initial production quantities."* (IEA Bioenergy report on decentralized small and micro-scale biomass-fired CHP ORC plants [8])

Table 2.1 summarizes, for illustration purposes, a global market overview of companies selling ORC power systems with power output $< 100\ kW_{el}$, including some already non-existent ones. Looking at the expanders for small systems (1–100 kW electrical power output), it can be summarized that they are either not in the market, are too expensive, or do not provide satisfactory performance. [7]

When focusing on micro scale or even domestic ORC CHP with electrical output in the order of less than $10\ kW_{el}$, many laboratory units and prototypes have been built and tested. Regardless of these R&D efforts, these micro scale systems mostly have not seen a commercialization, the rest have not yet

Table 2.1: Overview of manufacturers of $< 100kW_{el}$ ORC units

Manufacturer	Power output	Temperature level of source [°C]	Efficiency, technology	Web-site	Current state
GMK	32 kW–15 MW	>120°C	9%–21% depending on the heat source, Up to 500 kW screw expander	[9]	Number of references, most of small systems for ICE WHR
Bosch KWK Systeme	75 – 350 kW	100°C	11 %, R245fa, screw expander	[10]	A product with references, typically in larger systems
Ergion	4 –400 kW	120°C–300°C	13%–16%, Water-based with additives, modified screw expander	[11]	No references, no information on current state
WSK Energie und Umwelttechnik	52 - 65 kW	Exhaust gas from 490°C to 175°C	Average of 16.3 %, fluoric Hydro-carbons, screw expander	[12]	No references, no information on current state
Ormat	<4 kW, >200 kW		n-pentane	[13]	Global leader in ORC technology
Infinity Turbine	10-50 kW, >250 kW	90-200	R134a, R245fa	[14]	Offered mostly as kits and plans, missing reference
LTi REEnergy	30 kW	>160	-	[15]	Currently no ORC product
TRI-O-GEN	60-160 kW	>350	Toluene, turboexpander	[16]	A product with references
Eneftech	>5 kW	120-200	Scroll expander		Company ended operation
Electratherm	30-50 kW	>77	R245fa, Twin Screw Expander	[17]	A product with references
TransPacific Energy	10 kW - 5 MW	>30 - 480	TPE®	[18]	Offered but without references
Caltenix	<125 kW	>80	R245fa, high speed turbine	[19]	A product with references
DürrCyplan	40 kW - 1 MW	90 - 600	gross up to 22 %, low temperature up to 11%, turboexpander	[20]	A product with references
Enerbasque	5, 25, 100 kW	>85°C	Twin Screw Expander	[21]	A product with references
Enogia	5-100 kW	80-500	5-10 %, R245fa, R134a, new generation refrigerant, high speed turbine	[22]	A product with references
Kaishan	50 kW-several MW	-	Environmentally friendly refrigerant	[23]	A product with references; >100 kW
Orcan	20-100 kW, mobile <4 kW	-	-	[24]	A product with references
Rank	1-140 kW	>85 (micro units >140)	-	[25]	A product with references
Zuccato	30-300 kW		8 - 13.6 %, non-flammable HFC mix, radial turbine	[26]	A product with references, mostly biomass plants
Freepower	85-120 kW	110-270	10-22 %, micro turbine	[27]	Offered without references
POWER Engineering		>110	R245fa, single stage high speed turbine	[28]	Company ended operation

Table 2.2: Summary of experimental investigations of micro scale ($< 10kW_{el}$) biomass-fired ORC power systems

Reference	Th./Net el. output (kW)	Working fluid	Expander technology	Cycle layout	η_{is}/ η_{net} (%)	Fuel	Note
Kaczmarczyk et al. [29]	25/1.5 (gross)	HFE7100	4-stage radial turbine	Heat transfer loop, recuperated	71/6 (gross)	Wood pellets	Own radial turbine prototype and multi-fuel boiler
Qiu et al. [30]	47.3/0.9	HFE7000	RVE	Heat transfer loop, recuperated	53/1.4	Wood pellets	Ashwell boiler with added ORC circuit
Mascuch et al. [31]	42/1.9	MM	RVE	Direct heating, non-recuperated	61/4.3	Wood chips	Attempts for commercialization; own expander and boiler tech.
Jradi et al. [32]	9.5/0.5	HFE7100	Scroll	Heat transfer loop, recuperated	74.2/4.2	Wood pellets	Follows up on [16]; micro trigeneration system
Carraro et al. [33]	28/2.3	R245fa	Scroll	Heat transfer loop, recuperated	57/7.4	Wood pellets	Attempts for commercialization

been proven to be economically feasible and are very scarce on the market. Mainly because their installations face economical barriers with economy-of-scale, since downscaling the ORC power systems to micro scale results in high specific costs associated with low initial production quantities and large cost per installed kilowatt. [8] Table 2.2 presents some of the experimental research of biomass-fired micro scale ORC power systems available in the literature and summarizes the main results from the measurements.

As the expander constitutes a major share of the cost of the whole ORC power system, focusing on this device with a goal to improve its performance, reliability, lifetime and reduce its cost is of great interest. There are two fundamental types of expanders. The first is a volumetric expander including piston, scroll, screw, rotary vane or Wankel types. The advantage is that these expanders may often be derived from conventional volumetric compressors. They are considered to be well suited for small volumetric flow rates, while achieving decent efficiency and reasonably low rotational speed. [34], [35] The second option is a dynamic expander, i.e. a turbine. This is the standard for applications with a higher power output than about 500 - 1000 kW_{el}. In smaller applications they are rather uncommon. Their most common architecture types are radial inflow turbines (90° IFR), radial cantilever turbines and axial turbines.

For small systems, if a dynamic expander is utilized, single stage turbines are generally considered. Currently 90° IFR turbines are often favoured, for example [1], [36], [37], [38], [39], [40]. The reasons for this include their mass application in turbochargers for internal combustion engines and thus its availability and the theoretically achievable high efficiency. The design point of these turbines is though at a very high rotational speed for standard sized

wheels. The reasons for the limited number of actual commercial applications of this turbine type include the costs and life span of bearings for high rotational speeds, together with a complex geometry, where the customization of very small series is very expensive and time-consuming. Attempts of some companies to design a single design of a small unit for modular application (such as formerly offered Siemens SST-050 50 kW axial steam turbine) have not experienced the expected widespread either.

From turbomachinery aerodynamics point of view, an ORC turbine possesses unconventional solutions, since the character of organic working fluids is very specific, highly non-ideal and dramatically influences the fluid flow in the turbomachinery, which has to be carefully reflected within the design phase of the turbine. This work aims at designing a turboexpander for an already existing biomass-fired ORC CHP system, which is currently in operation with a volumetric expander and is in its early commercial phase of development. A dynamic turbomachine is only a logical innovation of the unit for several above-mentioned reasons. The thermodynamics of the fluid expansion and other boundary conditions are thus already given and the aerodynamic design has to respect it.

2.1 Definition of the essential flow parameters

For an easier orientation in the ORC turbine architectures and following discussions about ORC turbines in general, author reserves this space of the thesis for definitions of some further used essential parameters describing turbine stages.

For further reading about all of the concepts and parameters defined below, a fellow reader is redirected to the seventh edition of turbomachinery textbook by Dixon and Hall from University of Cambridge, where one can learn deeper about the fundamentals of turbomachinery. [41]

First, the convention for the thermodynamic states and quantities and also the velocity components is given. The turbine inlet is defined as state 1, intermediate state between stator and rotor state 2 and the turbine outlet state 3. This notation of the states and state quantities is shown in Fig.2.1.

Regarding the sign convention for the velocity components, the positive radial direction is considered as the radius from the turbine shaft increases, the positive axial direction goes along the shaft from the inlet to the outlet of the turbine and the positive circumferential direction goes in the direction of the circumferential blade speed. This sign convention is the same for the rotor and stator blades. The flow angles α, β are measured from the tangential of the blade towards the meridional direction. [0, π]. The sign convention for the sake of clarity is demonstrated on a velocity triangle in Fig.2.2.

Flow coefficient is defined as the ratio of the meridional flow velocity over the peripheral speed, as can be seen in Eq.(2.1). In axial machines, it collapses

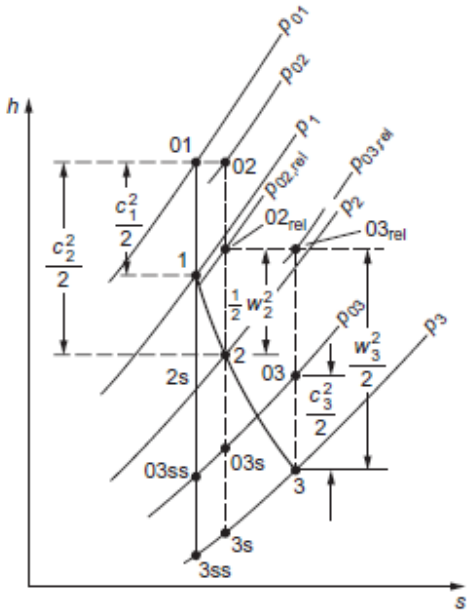

Figure 2.1: Convention for notation of the thermodynamic states and quantities; source [41]

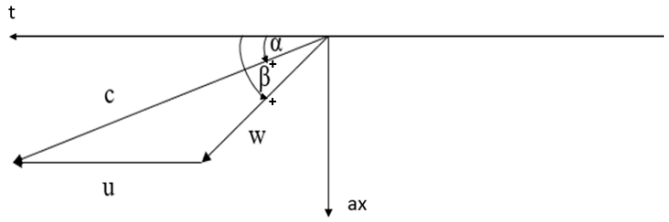

Figure 2.2: A demonstrative velocity triangle showing the convention and notation for velocities and flow angles

into a ratio of the axial component of the absolute velocity to the peripheral speed - see Eq.(2.2). Value of this coefficient determines the stage relative flow angles. This dimensionless parameter is often used for characterization of the turbomachine. Low values of ϕ implies highly staggered blades and highly tangential relative flow angles. High values of ϕ on the other hand mean low stagger and rather axial relative flow angles. When the geometry of the machine is given and rotational speed is fixed, mass flow increases as ϕ

increases (thus axial component of absolute velocity increases).

$$\phi = \frac{c_m}{u}[-] \tag{2.1}$$

$$\phi_{\text{ax}} = \frac{c_{ax}}{u}[-] \tag{2.2}$$

Stage loading coefficient is defined as the ratio of the static enthalpy drop in a stage over the square of the peripheral speed - see Eq.(2.3).

$$\psi = \frac{\Delta H_{\text{stage}}}{u^2}[-] \tag{2.3}$$

For adiabatic flows through an axial machine, this term is further reduced, as the static enthalpy drop is equal to the specific Euler work, which is defined as peripheral speed multiplied by the change in the tangential component of the absolute velocity in the rotor - see Eq.(2.4).

$$\psi = \frac{\Delta c_u}{u^2}[-] \tag{2.4}$$

High stage loading coefficient then implies large flow turning and means highly skewed velocity triangles. Stage loading coefficient can be considered a nondimensional measure of the work extraction from the fluid flow. It is though not possible to increase this value without any restrictions due to the limits of the mechanical integrity and also because very high stage loading coefficients negatively affect the efficiency of the machine.

The *degree of reaction* R is defined as the ratio of static enthalpy drop in the rotor and the static enthalpy drop in the whole stage as described in Eq.(2.5).

$$R = \frac{h_2 - h_3}{h_1 - h_3} = \frac{\Delta H_{\text{rotor}}}{\Delta H_{\text{stage}}}[-] \tag{2.5}$$

If an isentropic flow through a turbine is considered and neglecting compressibility effects, static enthalpy drop from the second law of thermodynamics can be roughly rewritten as Eq.(2.6):

$$Tds = dh - \frac{dp}{\rho} \overset{\text{yields}}{\longrightarrow} dh = \frac{dp}{\rho} \tag{2.6}$$

Degree of reaction R thus indicates the pressure drop across the rotor compared to the pressure drop in the whole stage. It can be also considered a nondimensional parameter which implies the asymmetry of the velocity triangles and describes the blade geometry. Degree of reaction R of 0.5 yields symmetrical velocity triangles and almost identical stator and rotor blade shapes. Degree of reaction close to zero means purely impulse stage, where all the pressure drop happens in the stator nozzles and the rotor blades are highly cambered.

As with all aerodynamic machines, the performance and efficiency of the turboexpander is significantly affected by the *Reynolds number Re*. Reynolds number Re for turbines is defined in Eq.(2.7) below according to the definition in [42], which follows the ASME Power test codes. Please note that in this definition, the characteristic dimension is the axial chord length at the midspan of the blade and the fluid properties are assumed at the rotor outlet. Other works can define Re with respect to blade passage or other characteristic parameters and the resulting Re values from different definitions are mutually incomparable.

$$Re = \frac{C_{ax} \cdot u_{2=3} \cdot \rho_3}{\mu_3}[-] \tag{2.7}$$

Mach number Ma is the ratio of the fluid flow velocity over the speed of sound at given point and conditions, see Eq.(2.8). Sometimes to describe the choking conditions in the rotor, *relative Mach number* Ma_r is used as defined in Eq.(2.9). The speed of sound is generally much lower for complex organic vapours when compared to air or steam, which results in highly supersonic flow conditions in most of the ORC turbines. This peculiarity is discussed in details in 2.3.

$$Ma = \frac{c}{a}[-] \tag{2.8}$$

$$Ma_r = \frac{w}{a}[-] \tag{2.9}$$

Specific rotational speed N_s is a non-dimensional parameter which separates the geometrical information of the turbomachine and describes only the effect of the rotational speed on the design of the turboexpander. It is often used in 0-D efficiency charts and plots for initial choice of the turbine architecture and an efficiency estimation. There are more definitions of this parameter varying mostly from historical differences in turbine design in Europe and the US. The one adopted in this thesis is defined in Eq.(2.10) below. in the following equations stands for the volumetric flow rate of the vapour passing through the rotor inlet.

$$N_s = N \cdot \frac{\sqrt{\dot{V}_2}}{\Delta H_{is}{}^{\frac{3}{4}}}[-] \tag{2.10}$$

Specific diameter D_s is yet another non-dimensional which describes the geometrical similitude of the turbomachine and provides an initial perspective on the design of the turbine - Eq.(2.11). It helps the designer to get an idea of the reference dimension with respect to the operating parameters.

$$D_s = D \cdot \frac{\Delta H_{is}^{\frac{1}{4}}}{\sqrt{\dot{V}_2}}[-] \tag{2.11}$$

These two parameters, D_s and N_s had historically been used for the initial choice and initial guess of the turbomachinery architecture and very preliminary design parameters, that were later iterated and refined during the first iteration step in the design of a turbine. For such initial choices, e.g. Baljé chart (see Fig.2.3) could be used.

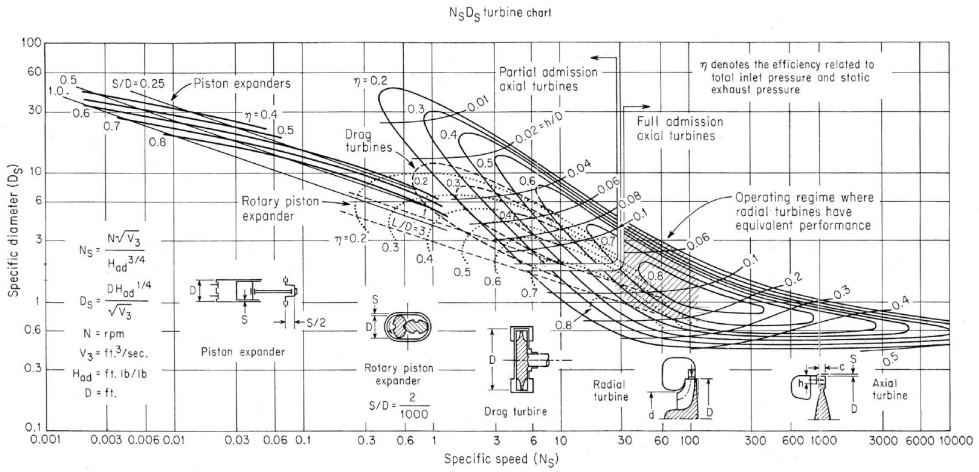

Figure 2.3: Baljé chart based on non-dimensional parameters Ns and Ds for preliminary turbine design and efficiency guess; [43], [44]

Pressure ratio PR is a basic design parameter of the turboexpander and is calculated as the ratio of the inlet static pressure over the outlet static pressure - Eq.(2.12) As for turbomachines for ORC, this number is inherently linked to the choice of the working fluid, temperature of the cooling fluid at the condenser inlet (i.e. the condensing temperature and pressure) and also the heat source temperature (thus the evaporation temperature and pressure).

$$PR = \frac{p_1}{p_3}[-] \tag{2.12}$$

Isentropic efficiency η_{is} of the turbomachine is defined in this thesis as the real turbine enthalpy drop over the isentropic enthalpy drop in the (adiabatic) turbine - Eq.(2.13). This relation can however be used only in describing models. In analysis of measured data, Eq.(2.14) has to be always used.

$$\eta_{is} = \frac{\Delta H}{\Delta H_{is}}[-] \tag{2.13}$$

$$\eta_{is} = \frac{P_{mech}}{P_{is}}[-] \tag{2.14}$$

Fundamental derivative in gas dynamics Γ is a quantitative measure of the variation of the speed of sound with respect to density in isentropic transformations. This value is a constant for a perfect gas from definition and is a key

to the understanding of real-gas flows in highly non-ideal regions. A definition by Colonna et al. [45] is used here (see Eq.(2.15)).

$$\Gamma = 1 + \frac{\rho}{c} \cdot \left(\frac{\delta c}{\delta \rho}\right)_{is} \tag{2.15}$$

The general form of *Euler's turbine equation* for an adiabatic turbine operating in a steady state is in this thesis defined as following Eq.(2.16):

$$W_{Eul} = (h_2 - h_3) = c_{u2} \cdot u_2 - c_{u3} \cdot u_3 > 0 \tag{2.16}$$

Rothalpy (rotational stagnation enthalpy) is a concept of an enthalpy, which remains constant along the streamlines in a turbomachine. It is particularly useful when studying or designing a rotational expansion machine. Rothalpy is defined as following Eq.(2.17):

$$I = h + \frac{1}{2}c^2 - c_u \cdot u \left[kJ \cdot kg^{-1}\right] \tag{2.17}$$

Non-dimensional mass flow rate (sometimes referred to as *swallowing capacity*) is an important compressible flow relationship used for turbomachinery as well. It is derived from the combination of the continuity equation and the Mach relations for compressible flows (pressure, density and temperature relations). Thanks to this relation, Eq.(2.18), the flow properties at different points within a compressible flow turbomachine can be related.

$$\frac{m \cdot \sqrt{c_p \cdot T_0}}{A \cdot p_0} = \frac{\gamma}{\sqrt{\gamma - 1}} \cdot Ma \cdot \left(1 + \frac{\gamma - 1}{2} \cdot Ma^2\right)^{-\frac{1}{2}\left(\frac{\gamma+1}{\gamma-1}\right)} \tag{2.18}$$

Any change in static enthalpy of the fluid (if we follow a single particle in space) cannot happen without an unsteady static pressure variation as described by Eq.(2.19).This is a so-called *Unsteadiness paradox* in turbomachinery, as we calculate the integral flow quantities in steady states yet the underlying mechanism of the work exchange from the fluid to the rotor blade is fundamentally unsteady and has to be unsteady, otherwise, no enthalpy change can occur.

$$\frac{Dh_{st}}{Dt} = \frac{1}{\rho}\frac{\delta p}{\delta t} \tag{2.19}$$

Where $\frac{D}{D_t}$ is a Euler's material derivative for a fluid particle moving through a turbomachine. (Viscosity effects are neglected in this simplified equation.)

2.2 Review of the most common ORC turbine architectures

Customization of the turbine designs for each specific application (diverse energy sources result in diverse operating conditions) together with highly specific flow conditions depending on a characteristic of the working fluid, resulted historically in several different ORC turbine architectures. Usually, there is also a niche of boundary conditions in which the architecture is superior to the others and some of them are even a domain of only a single company. A common denominator of the ORC turbine architectures may be the small enthalpy drops and low speed of sound, which together result in a rather compact machines with single or low number of stages with highly supersonic flows and unconventional flow components design.

The large variety of possible turbomachinery architectures is best displayed on the hydraulic turbine technology, where any possible configuration is viable for a specific combination of the fluid conditions. On the other hand, in the steam turbines segment and the gas turbine segment as well, the multi-stage axial reaction machines cover the major share of the market as a result of the goal of the machine to maximize the power output – large fluid flow rates and enthalpy drops – in a highly concentrated form.

For small to micro scale systems, it is often the case that 90°IFR are favoured due to their theoretically high efficiencies and similarities with mature segment of automotive turbochargers. If impulse axial single stage machines are adopted, it would often be necessary to adopt partial admission to get blade heights that are feasible to manufacture. A decision on whether to design the stage as an *impulse stage* ($R = 0$ in an ideal condition) or *reaction stage* ($0 < R < 1$) has to be done during the preliminary design. Both come with specific advantages and drawbacks.

The definition of an *impulse turbine stage* is that the majority of the fluid expansion takes place in the fixed turbine stator (nozzles). The flow is thereby accelerated and directed to the rotor through which it is diverted while the pressure is held near constant. The flow enters the rotor with a path close to the rotational direction, and is diverted to the opposite direction, thereby supplying the rotor with mechanical energy.

Purely *impulse turbine stage* with $R = 0$ (this is just an ideal model, in reality, degree of reaction is up to several percentage points even for impulse stage due to the irreversibility in the rotor) is able to work with very high PR per stage and with high stage loading. In addition, partial admission (i.e. not full 360° rotor wheel admission but only a segment or segments of the arc are admitted) can be utilized thanks to the fact that the whole pressure drop occurs in the nozzles, which is very advantageous for the small to micro scale turbines because the partial admission allows for longer blades that can be manufactured with sufficient accuracy. Impulse stages also operate with lower

tip leakage flows as a result of low pressure drop across the rotor.

The main drawback of an impulse stage is a lower isentropic efficiency in general due to higher flow velocities. From the definition of the degree of reaction, in an impulse stage, whole enthalpy drop of the stage happens in the nozzle, where it is converted into kinetic energy which is then utilized by the rotor blades (sometimes also called buckets for their specific shape). One of the design goals is to minimize the tangential component of the absolute velocity at the rotor outlet to avoid losses and to maximize the nozzle outlet velocity, which however goes against the favour of the profile and leads to secondary losses. With large flow deflection and highly cambered rotor buckets, boundary layer (BL) separation may occur and with that also an interaction of shocks with these separation bubbles. Schematic diagram of the working principle of an impulse stage is described on an axial stage in the Fig.2.4a).

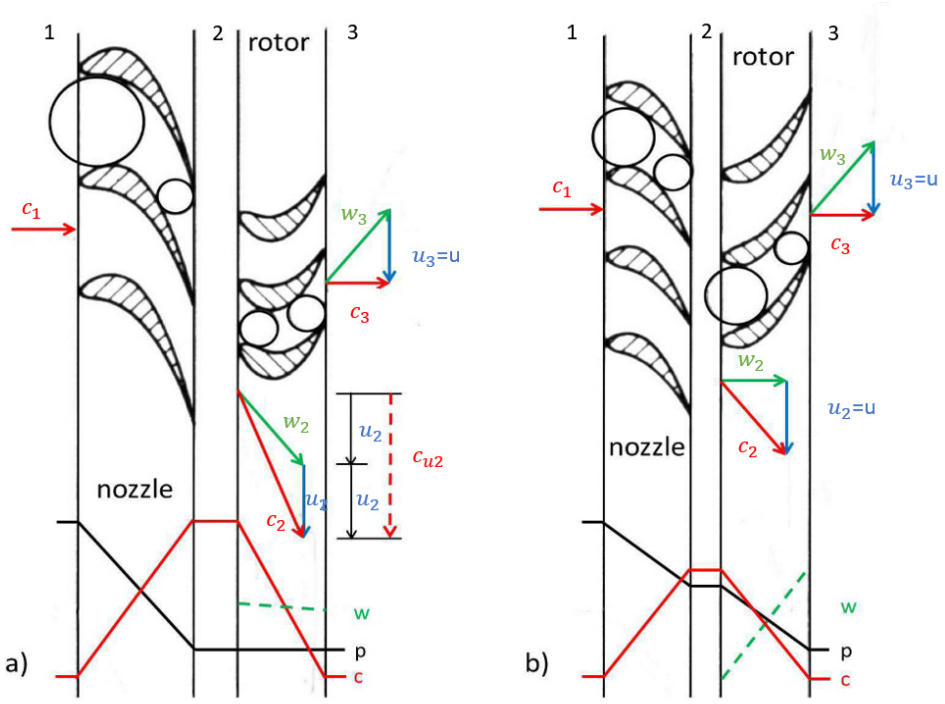

Figure 2.4: A working principle of an impulse stage (a) and a reaction stage (R=0.5) (b) of an axial turbine; edited from [46]

Reaction turbine stages on the other hand have the enthalpy and pressure drop distributed (not necessarily equally) in between both nozzles and rotor blades. An often-used reaction stage with $R = 0.5$ is shown in the Figure 2.4b). The specific of this configuration is that the inlet and outlet rotor velocity triangles are symmetrical and thus stator and rotor blades have similar shapes which leads to reduced production cost. It is often preferred in the multistage

turbine rows due to higher isentropic efficiency as the nozzle outlet velocity is significantly lower than in the impulse stages and thus the flow losses are lower as well. Also, the losses in the rotor are in general lower compared to the impulse rotors as the flow deflection is lower. In some cases, for ORC turbines, favouring multiple axial reaction stages may result in subsonic flow condition throughout the expansion machine and therefore further reduction of shock losses.

The drawbacks are for instance the inability to work with partially admitted rotor wheel, higher leakage losses, increased thrust on the rotor bearings and also a higher amount of stages needed to expand between the same admission and emission conditions compared to an impulse stage, which means the turbines are larger, with higher number of blades, thus heavier and more expensive.

2.2.1 Radial inflow (centripetal) turbines

Radial inflow or centripetal turbines are turbomachines in which the main fluid flow in absolute frame of reference is towards the centre of the rotor. There are two main types: cantilever radial inflow turbines and radial inflow – axial outflow turbines (sometimes called 90°IFR or Rad-Ax turbines). The cantilever type has both the inflow and outflow of the rotor blades in radial direction. On the contrary, the 90°IFR has as its name implies, a 90°change of the flow direction in the rotor with corresponding complex 3-D blade shape.

One of the great advantages of this concept is that a radial turbine may be controlled by variable inlet guide vanes (IGVs). By adjusting the guide vane outer ring, the flow cross section area and angle of attack may be adequately controlled to fit the ideal flow conditions for optimal efficiency of the turbomachine even in the off-design conditions. As the rotational speed is usually kept constant and thus also the circumferential velocity is constant, to achieve the regulation, IGV varies the leading-edge angle of attack to compensate for the change in the flow rate and thus the axial component of the velocity vector. Another option to compensate for the change in the fluid flow conditions is to maintain an optimal axial velocity by a variable partial admission nozzle ring. This option is suitable only for a partial decrease in the flow rate though, and does not provide any possibility for its increase.

90°IFR with variable IGVs are widespread in the automotive industry as a flue gas turbocharger to drive a 90° outflow radial air compressor. The turbine architecture is displayed in Fig.2.5. The conventional regulation method for ORC turbines would be to regulate the admission pressure upstream and that is connected with entropy production while throttling the organic vapour. The turbine itself then has fixed nozzle geometry. The benefit of the variable IGV regulation and omitting the control valve at the admission to the turbine is great also for ORC power plants. By the concept of variable IGVs, it is also possible for the turbine to compensate for changes in the condenser pressure

downstream, which may vary for example with the ambient conditions if it is cooled e.g. by a dry cooler or with the return hot water from the building if it is a CHP ORC unit with a variable thermal load. Centripetal turbines for ORC plants are a domain of only several manufacturers, for instance, Atlas Copco or GE Rotoflow. To the best knowledge of the author, cantilever IFR turbines (see Fig.2.6) are not currently available at the market, though some companies are currently investigating this as an option to further extend their portfolio. [47]

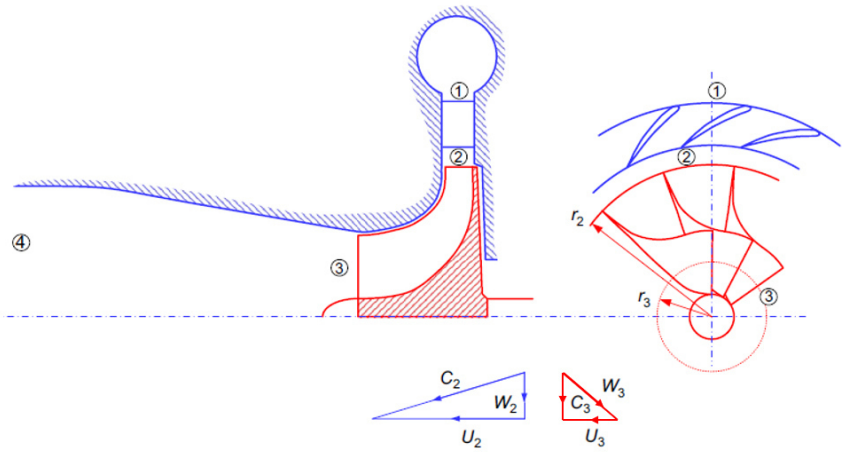

Figure 2.5: A meridional view, a side view and velocity triangles of a 90°IFR turbine; edited from [1]

2.2.2 Radial outflow (centrifugal) turbines

Radial outflow or centrifugal turbines are turbomachines in which the main fluid flow in absolute frame of reference is outwards from the centre of the rotor. Radial outflow turbine (ROT) or centrifugal turbine is a type of a turbine architecture originally conceived by Ljungstrom [48]. The working principle is displayed on Figure 2.7. The major improvement in comparison with traditional ORC turbine solutions is that it is better suited for large volumetric flow rates as the flow cross sectional area is inherently increasing as the fluid flows outwards from the centre of the rotor. This way, the increase in the cross-sectional area respects the nature of the fluid during the expansion. It is also possible to build compact machines with large number of stages and large enthalpy drops at rather low RPM avoiding highly supersonic flow conditions in this way. Spadacini, CEO of EXERGY S.p.A.[1] – a

[1] http://exergy-orc.com/

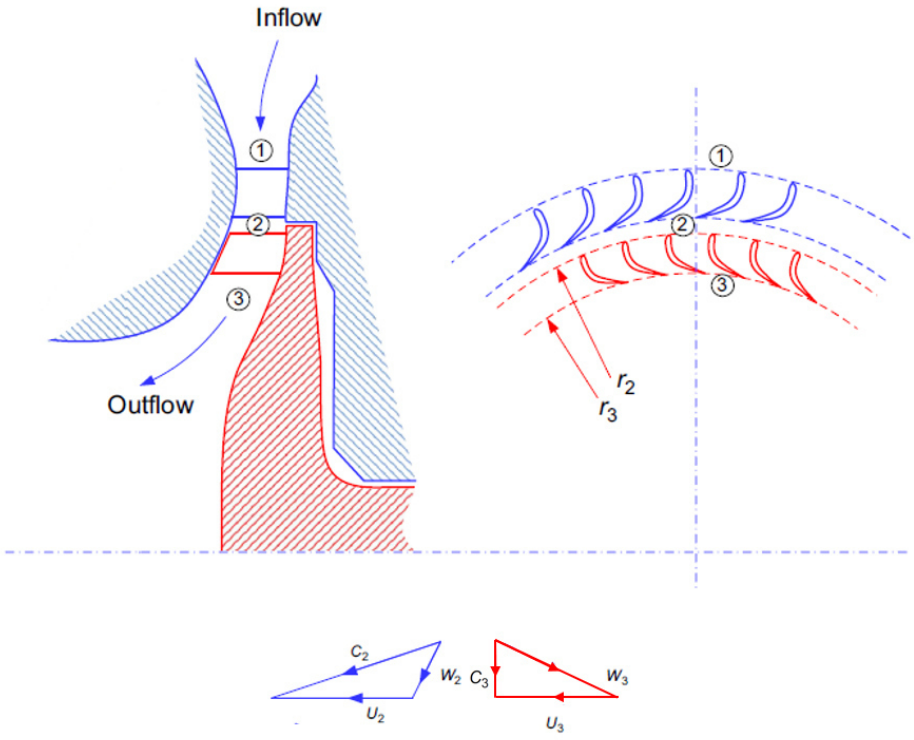

Figure 2.6: A meridional view, a side view and velocity triangles of a radial cantilever turbine; edited from [1]

company that since 2009 has successfully commercially delivered ORC systems equipped with ROTs and is considered a pioneer in ROTs, discusses the advantages and drawbacks in more details in [49]. Generally speaking, less critical aerodynamics of the fluid flow, smaller risk of choking the flow and possibility to build compact machines with large power output at low rpm. In spite of the potential of the ROTs, a clear evidence that they are superior in terms of efficiency or reliability to an axial machine with the same number of stage and similar reaction degree, stage loading and flow coefficient is still not available and more operational hours are needed to collect such information. [50] Another drawback associated with this turbine architecture is that a volute is needed to be implemented downstream of the ROT, which may induce additional losses to the turbomachine.

2.2.3 Axial turbines

Axial turbines are turbomachines in which the main fluid flow in absolute frame of reference is aligned with the axis of the rotor shaft. According to the statistical data, axial-flow turbomachines are the most preferred solution for

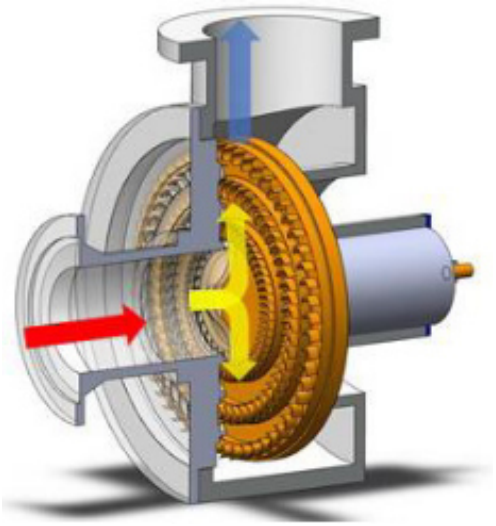

Figure 2.7: A schematic figure displaying an ROT in a cutaway; from [51]

the conversion of potential energy of a working fluid within a thermodynamic power cycle into mechanical, respectively electrical energy. Actually approximately 90 % of the electricity produced worldwide comes from axial-flow turbines (sum of the electrical energy produced in fossil fuel power plants, nuclear reactors, geothermal turbines, biomass steam turbines, hydro axial-flow turbines and axial wind turbines). [1]

Axial turbines are most often working either with steam, flue gases, air or water. Nevertheless, as ORC applications are increasing their number of applications, so is the interest in these turbomachines. Axial flow turbines for ORC technology are the common technology for the global ORC market leaders as Ormat or Turboden. [52] Axial turbines are an interesting option for ORC power system as the number of stages is usually very low. The entire expansion machine is then very compact even for large scale power systems. The large volumetric expansion ratio results in large spanwise differences of the fluid quantities across each cascade, which may negatively impact the performance, if not respected in the blade shape design. As highly supersonic conditions of the fluid flow due to very low speeds of sound are anticipated at the stator outlet, nozzles are usually designed as convergent-divergent.

2.3 The peculiarities of designing a turbine for ORC

Contrary to the steam turbine design and manufacturing procedure, where usually the turbogenerators are produced in a set of nominal power outputs and the cycle is built around them to fit for the nominal conditions, it is not of

an exception for ORC that the turbomachine is custom tailored for every single power plant (especially for site-specific waste heat recovery and geothermal applications). The off-the-shelf components are not usually available and a careful design procedure is applied for every single machine. This peculiarity brings even more attention towards additive manufacturing as customized solution and single-piece production is a domain where this technology excels.

The reasons for such significant differences are caused mainly by the added degree of freedom in the working fluid selection, and therefore the conditions of the fluid flow. These may vary dramatically for different working fluids, for instance the difference between critical temperature of a generic refrigerant R245fa and a cyclosiloxane D5 reaches to 200°C. The derivative of the slope of the saturated vapour curve ($\frac{ds}{dT}$) of the working fluid may get into three regions by which the working fluids are separated in three groups – the slope may be either:

- negative – "wet fluids" with simple molecules such as water, ammonia or lower alkanes
- positive – "dry fluids" with complex molecules such as siloxanes, toluene or complex refrigerants
- $\frac{ds}{dT} \approx 0$ – "isentropic fluids" such as R11 or Fluorinal 85©

Then there is the aspect of the cycle configuration as it is often the case that the Rankine cycle may operate in either subcritical, supercritical or transcritical region. All of these factors have direct effect on the turbine design and cannot be solved independently from it. As the cycle is usually optimized to utilize maximum waste heat from the source or to have the highest efficiency depending on the purpose of the system, the turbine design has to follow the ever-changing cycle parameters.

Another factor is the high molar mass and the molecular complexity of the organic fluid which results in low volumetric flow rates and volumetric ratios, low enthalpy drops along the expansion line and very low speed of sound. These aspects highly influence the turbomachinery design.

The implications of that are severe and of various character. On one hand, it helps to design very compact and little loaded machines resulting in rather cheap turbomachinery. On the other hand, low speed of sound means that the presence of a supersonic flow is inevitable and the blade design is rather nonconventional with convergent-divergent nozzles and the occurrence of shock waves and their interactions with boundary layer and therefore an entropy production within the flow channels.

High volumetric ratios for very complex molecules lead to difficulties in processing the large difference in the volumetric flow rate in a single-stage machine which often has to be compensated by a significant change of the blade height along the streamline, partial admission and very high flow deflection

angles. The variation of blade height comes with a penalty in the form of lower stage efficiency as it leads to an increased vorticity of the flow caused by the perpendicular velocity component and therefore increased secondary losses. The losses are furthermore increased by the high deflection blade shapes. A great advantage is though in the possibility to expand the fluid close from the or directly from the saturated vapour state without any danger of liquid droplets formation (and therefore without the risk of the rotor leading edge erosion) as high molecular complexity implies the positive $\frac{ds}{dT}$ slope of the saturated vapour curve.

For micro to small scale ORC applications - be it automotive internal combustion engine bottoming ORC, domestic CHP units or small scale concentrated solar power plants - the expander cost makes the major share of the cost of the entire unit. Therefore, the aim is not to maximize the isentropic efficiency of the machine at any costs (as Nicolas S. Carnot already noted in 1824, see the quote in the preface) but rather to optimize it for reasonable price while reaching sufficient efficiencies and reliability. A single stage turbomachines or volumetric expanders are thereby preferred in such systems over multistage optimised turboexpanders.

High rotational speeds are often avoided during the design of a steam turbine. On the contrary for ORC turbines this is not the case as the blade loading is usually very low due to much lower enthalpy drop and the temperature ranges in which the turboexpanders operate are also much lower compared to conventional steam turbines. Hence, the blades are much less mechanically stressed and high rotational speeds are not such a large concern. Also, the turboexpander as a whole is generally smaller and it is possible to apply permanent magnet high speed generators.

For all of the above stated reasons, a design approach of an ORC turbine cannot be simply derived from the design methodology of a steam turbine and has to follow a completely different method taking into the account all the aspects, specifics and peculiarities of the organic fluid flow. Traditional zero-dimensional statistical diagrams such as Smith charts or Baljé map can provide only a very rough estimate for the isentropic efficiency, because they are calibrated for large scale steam turbines. [53] The effect of highly supersonic flows at the stator outlet and strong shocks, large blade height variation and high deflection buckets should not be neglected even in the rough estimate.

The complex organic fluids show a very non-ideal behaviour especially in the region which is of the upmost interest in turbomachinery – the vapour single phase region. As the consequence, rather complicated real gas Equations of State (EoS) has to be utilized during the design phase (nowadays possible thanks to fluid properties libraries such as REFPROP or CoolProp). Siloxanes as members of so called *Bethe-Zel'dovich-Thompson (BZT) fluids family* exhibit in the single vapour phase region a negative fundamental derivative in gas dynamics Γ - Eq.(2.15), therefore all the thermodynamic properties show high sensitivity to its values and thus for precise enthalpy calculation, many

experimental data and specific EoS (e.g. *Peng-Robinson-Stryjek-Vera* EoS) are needed. [45], [54], [55]

The negative Γ region may be a benefit for an ORC turbomachine operating with such BZT fluid. As shock waves are almost inevitable in most of the turbine designs and thus also their interactions with *boundary layers* (BL) leading to BL detachment and therefore entropy production and reduced lift. In BZT fluids on the other hand a phenomenon replicated in many studies occurs that for appropriately chosen thermodynamic conditions upstream, it is possible to obtain a shock-free fully attached flow. The physical foundation behind this phenomenon is still under investigation and the details exceed the scope of this work. [56], [57], [58]

2.4 Review of small-scale micro turboexpanders

Research and development in similar field and of similar ORC small scale turboexpanders takes place on several institutes in the world, amongst which, with the greatest and most reliable results, are for example TU Delft leaded by prof. Pierro Colonna in cooperation with the company Triogen, Politecnico di Milano under prof. Marco Astolfi primarily for company the Turboden or OTH-AW under prof. Andreas P. Weiss, where cooperation exists with the company DEPRAG.

Table 2.3 provides a summary of experimental research in ORC turboexpanders of small-scale (of under 10 kW_{el} power output) in the available literature. Note that in some works, reported efficiency is however not properly evaluated from measured power output, but only from measured inlet and outlet enthalpy, which is known to overestimate the real value for small scale systems, so these numbers are rather indicative than conclusive. These values are marked by an asterisk.

There are several companies that manufacture ORC micro turboexpanders ($< 10\ kW_{el}$) either for their ORC CHPs or supply them to the ORC manufacturers. For instance: Enogia[2], DEPRAG GET[3], Rank.®[4] or Infinity Turbine LLC[5]

2.5 Available ORC turbine design tools

Several codes and design tools specifically for design and optimization of axial-flow ORC turboexpanders have been developed in the past decades. For instance, *AxTur* [53] developed in 1980s by Macchi for Turboden and much

[2] http://enogia.com/wp/

[3] https://deprag.com/en/green-energy/green-energy-turbine/

[4] https://www.rank-orc.com/rank-technology/

[5] https://infinityturbine.com/axial-turbine-generator-waste-heat-to-power/

Table 2.3: Summary of the experimental investigations of ORC turboexpanders of micro-scale power output ($< 10\ kW_{el}$)

Reference	Working fluid	Turbine type	PR	P_{el} [kW]	η_{is} [%]
Kaczmarczyk et al. [59]	HFE7100	4-stage radial	7	2	70
Żywica et al. [60], [61]	HFE7100	1-stage axial	3.1	1	73
Riffat & Zhao [62]	n-pentane	1-stage axial	5	3.7	n.a.
Hernandez-Carillo [63]	R245fa	Radial inflow	n.a.	1.2	66
Pu et al. [64]	R245fa; HFE7100	1-stage axial	3.5	2	60
Li et al. [65]	R123	1-stage axial	6.3	6.1	58.5
Pei et al. [66]	R123	Radial inflow	7.5	3.3	66
Nguyen et al. [67]	n-pentane	Radial inflow	4.1	1.5	50
Yagoub et al. [68]	HFE-301	Radial inflow	n.a.	1.5	85*
Yagoub et al. [68]	n-pentane	Radial inflow	n.a.	1.5	40
Klonowicz et al. [69]	R227ea	1-stage axial impulse	2.9	10.1	59
Shao et al. [70]	R123	Radial inflow	3	3.4	83.6*
Seume et al. [71]	Ethanol	1-stage axial impulse	50	8	58
Kosowski et al. [72]	Ethanol	1-stage axial impulse	17.3	2	n.a.
Weiß et al. [47]	MM	1-stage axial impulse; radial cantilever	18.8	5.6-14.1; 5.1-16	up to 73.4; up to 76.8
Gazet et al. [73]	HFE	1-stage axial impulse	3	10	70
Yue et al. [74]	R245fa	1-stage axial	n.a.	5	56.4
Guillaume et al. [75]	R1233zd	Radial inflow	4	3.5	75
Demierre et al. [76]	R134a	Radial inflow	4.3	2.4	67
Cho et al. [77]	R245fa	1-stage axial	4.8	2.2	n.a.
Al Jubori et al. [78]	various	Radial inflow	1.2-2.2	up to 4.8	up to 78.3

younger *TURAX* [79], [80] (freeware) by Meroni, both originated at Politecnico di Milano, *AxialOpt* [81] (open source Matlab code shared on GitHub) from NTNU Trondheim, Micro-turbine-generator construction kit (*mtg-c kit*) developed in cooperation of OTH-AW with DEPRAG Schulz, GmbH [82] or *Hojo Stodola*[6] (now in closed Beta), developed by a Dutch company Asimptote together with TU Delft. All this software is using REFPROP fluid property database ([83]) except for Asimptote's Hojo Stodola that works with their in-house developed library Fluidprop[7].

These design codes are all based on a 1-D mean-line approach with efficiency guess in the first step and empirical correlations for loss estimation and efficiency iteration. Initial rough efficiency guesses are usually carried out with the help of available 0-D performance maps based on similitude approach, such as Baljé chart (Fig.2.3) or from the company's own performance maps. New efficiency charts have been presented in the past years especially designed for ORC axial turbomachinery, these are variations to Smith and Baljé charts with updated loss models for ORC. [84], [85] Common profile loss models from conventional large steam turbines are usually applied. [86], [87], [88], [89], [90], [91], [44], [43] An exception to that is the mtg-c kit which uses an empirical correlation from more than half a century old NASA turbopump measurements instead. [92], [93]

All the design tools need input parameters – stator inlet pressure and temperature, rotor outlet pressure/temperature, working fluid, rotational speed, mass flow rate of the fluid, midspan diameter and several guesses of geometrical parameters. Then the flow variables are calculated from inlet to the outlet of the turboexpander by the principles of *conservation of mass and rothalpy* (Eq.(2.17)) i.e. an alternative expression to the *Euler's turbine equation* (Eq.(2.16)). Using trigonometric relations, velocity triangles are calculated and displayed. Thanks to the EoS of the fluid library, thermodynamic properties of the working fluid downstream are calculated. Compressible flow relations are necessary as the fluid flow in ORC turbines is generally in most of the cases over *Mach number* 0.3 (Eq.(2.8)), *swallowing capacity* or *non-dimensional mass flow rate* is calculated using Equation 2.18, which yields as a combination of compressible flow relations and the continuity relation. Flow deviation at the outlet of the cascade and losses within it are calculated using empirical correlations.

There are also very few commercial codes and software, such as Concepts NREC[8] and their AXIAL™CAE software for meanline design of multistage axial turbomachinery including compressors, gas, steam, and hydraulic turbines, supports design-point and off-design analysis for subsonic and supersonic designs through an advanced pressure-based formulation. AXIAL works

[6] http://www.asimptote.nl/hojo-stodola-beta-tester/

[7] http://www.asimptote.nl/software/fluidprop

[8] https://www.conceptsnrec.com/solutions/software/computer-aided-engineering/preliminary-designs/axial

with REFPROP and the following industry-standard loss models (Ainley-Mathieson, Dunham-Came, Kacker-Okapuu, Moustapha-Kacker), which allow for the independent selection of loss models by blade row and loss split by loss component (i.e., profile, secondary flow, partial admission, wetness losses etc.)

Chapter 3

Additive Manufacturing for Micro Turboexpanders

As ORC micro turboexpanders are most likely not going to be ever produced in large series and customization is key for quality performance, a possibility to effectively tailor the turboexpander design to the desired operating conditions of the cycle is a necessity. That comes with increased costs mainly on two fronts – the turbomachinery design and its manufacturing. The design part is tackled usually by specialized design tools as discussed in Section 2.5. Cost-effective manufacturing of single-piece produced customized ORC turbines was not possible for the most part of the history of ORCs. It was not until the last decade since AM technology allowed to produce technically feasible products while being a cost-effective option in comparison with conventional manufacturing technologies. Utilization of this novel manufacturing approach allows for fully Engineer-to-Order approach, where from the order to the final product, a digital thread is kept uninterrupted.

3.1 Review of the most common AM methods for turbomachinery

To present the current state-of-the-art of AM for turbomachinery, a brief overview is presented. For a more detailed and thorough review, a fellow reader is referred to author's collective previous work. [94] Summary of the possible additive manufacturing methods and their division according to ISO/ASTM 52900:2015 terminology is presented on a tree chart in Fig.3.1.

Additive manufacturing has found its way towards large-scale turbines and major industrial manufacturers but not as a manufacturing technology for entire wheels or blades, but rather repairs, maintenance and overhaul of the current machines. The author's collective sees further interesting potential of some of the above-mentioned technologies also for small to micro scale low

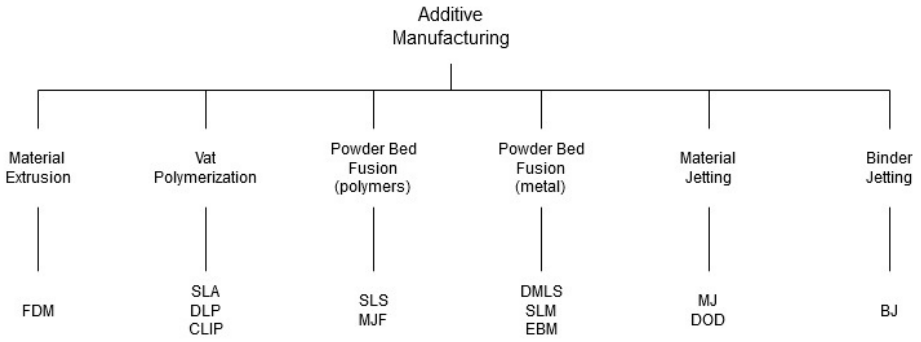

Figure 3.1: A tree chart of additive manufacturing technologies according to ISO/ASTM 52900:2015

Table 3.1: Summary of AM technologies for small turbines; source [82]

Technology	Possible applications	Materials	Maximum temperature	Advantages	Drawbacks
FDM	Low demand parts, other parts with limits	ABS, Ultra ABS, PETG, composites	∼100°C	Cheap, widely available	Rough surface in as-printed, need of supports, non-uniform properties
SLS	Any part	Nylon based, carbon, TPU, PP	∼80°C	Cheap, no support, good accuracy	Limited T ∼80°C
SLA	Stationary parts, rotor with limits	Resins	>200°C	Good resolution and surface quality	Most expensive plastic method, needed supports, fine features and tolerances are a problem
DMLS	Flow components	Metals (steel, Al, Ti)	>1000°C	Most available metal AM technology	Expensive, sensitive to fine-tuning, Rough surface in as-printed, need of supports
MJF	Any part	Nylon based	∼80°C	Cheap, no support, best tolerances, fastest	Limited T ∼80°C; domain only of HP
EBM	Flow components	Metals (steel, Al, Ti)	>1000°C	Fast, well-tuned properties	Very expensive

temperature applications, as plastics can be utilized and lower stage loading is usually obtained. Based on the literature review as well as on in-house tests, an overview of AM applicability for micro turboexpanders was created and presented in Table 3.1.

3.1.1 Stereolithography

One of the first AM technologies was *stereolithography (SLA)*, whose core functional principle is UV curing of a liquid resin. Most of the resins have a temperature limit of around 70°C which significantly reduces its potential for turbomachinery applications, but special high-temperature resins that can withstand temperatures up to 290°C for low loaded parts exist. Novel mod-

ifications of SLA such as continuous liquid interface polymerization (CLIP) promise fine tuning of properties of the end product, improved precision and print speed. [95], [96] Radial inflow air turbine of a kW-scale made entirely by SLA was reported. [97] Please note that maximal rotational speed in the experiments was below the nominal design point, suggesting issues either in bearings or the material itself. In addition, SLA was tested as a method to manufacture diffusor vanes for a small scale experimental centrifugal air compressor [98] or for models and cold aerodynamic tests in fluid dynamics research of companies and research institutes. [99], [97]

SLA has obvious advantages in surface quality similar to glass, rather high precision of the print with layer thickness up from 25 μm and thin sharp structures useful for trailing edges of blades, which suggest good applicability. On the contrary, regardless being the most expensive plastic AM method, the main drawback is the accuracy of the product. The circular tolerance can be up to 0.5 mm for a wheel of 120 mm in diameter with a state-of-the-art SLA printing machine. The accuracy according to the author's experience has not improved regardless of trials with various materials and settings. Support structures are also needed for SLA and leave burrs, which need to be manually polished. Lastly, the resin components are rather brittle and fragile, which has also been unfortunately experienced by the author by several incidents resulting in complete shattering of the turbine wheel.

3.1.2 Fused Deposition Modelling

Fused Deposition Modelling (FDM) is certainly the most common AM technology amongst the private applications and is widespread at the market for reasonable prices. Nonetheless, the quality of its prints is usually not able to fulfil requirements and criteria for turbomachinery operation. The product inhomogeneity is rather large, which is a large issue for rotating parts. The minimum layer thickness is also very low of around 80 μm (typical < 150 μm) but thermal effects cause large deterioration of accuracy. The circular tolerance on a wheel of 120 mm in diameter with professional FDM manufacturing exceeded 0.5 mm. Support structures are essential, especially for overhanging structures and they leave burrs after removal. In general, the surface quality is quite rough and requires additional treatment. Concerning the materials and their temperature resistance, FDM prints can sustain temperatures of over 80°C and exceptionally above 100°C (Ultra ABS material). A reference for small-scale turboexpander – a prototype of a 90° IFR 1 kW scale turbine – was found in [100]. An experimental investigation of another FDM manufactured turbomachine was presented in [99], FDM was used only for nozzles while the rotor was machined from glass reinforced polyether-ether-ketone (PEEK). Air tests have proven operation at speed of more than 32 000 rpm, maximum aerodynamic efficiency around 65 % and predicted efficiency in ORC with R245fa up to 66 %. This AM technology finds many application in less stressed tur-

bine parts, where surface quality is not critical, such as radial inflow turbine casings. [100], [101] Suggestions to use this method mostly for stator components can be supported also by studies of NASA, which tested the possibility to manufacture guide vanes for turbojet engines by FDM from materials as thermoplastics or Ultem®with carbon fiber. [102], [103]

3.1.3 Selective Laser Sintering

Selective Laser Sintering (SLS) is an AM method of selective sintering of a polymer powder – usually nylon powder and composite mixtures – by a high-power laser. This technology provides and interesting option for small-scale turbomachinery. The height of individual layers could start from about 60 μm. Together with no need for supporting structures, it provides decent surface quality, even without further polishing. The circular tolerance on a test piece of 120 mm in diameter proved the best numbers out of the tested AM technologies, reaching under 0.25 out of several test prints. The temperature resistance of the materials is usually around 80 – 100°C and a bit over 100°C for composite materials. No turbomachinery applications nor references have been found in the literature which is to the upmost of interest to the author as its features, such as accuracy, rigidity, price and surface quality make SLS a truly promising technology for small to micro scale low temperature turbomachinery applications.

A very similar technology to SLS is HP's *Multi Jet Fusion (MJF)*. It also belongs to the polymer powder bed fusion family of the AM methods, and it also uses nylon as the main material. The main difference between MJF and SLS is the heat source. SLS uses a laser to scan and sinter each cross-section, while in MJF an ink (fusing agent) is dispensed on the powder that promotes the absorption of infrared light. An infrared energy source then passes over the building platform and fuses the inked areas. Essentially, MJF is a combination of the SLS and Binder Jetting technologies. The fusing agent currently used in MJF systems is black in colour because dark materials absorb radiation more effectively. As a result, MJF parts have a light grey appearance. An optional post-processing dyeing step can be applied to achieve a uniform black finish. This technology has the advantages of nylon SLS technology and is cheaper per printed piece. Also, the dimensional accuracy is highest amongst all of the additive manufacturing methods. This makes this technology excellent for prototyping of turbine flow components for cold aerodynamic testing.

3.1.4 Direct Metal Laser Sintering

Last but not least, *Direct Metal Laser Sintering (DMLS)* technology is presented as one of the major AM technologies, which works on a similar principle as SLS, but with metal powders. The minimal layer height is similar to SLS but the support structures are necessary and resulting surface roughness is

rather high. Altogether these factors limit the application for turbomachinery in the as-printed state. On the other hand, majority of references have been found for this AM technology in the literature such as [38], [104]. The possibility to print cooling channels directly without a need of drilling has been successfully explored for high temperature turbochargers for automotive. [105], [106]

3.2 Post-processing of AM components

Almost any part produced by AM in its as-printed state is not fulfilling the requirements for turbomachinery operation. Post-processing is therefore an essential part of the manufacturing process and is the finishing operation with a goal to improve the quality of the part and to meet the design specifications. The printed part has to account for additional material that is removed during the post-processing, as most of the methods have effects on geometry.

3.2.1 Metal parts

As was mentioned above, metal parts produced by AM are most often manufactured by methods based on powder bed fusion. Post-processing of components that are manufactured by this technology starts by removing and recycling the unused powder from the build volume. Since the printed part gets basically welded to the support plate during the print process, it needs to be removed from the base plate, which is usually done by *wire electrical discharge machining* (WEDM) or by band saw machining. Before that is done, stress-relief heat treatment is usually applied. The residual stress in the printed parts is a result of the layer-by-layer printing and large temperature differences during the manufacturing. This procedure has to be done before the blade is removed from the support plate, otherwise the part may get cracked or damaged.

Heat treatment of the separate part is usually done before the machining or finishing process. A furnace with the ability to regulate the environment in the oven (heat treatment temperature and cool-down process regulation) is needed. Heat treatment of AM parts follows standardized procedures by *American Society for Testing and Materials* (ASTM). [107] Alternative method is Hot Isostatic Pressing (familiarly sometimes called “HIPing”), which is often adopted in aerospace printed parts and whole metal turbine blades to reduce the porosity of the material and improve the fatigue resistance of the part. [108], [109], [110] Fatigue strength of AM parts is one of the main barriers that limits widespread use of AM also for critical parts of turbomachines. [111] The microstructure of the part is full of impurities and voids introduced during the layer-by-layer method and this may initiate a crack that leads to fatigue failure of the part. [112] Several methods might be

adopted to increase fatigue strength of an AM part, e.g. shot, ultrasonic or laser peening or heat treatment for residual stress recovery. [111]

Another issue is the surface quality of the part in the as-printed state. The roughness is usually not sufficient and not suitable for turbomachine parts as it would lead to very high friction losses in the fluid flow channel. Hence, machining or polishing of the functional surfaces is very often applied. If very low surface roughness is to be obtained, it might be necessary to polish the blade surface using sand or bead blasting. *Electrochemical machining* (ECM), *abrasive flow machining* (AFM) or a combination of these have been successfully used as conventional methods for turbine blades made by standard manufacturing methods and now are recommended and explicitly configured for AM parts. [113], [114]

As the AM methods differ, also the post-processing is very specific to each of the AM technologies. However, there is a trend to fully automate the process using collaborative or even fully automated manufacturing robots also for post-processing. These also enable to keep the digital manufacturing thread from initial order, CAD model to the ready-to-use end product. [115]

3.2.2 Plastic parts

Additional heat treatment is not common for plastic parts as these are usually much less loaded then metal parts. [116], [117] Nevertheless, it still significantly improves the material properties, as has been shown for FDM parts in [118], [119]. Some improvements have been achieved also for nylon SLS parts. [120] SLA methods are usually post-cured by UV light rather than thermally treated.

Surface quality treatment has similar possibilities as for metal AM parts. Additional option is using suitable solvent vapours and chemical treatment for smoothing of the surfaces with very little to negligible impact on the final geometry of the product. Also, typically for SLS, coating of the part can be applied. [121]

3.3 Additive manufacturing application scenarios for turbomachinery

This section aims at describing possible application scenarios for additive manufacturing in turbomachinery industry.

3.3.1 Rapid prototyping

Additive manufacturing enabled to introduce a new procedure for development of new products and a new way of their prototyping. Conventional method uses testing as a validation of the design result, on the contrary, it is an integral part of the iterative process for rapid development. The testing results bring

information, which is used for adjustments in the design of the part. Therefore, the development cycles can run in parallel and much faster in comparison with conventional methods. The process is briefly described also in Fig.3.2. For extreme cases, the lead time can be reduced from months to single days before an operative field-testing of the prototype.

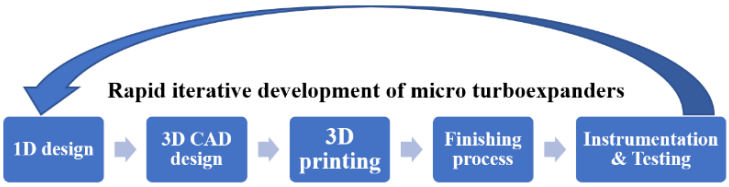

Figure 3.2: Rapid iterative development of micro turboexpanders; source [122]

3.3.2 Customization of end-product

Small scale production of any parts is cost-intensive. This is due to various reasons. Stocking of these models, their logistic and supply chain, switching the production process to another model, are all what keep the prices of the final product high and brings further complexity into the manufacturing process. With AM, customization is only a quick matter of adjusting several dimensions in the CAD software and switching to manufacturing a different model brings little to none additional costs. Tailored turbomachinery for available price and for wide range of custom applications such as distributed energy systems is now possible thanks to this.

3.3.3 Temporary replacements

Often it is the case that some highly specific spare parts are needed urgently and any minute of downtime brings severe loss of profits. In these situations, 3-D printing can often provide at least temporary replacement even though it may have slightly worse performance. Replacing it with the original part in next servicing stop is the following step and more substantial losses are avoided.

3.3.4 Rapid repair

Similar to previous application scenario, custom rapid repairs of the parts that are facing the toughest and harshest conditions with the lowest lifespan is another great potential for AM. Maintenance of such parts as gas burner tips or leading edges of blades in the first turbine stage in a gas turbine means replacing the entire part or taking it out and repairing it by braze restoration or welding process, which is costly and time-consuming. AM helps to reduce

the lead time of an overhaul and also the amount of material used for such repairs. Rapid repairs using AM also bring an opportunity to upgrade the damaged parts according to the latest design. [123], [124], [125]

Chapter 4

Design of the ORC Micro Turboexpander

This chapter presents the design methodology and procedure for an ORC micro scale turboexpander. The design procedure of the ORC micro turboexpander follows several generations from the proof of concept unit for preliminary cold air testing towards the prototype of the turbine working with organic vapour.

The designed turboexpander is to be installed into a small scale biomass-fired μCHP ORC plant instead of a currently used volumetric rotary vane expander (process flow diagram of the plant is displayed in Appendix D). This ORC system is being developed at Laboratory of Organic Rankine Cycles and its Applications at University Centre for Energy Efficient Buildings of Czech Technical University in Prague.

The parameters relevant to the turbine design are displayed in Table 4.1. Main relevant parameters of the cycle that determine the turbine design are the following: expander inlet and outlet pressure, inlet temperature, nominal mass flow rate and the nature of the working fluid; these cycle boundary conditions are supposed to be conserved with a new expander as well.

Table 4.1: Turboexpander design boundary conditions defined by the cycle performance

Parameter	Value	Units
Expander inlet pressure p_1	650	kPa
Expander inlet temperature T_1	190	°C
Expander inlet superheating T_{SH}	10	K
Expander outlet pressure p_3	55	kPa
Working fluid	MM	–
Working fluid mass flow rate $\dot{m}_{wf}$	0.3	$kg \cdot s^{-1}$

According to Table 4.1, one may observe that the design pressure ratio for the turboexpander is around 12, and the inlet temperature of the superheated organic vapour is 190°C. For these inlet conditions, the speed of sound is 123 m/s, and it is quite obvious from this preliminary estimate that the fluid flow at the nozzle outlet for an isentropic enthalpy drop of around 50 $kJ \cdot kg^{-1}$ will be highly supersonic. For ORC turbines with such high Mach numbers (above 1.4), it is necessary to design the nozzles as uniquely-shaped convergent-divergent to respect the nature of the supersonic fluid flow. [126]

The working fluid selection – hexamethyldisiloxane (MM) impacts the design of the turbomachine heavily. Due to its nontoxicity, excellent thermal and chemical stability, and limited flammability, it can be possibly considered as the most suitable fluid for such high-temperature ORC from an engineering point of view. [45], [127], [128] Other reasons for its application were also a reasonable price, that it remains liquid under ambient conditions, solubility of oil and previous unpleasant experiences with hydrocarbons as working fluid.

The micro turboexpander designed in the scope of this work would then replace the rotary vane expander within the system. There are several changes though that are needed to be done before the replacement. The emergency bypass would have to be changed for a regulated control by-pass valve for start-up and shut-down operation of the turbine. The electrical power extraction from the turbomachine would have to be solved in a completely different manner. As the nominal rotational speed of the turbine will for certain exceed 50 Hz, a permanent magnet high-speed generator integrated into the shaft of the rotor wheel and power electronics to supply the electrical power to the grid is a necessity and brings added costs to the update of the system.

4.1 Evolution of the designed micro turboexpanders

The investigation of micro scale turboexpanders for distributed power systems started in 2017 with research on possibilities of additive manufacturing for small scale turbomachinery for low-temperature distributed power systems and applications. In the scope of this project, two designs (here called *generations*) were created and experimentally verified at the pressurized air test rig. The design of the ORC micro turboexpander discussed within this thesis is, therefore, an evolution of the previous generations. Even though it is based on very different design methodology, it builds on the knowledge and experience gained from the design and experimental trials of the first two generations.

The *first generation* was designed specifically for air as a proof-of-concept of the whole turbine test stand. The design methodology and aspects discussed in Section 5.1.2 with further details provided in [122]. Various assemblies of stator and rotor wheels made of different materials and by different additive

manufacturing technologies were experimentally tested, and the results are reported in Section 5.4.

The *second generation* then followed up on the first generation design with several evolutional upgrades and some solely new concepts. The main difference is in the stator nozzles. Whereas in the first generation, there was a full stator wheel and then a large part of the admission arc was blocked, this concept brings only one nozzle segment which consists of three nozzles, which are then mounted in a metal frame. Also, the nozzles and rotor blades were designed for hexamethyldisiloxane vapour with a simple 1-D model according to [82]. The rotor blades were designed with a constant blade length, and the buckets were shaped according to the continuity equation for non-compressible fluids. The nozzle segments and rotor wheels were again manufactured by various AM methods and from different materials and tested at the pressurized air test rig. The results from these measurements are part of Section 5.4.

The *third generation* of the micro turboexpander is finally the output of this thesis, discussed in the following Sections 4.2, 4.3. This generation partially builds upon the rotor design methodology introduced in the second generation. Still, the approach to the nozzle design and the overall turbine stage is developed from scratch with inspiration from various ORC turbine design tools discussed in Section 2.5. This generation is finally designed from the beginning to be tested and verified in the ORC power unit and with an attempt to finally operate as an expander of the biomass-fired CHP plant discussed earlier in this chapter. The design of the third generation turbine was not yet experimentally tested at the time when this thesis is finalized, and it will be together with a thorough CFD analysis and mechanical design of the shaft assembly a subject of the future work of the author's collective as discussed in the conclusions in Chapter 6. This design continues in the modular design concept adopted in previous generations so that new loss models and geometries can be easily varied.

4.2 Detailed 1-D meanline design tool of the 3^{rd} generation turbine

The 1-D meanline design of the axial impulse stage turbine is based on energy and mass balance in each state of the turbomachine and with several assumptions:

- Steady states at 1, 2 and 3 at all the radii
- The thermodynamic properties are calculated for midspan diameter
- Conservation of rothalpy principle is applied
- Conservation of moment of momentum

- Cycle boundary conditions are to be conserved and not affected by the replacement of the expander
- The kinetic energy of the working fluid at the inlet is neglected
- Any heat losses from the turboexpander to the environment are neglected
- All design variables have to be kept within the limit of manufacturability
- The kinetic energy at the outlet is considered not to be recovered
- Rotor buckets designed with constant channel width and equal but opposite relative flow angles
- The incidence and deviation angles are assumed to be zero

The model was created using MS Excel with VBA and REFPROP add-in for fluid properties.

Since the designed turboexpander is meant to be affordable and simple to manufacture, assembly and operate, the desired combination of high power output and a compact design makes the impulse turbine a favourable choice compared to the reaction turbine. These may offer higher efficiency, at the cost of a larger machine. An axial configuration is chosen for the simplicity of manufacturing and easier design of the turboexpander. Also, partial admission can be easily adopted for axial impulse stage turbines. Finally, there were previous experiences from the experimental trials with cold aerodynamic tests of axial impulse stage turbines from the first two generations.

High pressure ratios, transonic flow velocities and compressible flow effects along with the proximity of the saturation curve lead to the complicated combination of a non-ideal gas and compressible flow. In the common 1-D meanline models, one of the two usually assumes the absence of the other. In the designed model, real fluid behaviour is therefore assumed, with a non-ideal gas model, the heat capacity ratio thus cannot be considered constant and is calculated for each state of the turbine. The design procedure is shown on a simplified flowchart in Fig.4.1.

For the initialization of the turboexpander design, some of the design variables had to be chosen with respect to the rotational speed, diameter of the machine and some other geometrical components. Another very important parameter to be estimated in the first step of the design is the isentropic efficiency of the turboexpander. These initial values and guesses are reported in Table 4.2. Some of these parameters were kept constant throughout the design phase and some were optimized, such as the rotational speed of the turbine and the blade height. The optimization parameters and the overall impact onto the isentropic efficiency of the designed turbine is displayed in the end of the Section 4.2 in Table 4.8. Please note that the calculations in

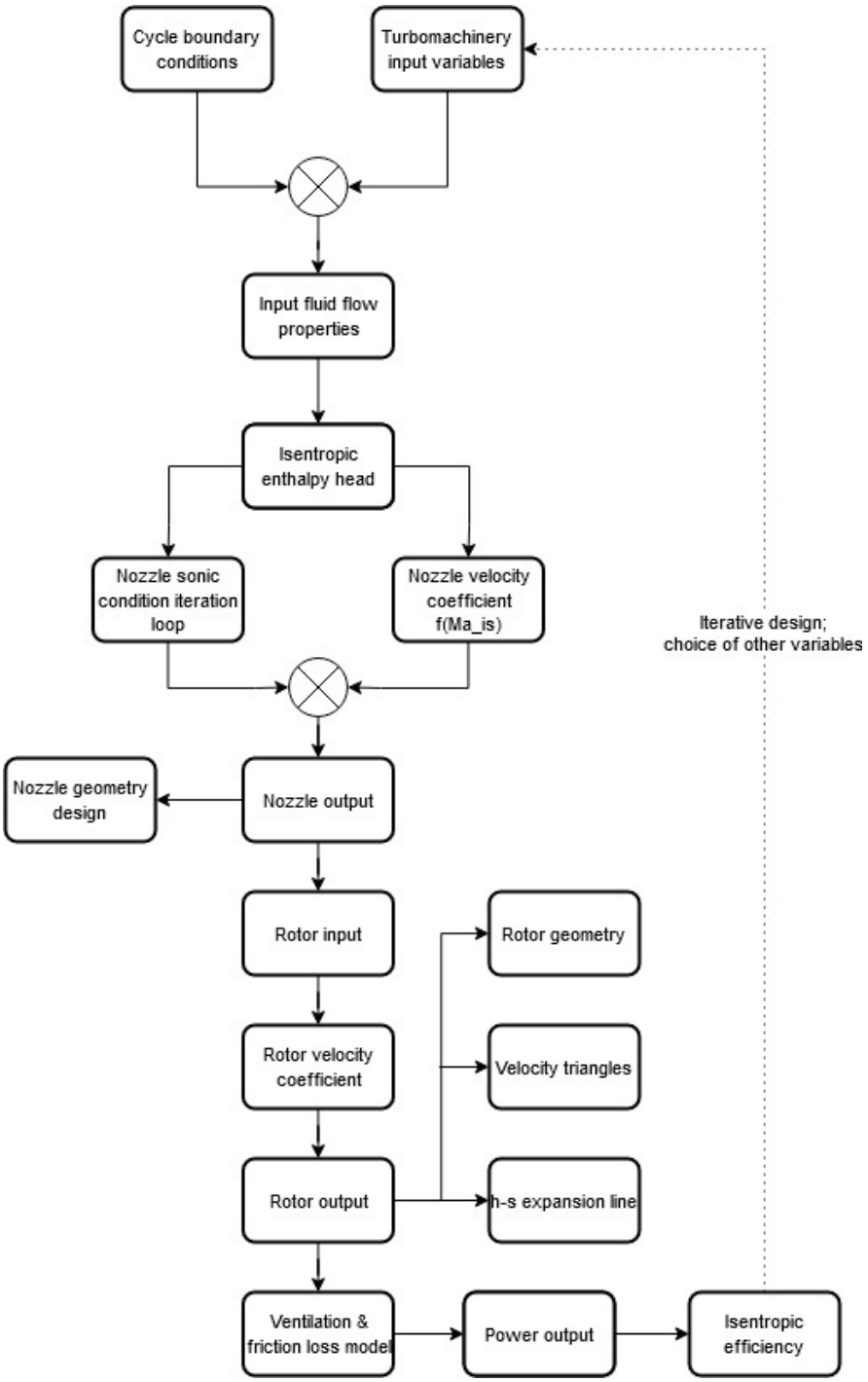

Figure 4.1: A simplified flowchart of the turboexpander design methodology

Table 4.2: Turboexpander design - chosen input parameters and guesses; parameters denoted with $'$ were later optimized

Parameter	Initial value	Units
Rotational speed n'	24 000	rpm
Midspan diameter D_{mid}	100	mm
Nozzle outlet flow angle α_2	13	°
Isentropic efficiency guess	70	%
Partial admission e'	58.5	%
Blade height ratio $\frac{h}{D_{mid}}'$	0.1	-
Minimum blade height h_{min}	5	mm
Rotor blades aspect ratio AR	2	-

the equations below are reported with values of already optimized values of the chosen parameters.

The nozzle outlet flow angle was assumed from the common and recommended values for axial flow impulse stage turbines. The midspan diameter was chosen concerning the spatial constraints within the ORC power system and also as a compromise between the high rotational speed and a large wheel size.

From the initial boundary conditions given from the cycle performance, the following midspan thermodynamic parameters are calculated using REFPROP add-in.

From the given pressure and temperature at the inlet, the enthalpy of the working fluid can be assessed in the Eq.(4.1), which is an illustrative example to outline the methodology of calculating fluid flow properties.

$$h_1 = \text{ Enthalpy } (MM; tp; SI \text{ with } C; T_1; p_1) = 340.62 \text{ kJ} \cdot \text{kg}^{-1} \tag{4.1}$$

And also, other thermodynamics state quantities, such as entropy or density at the inlet are calculated. Please note that for the sake of simplicity, the syntax of calculating the fluid properties using REFPROP is not repeated for every single parameter.

The enthalpy at the outlet of the turbine considering an isentropic expansion process can be calculated from the outlet pressure and the assumption of constant entropy in Eq.(4.2).

$$h_{3_{is}} = \text{ Enthalpy } (p_3; s_{1=3}) = 289.05 \text{ kJ} \cdot \text{kg}^{-1} \tag{4.2}$$

The isentropic enthalpy drop in the turbine stage is then equal to Eq.(4.3):

$$\Delta H_{is} = h_1 - h_{3_{is}} = 51.57 kJ \cdot kg^{-1} \tag{4.3}$$

From the chosen rotational speed, the circumferential velocity can be calculated - Eq.(4.4).

$$U = \frac{\pi \cdot D_{\text{mid}} \cdot n}{60} = 146.61 \text{ m} \cdot \text{s}^{-1} \tag{4.4}$$

And the isentropic absolute velocity at the nozzle outlet is then Eq.(4.5):

$$c_{2_{is}} = \sqrt{2 \cdot \Delta H_{is} \cdot 1000} = 321.15 \text{ m} \cdot \text{s}^{-1} \tag{4.5}$$

The isentropic Mach number at the nozzle outlet is calculated again using fluid properties and isentropic absolute velocity - Eq.(4.6).

$$Ma_{2is} = \frac{c_{2is}}{a_{2is}} = 2.19(-) \tag{4.6}$$

There are some well-known turbine loss models in literature like Craig and Cox profile loss, Macchi and Deich supersonic flow expansion loss models and other mentioned in Section 2.5, e.g. those by [86], [129], [130] etc. Most of them are mainly developed for and based on data from subsonic MW-class axial multistage steam and gas turbines working with full admission. Macchi [53], Da Lio [85] or Aungier [87] formulated specific loss models for ORC turbines with lower power output.

These sophisticated loss models consider a vast number of flow and geometry parameters for predicting total pressure loss or enthalpy dissipation per blade row. However, the model in this thesis focuses on the design of a single stage supersonic ORC micro turbine in the few or several kW-class, which often operates with partial admission. In reference [69] was broadly discussed that the conventional loss models could lead to differences in turbine stage efficiency in the magnitude of more than ten percentage points, especially for low specific speed turbines. This fact is not only a problem in terms of turbine performance but also in terms of turbine geometry design: since the required flow area depends on thermodynamic flow condition, which is directly influenced by losses. Thus, an approach from [131] was adopted, based on correlations from turbine drives of rocket turbopumps.

Generally, in small scale ORC applications, the required turbine pressure ratio leads to supersonic Laval nozzles due to very low speed of sound, resulting in highly supersonic fluid flow. The velocity coefficient of the supersonic nozzle is calculated by Eq.(4.7), which is derived from the data given in [93]

$$\begin{aligned}\phi_{No} = (1 - (2.9 \cdot 10^{-3} \cdot Ma_{2,is}^3 - 5.2 \cdot 10^{-2} \cdot Ma_{2,is}^2 - 2.241 \cdot 10^{-1} \cdot Ma_{2,is} \\ -8.77 \cdot 10^{-2}))^{\frac{1}{2}} = 0.899\end{aligned} \tag{4.7}$$

The absolute fluid flow velocity at the nozzle outlet is then equal to Eq.(4.8):

$$c_2 = \phi_{No} \cdot c_{2is} = 288.58 \text{ m} \cdot \text{s}^{-1} \tag{4.8}$$

Table 4.3: Resulting non-dimensional parameters of the designed turbomachine

Parameter	Initial value	Value after optimization
Stage loading coefficient ψ	47.26	55.13
Specific rotational speed N_s	0.04	0.047
Specific diameter D_s	0.083	0.083

The resulting non-dimensional parameters of the design turbomachine for reference with other turbines are reported in Table 4.3.

A simple iteration loop to calculate the critical fluid properties (noted with a "*") is implemented. The critical temperature of the fluid when the ideal gas model would be used would result in the following Eq.(4.9).

$$T^*_{id} = \frac{2}{\gamma + 1} \cdot (T_1 + 273.15) - 273.15°\text{C} \tag{4.9}$$

This is used as an initial guess in the iteration loop to reach the actual iterated real gas model T*. The iteration loop searches for a value of T* for which the Equation (4.10) is valid with a marginal iteration error.

$$\frac{a^{*2}}{2} = (h_1 - h^*) \cdot 1000 \text{ kJ} \cdot \text{kg}^{-1} \tag{4.10}$$

The iterated T* values are then used to calculate the other fluid properties in the throat area of the nozzle, which are later used for the design of the nozzle itself. From these equations, the total nozzle throat area A* is calculated as follows - Eq.(4.11). This model assumes that all energy during the expansion in the convergent part of the nozzles converts into the kinetic energy, the heat production being neglected.

$$A^* = \frac{\dot{m}_{wf}}{a^* \cdot \rho^*} = 111.18 \text{ mm}^2 \tag{4.11}$$

From the fixed nozzle height of 6 mm, the total nozzle throat width b* is calculated. Eq.(4.12)

$$b^* = \frac{A^*}{h_{No}} = 18.53 \text{ mm} \tag{4.12}$$

Table 4.4 then summarizes the calculated thermodynamic midspan properties at the nozzle outlet characterizing the fluid flow.

Interestingly enough, one may notice that the speed of sound indeed increased along the expansion in the de Laval nozzle ($a_1 = 123m \cdot s^{-1}; a^* = 135m \cdot s^{-1}; a_2 = 148m \cdot s^{-1}$), contrary to the expected ideal gas alike behaviour. This effect is caused by the highly non-ideal behaviour of the working fluid caused by the high molecular complexity and molar mass of the organic

Table 4.4: Midspan fluid properties at the nozzle outlet (state 2)

Parameter	Value	Units
T_2	157.91	°C
p_2	55	kPa(a)
h_2	298.98	$\mathrm{kJ \cdot kg^{-1}}$
c_2	288.58	$\mathrm{m \cdot s^{-1}}$
ρ_2	2.54	$\mathrm{kg \cdot m^{-3}}$
a_2	148.02	$\mathrm{m \cdot s^{-1}}$
Ma_2	1.95	–
v_2	$3.8 \cdot 10^{-6}$	$\mathrm{m^2 \cdot s^{-1}}$

fluid. In this thermodynamic region in which the nozzle operates, the intermolecular forces are not negligible anymore and strongly affect the fluid flow. The fluid properties library is equipped for these real gas effects thanks to the experimental facilities such as FAST [132] or ORCHID [133] at TU Delft, the CLOWT ([16]) at Muenster University of Applied Sciences, the Imperial College Dense Gas Blowdown Facility [134], and especially the Test Rig for Organic VApors (TROVA) [135] at the Laboratory of Compressible fluid-dynamics for Renewable Energy Applications (CREA Lab) of Politecnico di Milano, which focuses especially on experimental campaigns with siloxanes and MM.

An interesting phenomenon is a difference in the heat capacity ratio γ in between the states 1 and 2 as displayed in Eq.(4.13,4.14).

$$\gamma_1 = \frac{c_{p_1}}{c_{v_1}} = 1.096 \tag{4.13}$$

$$\gamma_2 = \frac{c_{p_2}}{c_{v_2}} = 1.032 \tag{4.14}$$

This clearly shows how impactful are the real gas effects and that using an ideal gas model brings very unsatisfactory results, especially for the nozzle design.

These midspan thermodynamic fluid flow properties are used to obtain the basic geometrical parameters for the nozzle and rotor design. First, from the continuity equation, the total area at the nozzle outlet is calculated - Eq.(4.15)

$$A_2 = \frac{\dot{m}_{wf}}{c_2 \cdot \rho_2} = 413.32 \text{ mm}^2 \tag{4.15}$$

Since the nozzle blade height is chosen to be an optimization parameter, as discussed earlier within the chapter, the total nozzle width can be now calculated - Eq.(4.16)

$$b_2 = \frac{A_2}{h_{\mathrm{nozz}}} = 68.89 \text{ mm} \tag{4.16}$$

Table 4.5: Velocity components values of the fluid flow at the nozzle outlet (state 2)

Parameter	Value	Units
$c_{2_{ax}}$	64.92	$\mathrm{m \cdot s^{-1}}$
c_{2_u}	281.2	$\mathrm{m \cdot s^{-1}}$
$w_{2_{ax}}$	64.92	$\mathrm{m \cdot s^{-1}}$
w_{2_u}	134.57	$\mathrm{m \cdot s^{-1}}$
c_2	288.58	$\mathrm{m \cdot s^{-1}}$
w_2	149.41	$\mathrm{m \cdot s^{-1}}$
u_2	146.61	$\mathrm{m \cdot s^{-1}}$
$\lvert\beta_2\rvert = \lvert\beta_3\rvert^*$	25.75	°

The degree of admission e is calculated from the nozzle outlet area and the total annular area A_{ring} in Eq.(4.17).

$$e = \frac{A_2}{A_{\mathrm{ring}} \cdot \sin(\alpha_1)} = 0.975 \tag{4.17}$$

The calculated velocities and angles for the nozzle outlet and rotor inlet respectively are reported in Table 4.5.

A very important parameter for assessment of the losses in the rotor blading is the relative Mach number at the inlet of the rotor Ma_{r_2} calculated as the ratio of the relative velocity component and the speed of sound Eq.(4.18).

$$Ma_{r_2} = \frac{w_2}{a_2} = 1.01 \tag{4.18}$$

The flow deflection ϵ in the rotor is calculated as the differential of the relative flow angles Eq.(4.19):

$$\varepsilon = \beta_3 - \beta_2 = 128.5° \tag{4.19}$$

The correlation for the blading velocity coefficient (defined in the Eq.(4.20) below) of the pure impulse blading is also taken from the former turbopump development (see [92]).

$$\phi_{bl} = \frac{w_3}{w_2}[-] \tag{4.20}$$

The basic profile velocity coefficient is a function of the blade relative inlet Mach number Ma_{r_2} and the flow deflection angle ϵ, Eq.(4.21).

$$\begin{aligned}\phi_{bl} &= 9.57 \cdot 10^{-1} - 3.62 \cdot 10^{-4} \cdot \varepsilon - 2.58 \cdot 10^{-2} \cdot \mathrm{Ma}_{r_2} + 6.39 \cdot 10^{-6} \cdot \varepsilon^2 \\ &+6.74 \cdot 10^{-2} \cdot \mathrm{Ma}_{r_2}^2 - 7.53 \cdot 10^{-8} \cdot \varepsilon^3 - 4.3 \cdot 10^{-2} \cdot \mathrm{Ma}_{r_2}^3 \\ &-2.38 \cdot 10^{-4} \cdot \varepsilon \cdot \mathrm{Ma}_{r_2} + 1.45 \cdot 10^{-6} \cdot \varepsilon^2 \cdot \mathrm{Ma}_{r_2} \\ &+4.25 \cdot 10^{-5} \cdot \varepsilon \cdot \mathrm{Ma}_{r_2}^2 = 0.853\end{aligned} \tag{4.21}$$

Table 4.6: Velocity components values of the fluid flow at rotor outlet (state 3)

Parameter	Value	Units
$c_{3_{ax}}$	52.97	$\mathrm{m \cdot s^{-1}}$
c_{3_u}	36.81	$\mathrm{m \cdot s^{-1}}$
$w_{3_{ax}}$	52.97	$\mathrm{m \cdot s^{-1}}$
w_{3_u}	-109.8	$\mathrm{m \cdot s^{-1}}$
c_3	64.5	$\mathrm{m \cdot s^{-1}}$
w_3	-121.91	$\mathrm{m \cdot s^{-1}}$
$u_3 = u_2$	146.61	$\mathrm{m \cdot s^{-1}}$
α_3	55.2	°

Table 4.7: Midspan fluid properties at the rotor outlet (state 3)

Parameter	Value	Units
T_3	159.91	°C
p_3	55	kPa(a)
h_3	302.71	$\mathrm{kJ \cdot kg^{-1}}$
h_{3_t}	304.8	$\mathrm{kJ \cdot kg^{-1}}$
ρ_3	2.53	$\mathrm{kg \cdot m^{-3}}$
a_3	148.41	$\mathrm{m \cdot s^{-1}}$
Ma_3	0.43	-
Ma_{r_3}	0.82	-
c_3	288.58	$\mathrm{m \cdot s^{-1}}$

This blading velocity coefficient is then corrected by the effect of the blade height and the chord length ratio and the final value is iterated - Eq.(4.22). The chord length is taken from the geometrical values of the rotor discussed within the next Section 4.3.

$$\phi_{bl_{corr}} = 0.816 \tag{4.22}$$

From the definition of the blading velocity coefficient, one may then calculate the relative velocity of the fluid flow at the rotor outlet and thus also the rest of the velocity components (summarized in Table 4.6). Also, the fluid properties at state 3, the rotor outlet are calculated and the results are shown in Table 4.7.

Finally, the velocity triangles of the impulse stage are displayed in Figure 4.2. It is apparent, that the optimal maximum efficiency point yields a slight resulting tangential component of absolute velocity. This is due to the contradictory effects of optimizing the rotational speed and reducing u_3 respectively and the increase in flow deflection ϵ and its effect on the blading velocity coefficient Eq.(4.21).

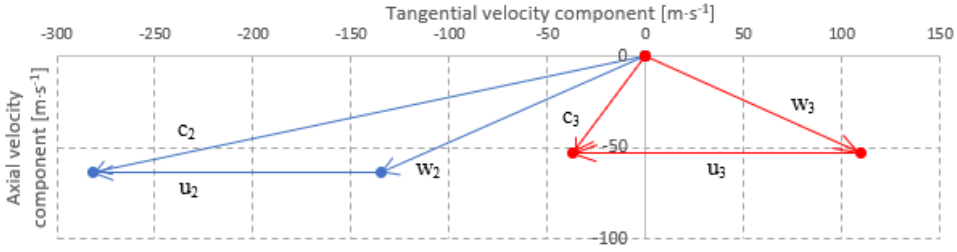

Figure 4.2: Velocity triangle of the design ORC impulse stage

The enthalpy rise at the outlet by the effect of kinetic energy loss in the rotor blading is equal to Eq.(4.23):

$$\Delta H_{\text{rotor}} = \frac{w_3^2 - w_2^2}{2} = 3730 \text{ J} \cdot \text{kg}^{-1} \tag{4.23}$$

This results in a slight degree of reaction in the impulse stage equal to Eq.(4.24):

$$R = \frac{\Delta H_{\text{rotor}}}{\Delta H_{\text{stage}}} = \frac{3.73}{37.91} = 0.098[-] \tag{4.24}$$

It can thus be observed that due to the effect of irreversibility in the rotor, a purely impulse stage can be obtained only in theory. A real turbine stage always possesses some losses within the rotor and thus a reaction degree of a few percentage points. In the design procedure, another iteration step should be included, in which now the stagnation pressure at the outlet of the turbine would be increased according to the slight degree of reaction.

Finally, the total power extracted from the fluid flow and transformed into the rotational energy of the turbine shaft can be calculated - Eq.(4.25).

$$P_{\text{turb}} = \dot{m}_{wf} \cdot u_3 \cdot (c_{3_u} - c_{2_u}) = 10856 \text{ W} \tag{4.25}$$

This total power output already excludes the profile and secondary losses within the nozzle and blading, which are accounted for by the velocity coefficient. The ventilation and friction losses are yet to be calculated by the following formulas.

The friction loss is calculated using the following Equation (4.26) from [131].

$$P_{fr} = 0.01 \cdot \rho_2 \cdot \left(\frac{n}{60}\right)^3 \cdot D_{\text{mid}}^5 = 26 \text{ W} \tag{4.26}$$

Ventilation losses in the rotor blading play a significant role for the considered small axial impulse stage turbines due to partial admission, which is often necessary. To estimate ventilation losses, based on the investigation of

Table 4.8: Optimization of chosen turbine design input variables and its effect onto the turbine performance

Parameter	Initial value	Optimized value	Units
Rotational speed n	24 000	28 000	rpm
Velocity ratio $\frac{u}{c_{is}}$	0.391	0.457	-
Blade height ratio $\frac{h}{D_{mid}}$	0.1	0.06	-
Partial admission e	58.5	97.5	%
Isentropic efficiency η_{is}	67	69.2	%
Mechanical power P_{mech}	10 467	10 809	W

[136], the basic blade velocity coefficient is adjusted by a correlation assuming that secondary losses are linearly coupled to basic profile losses and inversely proportional to the blade aspect ratio. The correlation (Eq.(4.27)) for the ventilation power P_V of a single impulse wheel is originally from [137] and has been adjusted to the design architecture by [47].

$$P_V = 0.925 \cdot \left[(1-e)\rho_3 \cdot \left(\frac{n}{60}\right)^3 \cdot D_{\text{mid}}^4 \cdot 4.5 \cdot h_{\text{rot}_{\text{out}}} \right] = 21 \text{ W} \tag{4.27}$$

The simple loss model does not consider Reynolds number. This may influence the correlation for low Re flows such as can be seen in the experimental values in Section 5.4.1 with cold air tests. For the design of the ORC turbine, it was investigated and proven that the ventilation power loss is not a strong function of the Reynolds number as the designed turbines are in most of the cases well above the critical Reynolds number region. The tip leakage is neglected as the rotor is designed as shrouded. The friction loss in the bearings is within this design stage neglected as well as the type of bearing is still to be defined.

Subtracting the power losses from the total power output, the mechanical power output of the turbine is calculated as Eq.(4.28).

$$P_{\text{mech}} = P_{\text{turb}} - P_{\text{fr}} - P_V = 10809 \text{ W} \tag{4.28}$$

The value of total-to-static isentropic efficiency of the turbomachine is finally calculated by comparing the mechanical power output to the isentropic power - Eq.(4.29).

$$\eta_{is} = \frac{P_{\text{mech}}}{\dot{m}_{wf} \cdot \Delta H_{is}} = 0.692 \tag{4.29}$$

A sensitivity analysis with respect to the effect of the velocity ratio $\frac{u}{c_i s}$ respectively the rotational speed of the turbine onto the isentropic efficiency was performed in order to optimize the design rotational speed of the machine and achieve maximum η_{is}. If put into the context of the mechanical design

and operation turbine, it is though questionable whether the increase of few percentage points in the isentropic efficiency of the turboexpander is justified by an increase of rotational speed by 4 000 rpm. This has to be further analyzed during the mechanical design of the whole 3^{rd} generation ORC turbine assembly. This sensitivity analysis is better shown in Figure 4.3.

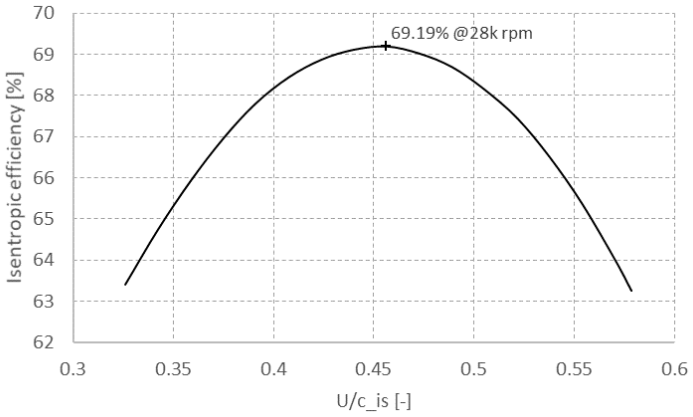

Figure 4.3: The sensitivity analysis on the rotational speed, respectively the velocity ratio $\frac{u}{c_{is}}$

Another optimization parameter was the nozzle height ratio defined as the ratio of nozzle height and the midspan diameter. This was optimized again in order to achieve maximum efficiency. The optimization of the nozzle height and eventually, the degree of admission e is shown in Figure 4.4. The maximum efficiency was reached with a full degree of admission. Due to the manufacturing issue, 5 mm nozzle height was chosen as a minimum value. To account for a finite trailing edge with of the nozzle blades, the degree of admission is reduced by 2.5 % according to an estimate of number of stator blades and a trailing edge thickness of 0.5 mm. The resulting nozzle height then equals $h_{No} = 6$ mm with $e = 0.975$. Additional 0.2 mm are added to the blade height in the rotor inlet to cover better the impinging jet fluid flow at the nozzle outlet and reduce the tip losses, the blade length at the rotor inlet yields $h_{rot_{in}} = 6.2$ mm.

The expansion process is described in Figure 4.5 in an h-s diagram. It can be observed that if the kinetic energy would be usefully employed and not entirely wasted, the fluid flow would expand to state 3^{+} instead of 3 and recover some of the pressure. Theoretical expansion with the same isentropic efficiency would yield higher enthalpy at the state 3 since it considers all the kinetic energy at the output as dissipated into heat and the 1-D meanline model considers it as a fully unrecovered loss even though it is further downstream utilized in the condenser.

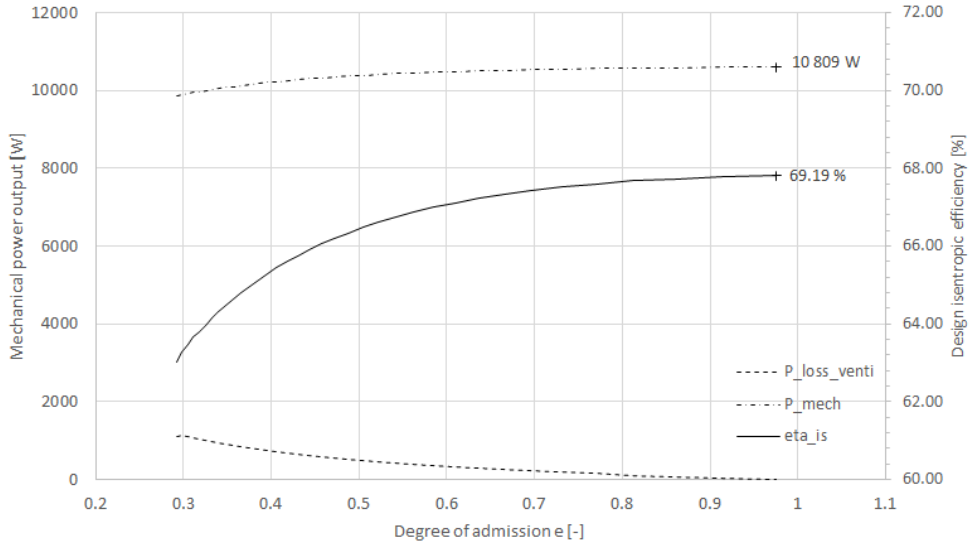

Figure 4.4: Sensitivity analysis for the degree of admission of the designed impulse stage turbine

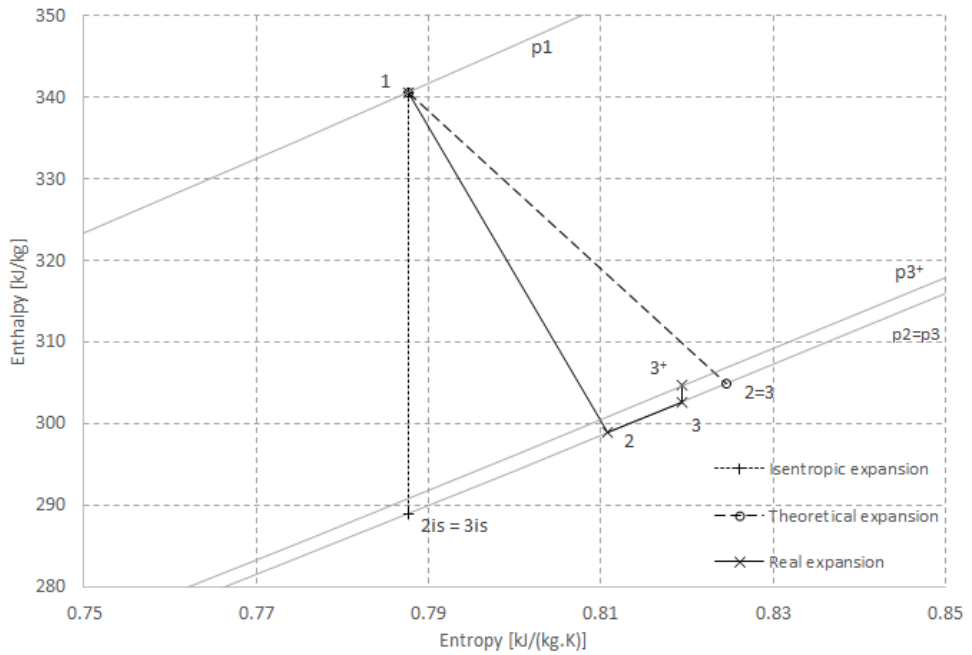

Figure 4.5: h-s diagram of the isentropic, theoretical and real expansion line

4.3 Design of the flow components

The resulting values from the 1-D meanline design at midspan are used to design the flow components.

The *stator* is designed as a series of *convergent-divergent de Laval nozzles*. As the flow suffers sever real gas effects and is highly supersonic, the resulting nozzle geometry is very unconventional, cambered and unlike any stator blade geometries that could be found in an airfoil atlas. The geometry of the nozzle is thus designed as a combination of the divergent part, which for such highly supersonic flow impacts the efficiency of the nozzle the most and therefore more effort is put into designing it, and the convergent part.

Several shapes of the divergent part of the nozzle can be used. The difference between them is in a few percentage points in nozzle efficiency. Still, more importantly, the more sophisticated designs shorten the length of the divergent part of the nozzle which saves the materials used, the weight and overall the cost of the component. Especially, for this reason, nozzle shapes are of utmost importance for aerospace engineers designing the rocket engines, where "every kilogram counts". The simplest design uses a *conical-shaped* divergent part with a constant divergent angle. This shape is the easiest to manufacture, but the nozzles have more unsatisfactory performance and are longer. More advanced design shapes and the most common ones in jet engines are nozzles with *bell-shaped* divergent part (named after its remarkable bell shape), an essential design issue is to contour the nozzle to avoid oblique shocks. Therefore, the nozzle has a high angle expansion section right after the throat, followed by a gradual decrease of divergent angle. Other common nozzle shapes are for example annular nozzles, spike nozzles or aerospike nozzles, which can be utilized in specific types of jet engines such as ramjets or scramjets. [138]

A simplified version of a bell-shaped nozzle named Rao nozzle is used for the design of the nozzle shape in the scope of this thesis. [139] This nozzle shape uses a rather simple circular arc for the throat section and a parabola for the divergent part, as can be seen in the Fig.4.6.

As for the bell-shaped nozzle, the expansion angle is higher closer to the throat section and decreases along with the nozzle. Optimal parabola angles for the maximum performance according to the nozzle expansion ratio were chosen according to the empirical results from the literature. [138]

From the knowledge of total nozzle throat area and total nozzle outlet area calculated in the previous Section 4.2, and the chosen number of blades, one may calculate and design the nozzle geometry. The selection of the number of blades for supersonic turbines is a topic not often discussed in the literature. Several different recommendations can be obtained from the literature for subsonic nozzles, such as in the work of Deich [140] or Zweifel [141], who introduced the Zweifel loading criterion for an optimum pitch-to-chord ratio for high deflection turbine cascades. For turbine cascade blades, there is an

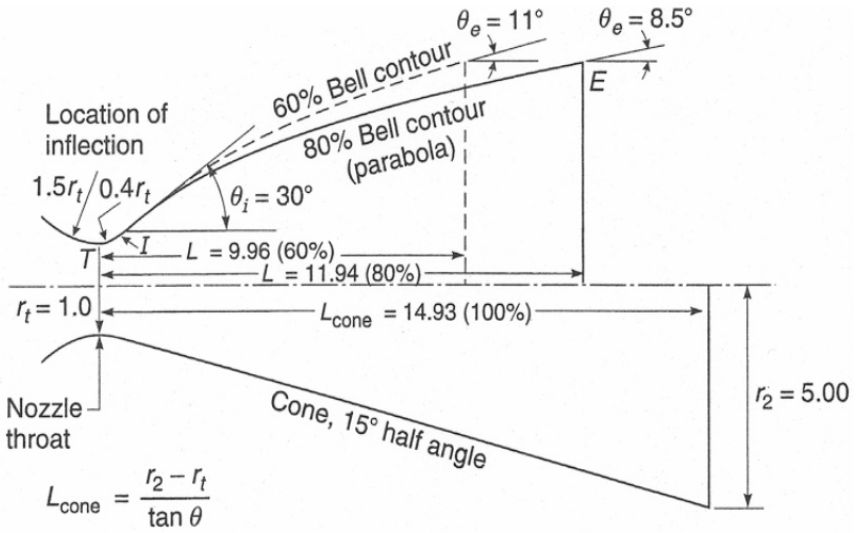

Figure 4.6: Rao nozzle geometry used to design the turbine stator compared to other nozzle geometries; source [139]

optimum pitch-to-chord ratio that gives a minimum overall loss. If the spacing between the blades is made small, the fluid receives the maximum amount of guidance from the blades, but the friction losses will be large. On the other hand, with the same blades spaced well apart, friction losses are small but, because of poor fluid guidance, the losses resulting from flow separation are high. Such criterion has to be formulated empirically from a series of experiments with turbine cascades, and unfortunately, such correlations are not available for highly supersonic turbines. The number of stator nozzles was therefore chosen with a different approach, from the manufacturability perspective and then checked with the Zweifel loading criterion and Ainley-Mathieson charts for minimum nozzle profile loss coefficient for given nozzle outlet flow angle and pitch-chord ratio for at least some reference, even though these charts were developed for subsonic flows. [89], [90]

The manufacturability limit was set to the least of 1.5 mm of the nozzle throat area. With this limitation, a number of 10 stator nozzles was chosen, resulting in the following design values. A single nozzle throat width of 1.85 mm and a single nozzle outlet width of 6.88 mm are obtained. With a nozzle height of 6 mm, this results in a nozzle throat area = 11.12 mm^2 and a nozzle outlet area = 41.33 mm^2. The rotor wheel is fully admitted by the flow out of the nozzles except for the flow area blocked by the trailing edges of the nozzles, which is accounted for by the reduction of the degree of admission to $e = 0.975$. The number of stator nozzles will be a parameter, which can be in the future both experimentally and by the method of CFD verified and updated to achieve maximum performance.

The turbine acts as a key element of the cycle, which separates the two pressure levels and determines the operation of the cycle. From the cycle perspective, the turbine must be able to swallow the required mass flow rate at a given temperature to generate the design inlet pressure for adequate cycle operation. As the nozzle operates in supersonic condition, the flow is choked. This means that an ideal gas flowing through such nozzle would keep constant *swallowing capacity* as defined in Eq.(2.18) and the turbine inlet pressure is proportional to it and fully independent of the turbine outlet pressure. Introducing the real gas compressibility effects, especially for hexamethyldisiloxane at given boundary conditions the heat capacity ratio increases for increasing turbine inlet pressure and so as does the density of the fluid, this in hand with an increase of Mach number would result in higher swallowing capacity and the choking point at higher pressures than for the ideal gas.

The *rotor blades* were designed as constant channel width buckets with geometry according to [142]. The shape of the buckets is again unconventional and highly cambered since it experiences large flow deflection. Thus, conventional airfoil for turbine rotor blades cannot be used, and the geometry is designed specifically for this type of application. The blades are simple cylindrical as they are easy to manufacture with standard technology. The increase in specific volume along the streamline is accounted for by means of linearly increasing blade length along the chord line of the blade. The aspect ratio (ratio of axial chord length to blade length) was chosen $AR = 2$ as recommended by Agromayor and Nord in [81] for this type of axial impulse supersonic turbines. The blades were designed as unshrouded due to the manufacturability constraints.

From the average rotor blade length, the *axial chord length* was then calculated and rounded up to 12.5 mm. The number of rotor blades was chosen with respect to manufacturability - a *trailing edge width* of 0.3-0.4 mm is required for a trade-off between structural strength and flow blockage resulting in thick wakes and according to the recommendation of Zweifel and Ainley-Mathieson for minimum profile loss for the selected *pitch-to-chord ratio* $\frac{s}{c}$. [89] The final iterated number of 35 rotor blades were selected with pitch s of 8.98 mm and thus 0.72 pitch to chord ratio $\frac{s}{c}$, whilst the optimum for given flow angles according to Ainley-Mathieson lays at 0.75. [143] The rotor blade length varies linearly along the axial chord from 6.2 mm at the inlet to 7.74 mm at the outlet of the rotor.

The deviation angle is considered to be zero, as for the highly supersonic turbines thin boundary layers at the blade exit for well-designed blades can be expected, which results in attached flow. Thus, the blade camber angle θ is matched with the flow deflection angle ϵ and equal to 128.5°.

As foreseen by the experiments at the Fluid machinery Laboratory at Politécnico di Milano, a gap between stator and rotor of 35 % of the stator axial chord length is used, in order to minimize the effect of *stator-rotor interaction* by shedding the wakes and vortices from the nozzle trailing edges and their

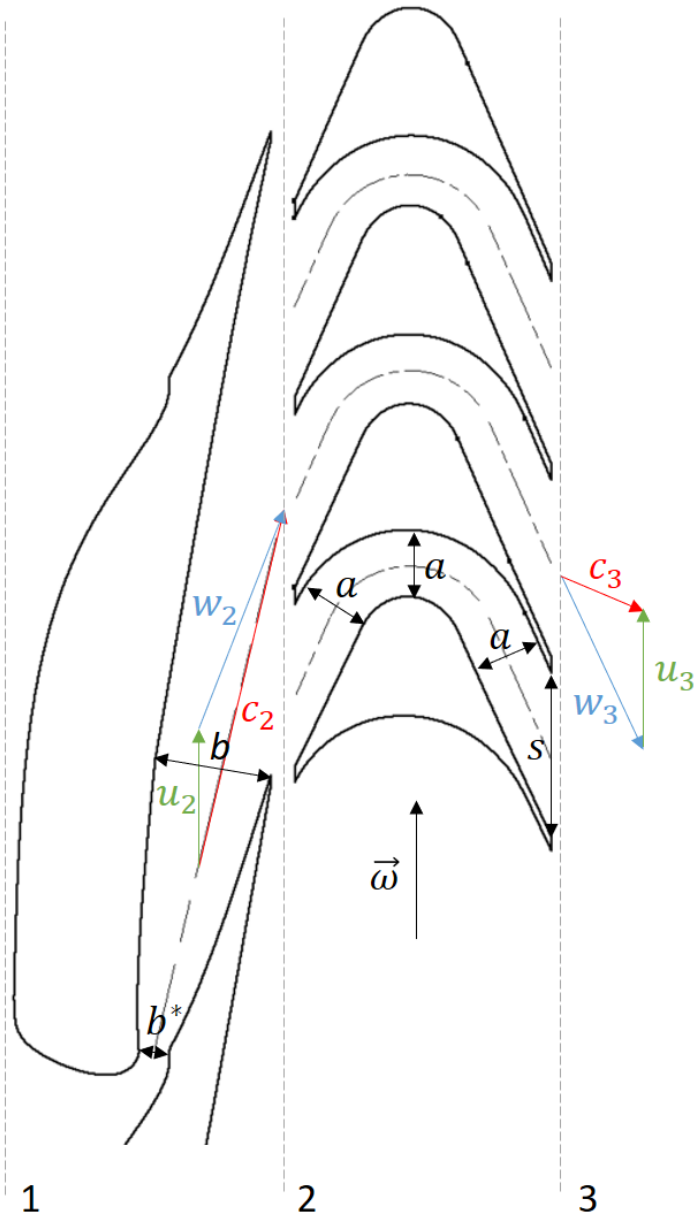

Figure 4.7: Blade-to-blade cross-section of the designed nozzle and bucket geometry with velocity triangles

interaction with boundary layer in the rotor. [144]

The designed geometry of stator nozzles and rotor blades along with the velocity triangles of the fluid flow is shown in Fig.4.7.

The Reynolds number of the fluid flow through rotor is calculated below to check the nature of the flow according to the Eq.(2.7). The characteristic

dimension is the hydraulic diameter of the rotor blade passage.

$$Re = \frac{C_{ax} \cdot u_2 \cdot \rho_2}{\mu_2} = 1222202[-] \tag{4.30}$$

Reynolds number in the order of 10^6 indicates the fluid flow is highly turbulent with a very thin laminar sublayer.

The whole stator-rotor assembly is displayed in Figure 4.8. The rest of the turbine – the shaft, bearings, housing, coupling etc. has not been discussed within the scope of the thesis and will be a subject of the future work. The stator and rotor are considered to be manufactured by 5-axis milling from aluminium alloy suitable for operation in high temperatures and thus are not designed as shrouded wheels.

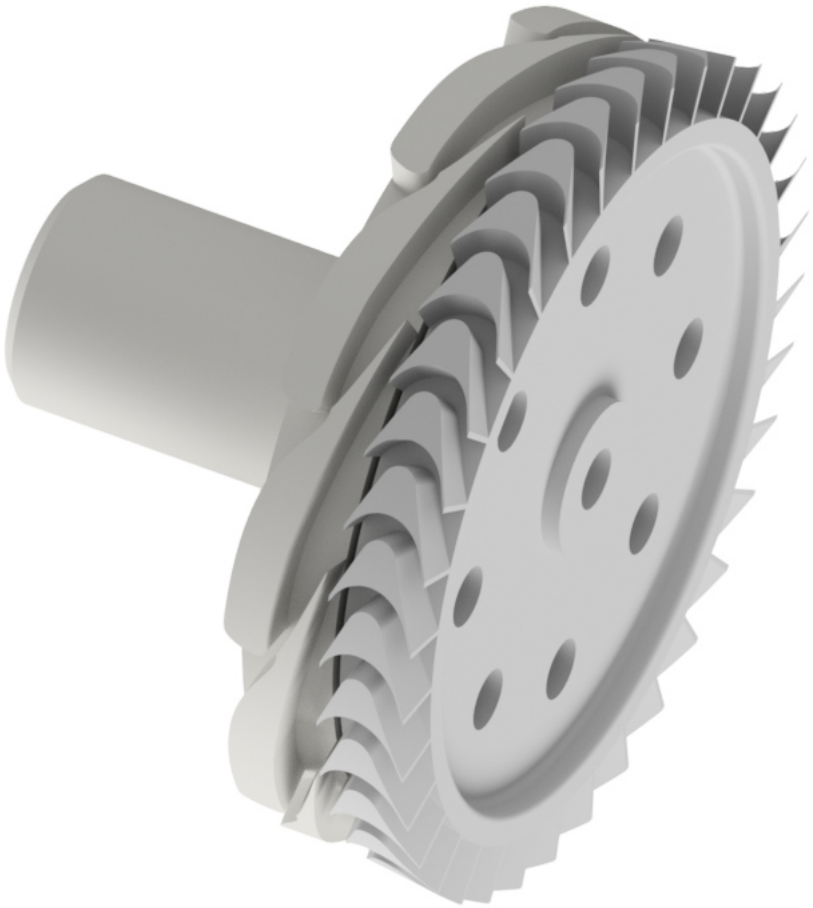

Figure 4.8: A render of the designed stator-rotor assembly

Chapter 5

Experimental Investigation of the First and Second Generation Turboexpanders

This chapter presents the methodology and results of the cold aerodynamic experimental trials of the 1^{st} and 2^{nd} generation axial impulse micro turboexpanders. The investigation aims at the evaluation of isentropic efficiency of the turboexpander generations as a whole but also even maybe more importantly, at the various effects of additive manufacturing on the turbomachinery performance.

5.1 Detailed description of the measured turbine generations and combinations

The evolution and the generations of the designed micro turboexpander were previously mentioned in Section 4.1. This subchapter brings more details on the design of the generations and their variations - distinguished by the additive manufacturing methods, post-processing and material - for the experimental investigation. An overview of the experimentally verified turbine assemblies is presented in the last part of the section.

5.1.1 Summary of the experimentally investigated turboexpander assemblies

Various combinations of rotor and stator wheel were tested to investigate several tasks. For the first generation, the combinations were made from stators and rotors made by DMLS, SLS, FDM and in two versions of chord length (only selected variations) – short chord and long chord. The DMLS

stator wheels were tested with different finishing methods and with added features to investigate these effects onto the turbine performance.

The list of the experimentally investigated flow components with further used notation follows:

First generation flow components:

- Stator wheels
  - SLSl – long chord selective laser sintered nylon stator wheel
  - SLSs – short chord selective laser sintered nylon stator wheel
  - FDMl – long chord fused deposition modelled ABS stator wheel
  - DMLSs – short chord direct metal laser sintered stainless steel stator wheel
    - DMLSs_ap – in as printed state
    - DMLSs_pol – polished by a hand polishing machine
    - DMLSs_supp – with functional supports as recommended by the manufacturer
  - DMLSl – long chord direct metal laser sintered stainless steel stator wheel
- Rotor wheels
  - SLS – selective laser sintered nylon rotor wheel
  - DMLS – direct metal laser sintered stainless steel rotor wheel

Additionally, DMLS long chord rotor with SLS long chord stator were also investigated. But due to its heavy weight and large inertia, it was impossible to operate it at higher rotational speed and thus the results are not reported.

Second generation flow components: For the second generation, there were three variants of nozzle segment manufacturing methods – SLA, SLS and DMLS - and three variants for the rotor - SLA, SLS and MJF. All combinations of the nozzles and rotors were investigated.

- Nozzle segments
  - DMLS – direct metal laser sintered nozzles from stainless steel powder, hand-polished
  - SLA – nozzle segments made of resin by stereolithography
  - SLS – selective laser sintered nozzles from nylon powder
- Rotor wheels
  - SLS - selective laser sintered rotor wheel from nylon powder

- SLA - rotor made of resin by stereolithography
- MJF – nylon rotor wheel manufactured using multi jet fusion

Detailed information regarding the first and second generation designs follow.

5.1.2 Proof-of-concept first generation turboexpander

This proof-of-concept 1^{st} gen turboexpander was designed to operate with air and 30 kJ/kg enthalpy head at a design pressure ratio of 1.4. The low design pressure ratio was chosen for the sake of a safe operation of the machine and not to run into high rotational speed and fluid speeds, respectively. The final design of the first-generation proof-of-concept experimental turbomachine is displayed at the Fig.5.1. The geometrical parameters of this turbine are then summarized in Table 5.1. The design procedure was extensively discussed in [122].

Apart from the design of the turbine, also the instrumentation and control of the power output and turbine operation were developed. The flow components of the micro turboexpanders of the first generation were designed according to the methodology and loss correlations for large scale steam turbines from the 1950s. The first generation was designed in two variations – *long chord* and *short chord*. These two differed in the number of blades in the stator and rotor wheel and as the name indicates, in the chord length, with approximately the same pitch to chord ratio $\frac{s}{c}$.

The main goal of the first generation was to prove that the concept is reliable and gives valid data for isentropic efficiency evaluation of turbine assemblies with flow components made of several different materials and additive manufacturing technologies. These AM technologies differ in the resulting surface roughness, geometrical precision and strength of the material, and the goal was to evaluate these effects on the overall efficiency of the turbomachine. In Fig.5.2 and Fig.5.3 are shown details of the blading of the 1^{st} gen stator wheels and the values of surface roughness of the blades are summarized in Table 5.2. The surface roughness measurements were performed inside the channel on the pressure side of the blade in the fluid flow direction, and the total values were averaged from five measurements with the lowest, and the highest values of Ra left out. The lowest Ra was measured for the polished stainless steel DMLS blades and the highest for the same blades in the as printed state. The plastic wheels were without any post processing, and the same goes for the stators as well as the rotors. A variation of the DMLS stator wheel with *functional supports* as recommended by the manufacturer was tested. These supports were added for improved print quality and the goal was to experimentally verify what will be the impact on the overall turbine performance with these extra features.

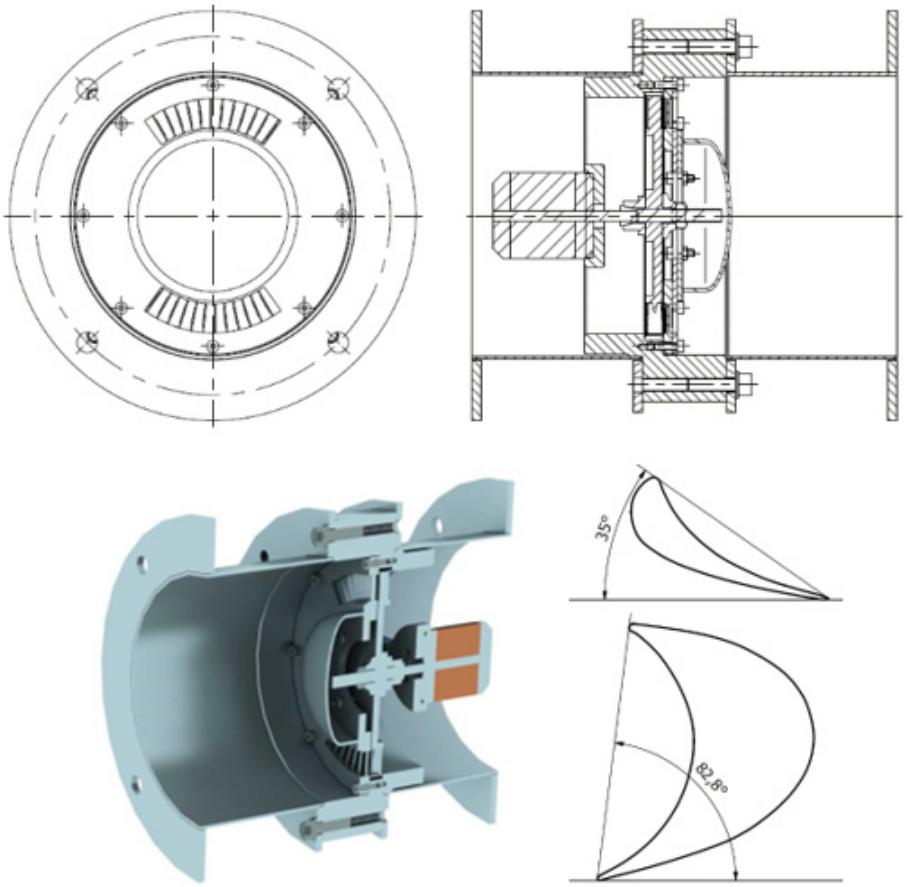

Figure 5.1: Design of the first-generation proof-of-concept turboexpander and detail of guide vane and rotor blade shapes S-90-12A and R-26-17A; source: [122]

The goal with this first generation proof-of-concept experimental turbine was to have a very simple design, on which the aspects of additive manufacturing can be investigated. Also, it was designed to be easily transported, assembled and disassembled and within the *plug & play* concept. During the experiments, the 1^{st} generation turboexpanders were operated with only one admitted stator nozzle for long chord stator wheels and 3 nozzles for short chord wheels (equal to the degree of admission ϵ of 6.7 %) to reduce the power output and the cost and size of the power electronics.

5.1.3 Second generation micro turboexpander

As a next step forward in the research of micro turboexpanders towards an ORC application, another geometry of the rotor and stator nozzles were de-

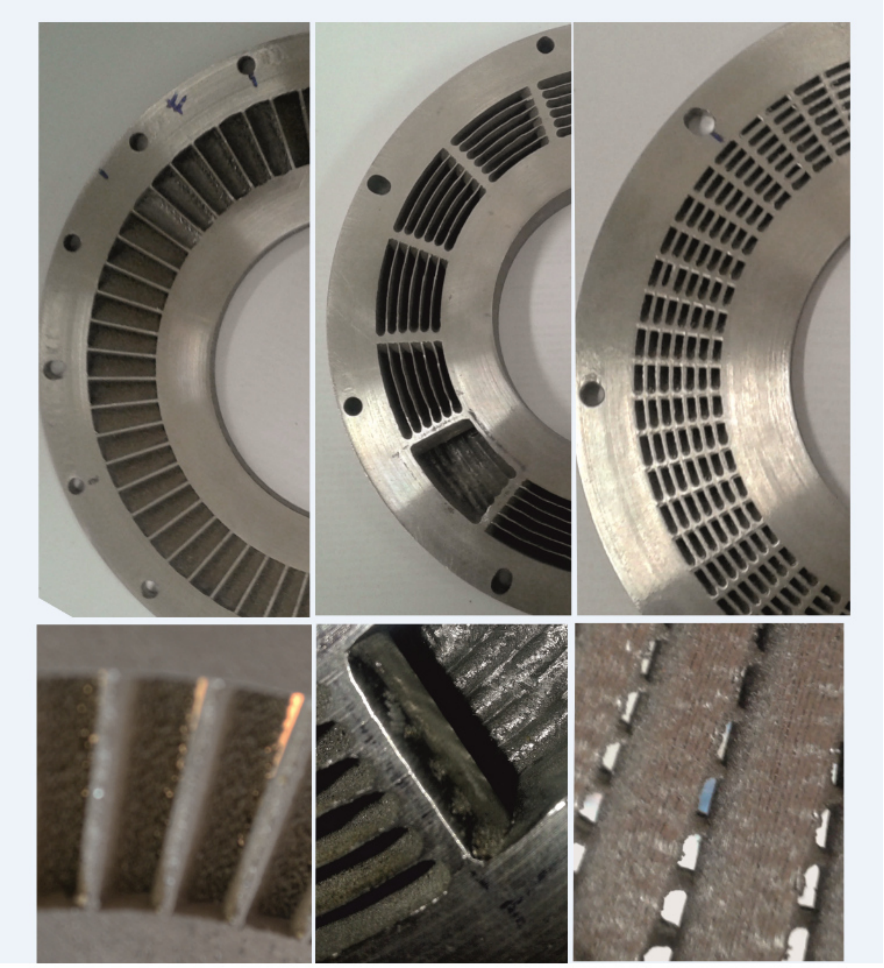

Figure 5.2: Investigated DMLS stator wheels, from the left - as-printed short chord stator, polished long chord stator and the stator with *functional supports*

signed specifically for the hexamethyldisiloxane and with supersonic convergent-divergent Laval nozzles. The second generation design is displayed in the drawings and a cross-section in Fig.5.4. These flow components were designed in a way that it would also be possible to test this combination with pressurized air in the same test rig as the first-generation turbine and verify the possibility to transfer the results obtained from the cold aerodynamic testing to the hot-fired ORC tests.

This second generation also featured improved sealing and fitting of the assembly, which significantly reduced lead time for changing the flow components. With pressurized air though, the second generation of course operated in highly off-design condition and the results yield from these experiments cannot be fully compared with the first generation. Experiments with the

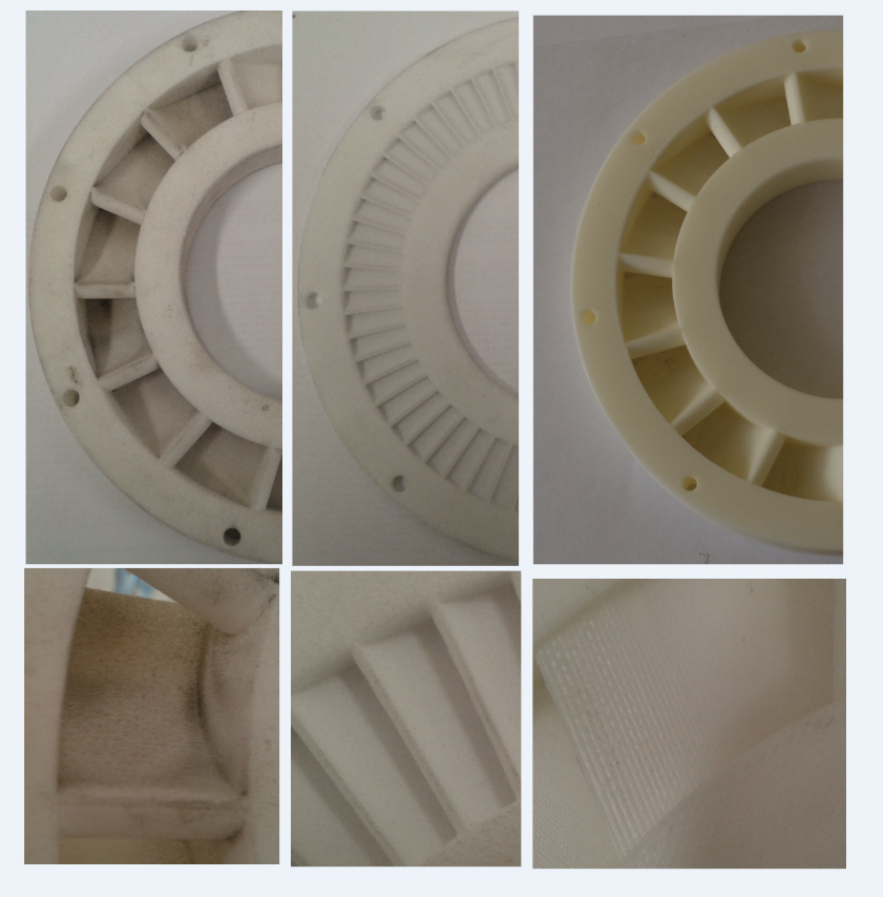

Figure 5.3: Experimentally tried stator wheels; from the left – SLS long chord, SLS short chord, FDM long chord

second-generation design were more focused onto gaining experience operating the turbine, which will be run with organic fluid and also to try and compare various combinations of AM methods and materials for 3-D printing with different surface quality and geometrical precision.

The nozzle segments and rotor wheels that were experimentally investigated are shown in Fig.5.5 and Fig.5.6, respectively. Note the apparent drilling holes from the dynamic balancing of the rotor wheels and that the SLA wheel on the left is after an accident. The rotors had been dynamically balanced to the precision of G 1.2 according to ISO 1940-1 by an accredited laboratory.

Again, as for the 1^{st} gen turboexpanders, the surface roughness of the nozzles was measured and with the same procedure. The results of the surface roughness measurement are reported in Table 5.3.

Table 5.1: Resulting design parameters of the first-generation proof-of-concept turbine; source [122]

Design parameter	Value	Units
Stator vanes outlet angle α_2	14.3	°
Rotor blades inlet angle β_2	19.2	°
Rotor blades outlet angle β_3	19.1	°
Chord angle Cα_y	35	°
Chord angle Cβ_y	82.8	°
Stator chord C_1	8.1/32.2*	mm
Rotor chord C_2	9.8/38.5*	mm
Midspan diameter D_{mid}	120	mm
Blade length l_1	17.2	mm
Blade length l_2	18.2	mm
Number of stator blades z_l (for full admission)	60/15*	–
Number of rotor blades z_2	55/15*	–
Partial admission ε	34	%
Partial admission segments i	2	–

* (short / long blades version)

Table 5.2: The surface roughness of the first-generation stator blades, measured inside the channel in the fluid flow direction with a declared accuracy of ±10 %; averaged from five measurements (Roughness meter INSIZE ISR-C002)

AM technology	Value	Units
Selective Laser Sintering (SLS, nylon)	5	μm
Fused Filament Extrusion (FDM, ABS)	7.1	μm
Laser Powder Bed Fusion (DMLS, stainless steel) - as printed	20	μm
Laser Powder Bed Fusion (DMLS, stainless steel) - polished	0.9	μm

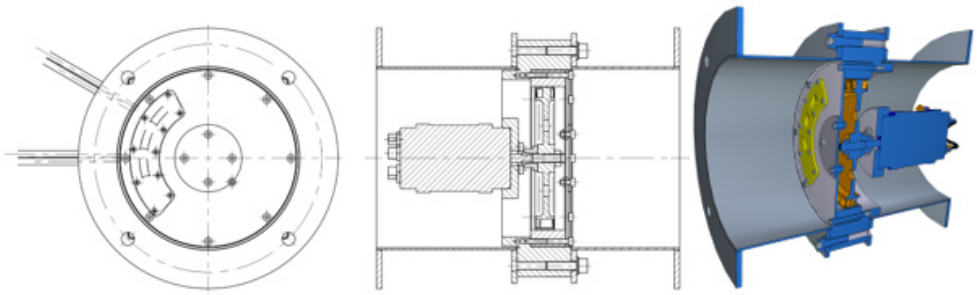

Figure 5.4: Design of the second-generation ORC turboexpander and a cross-sectional view of the model

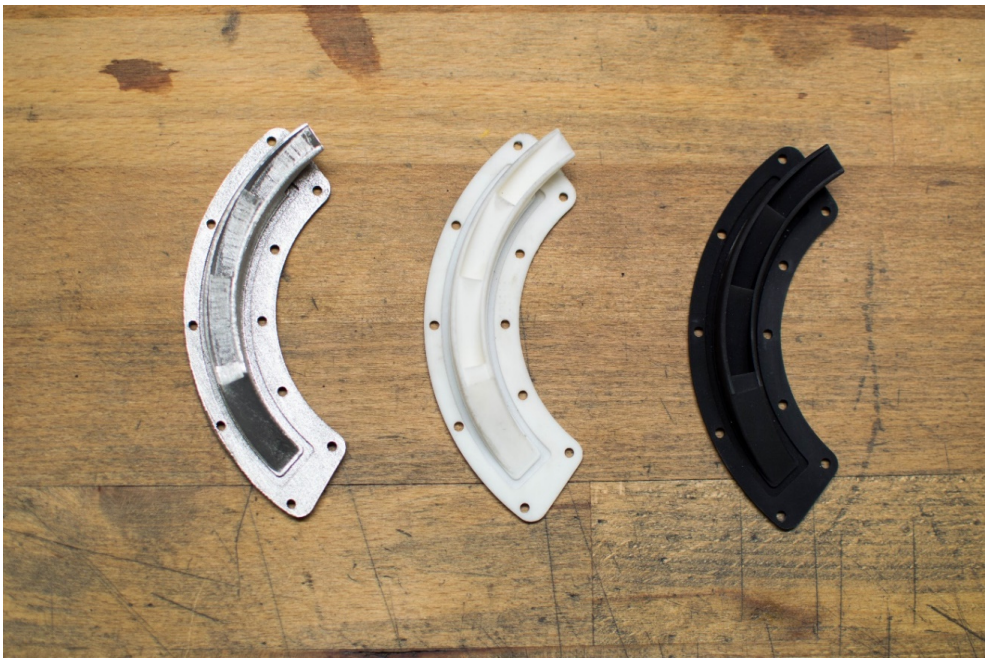

Figure 5.5: Experimentally investigated nozzle segments made of different materials by different AM methods; from left to right: DMLS stainless steel, SLS nylon, SLA resin

Table 5.3: The surface roughness of the second-generation nozzle elements, measured inside the channel in the fluid flow direction with a declared accuracy of ±10 %; averaged from five measurements (Roughness meter INSIZE ISR-C002)

AM technology	Value	Units
Selective Laser sintering (SLS, nylon)	5.7	μm
Stereolithography (SLA, resin)	5.4	μm
Laser Powder Bed Fusion (DMLS, stainless steel) - polished	3.1	μm

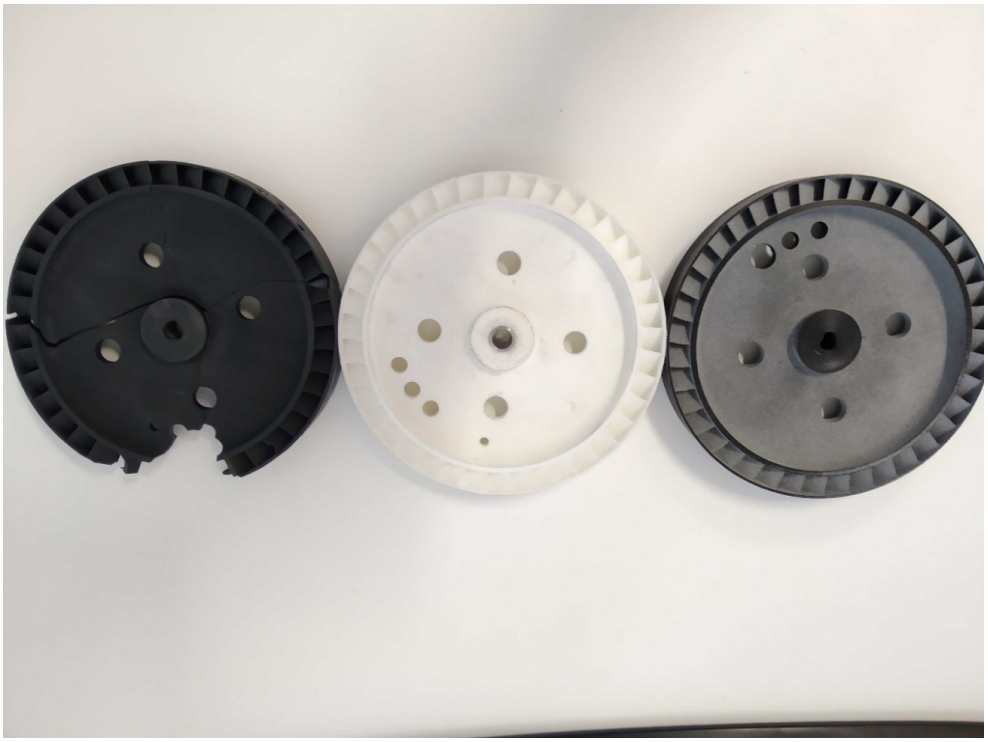

Figure 5.6: Experimentally investigated 2^{nd} gen. rotor wheels made of different materials by different AM methods; from left to right: SLA resin (shattered), SLS nylon, MJF nylon

5.2 Description of the test rig

The main goal of the experiments performed within the scope of this thesis was to verify a proof-of-concept additive manufactured micro scale turboexpander that can be safely operated with cold air and easily transported with a possibility of quick replacements of the flow components. Experiences from these experiments and cold aerodynamic tests will then be utilized for the design and future operation of the turbine with organic fluid. A secondary objective was to test various additive manufacturing methods and their feasibility for turbomachinery, respectively how their accuracy of the prints, mechanical properties and the surface roughness affects the overall isentropic efficiency of the machine.

To perform such experiments, some equipment of the test rig was designed and built with a configuration according to Fig.5.7 exclusively for this purpose. As the measurements were conducted during an internship in the PDLT laboratory of Strömungsmaschinen & Thermische Maschinen, Drucklufttechnik, Fakultät Maschinenbau / Umwelttechnik at OTH-AW, in collaboration with Prof. Dr. Andreas P. Weiß and his colleagues, major part of the in-

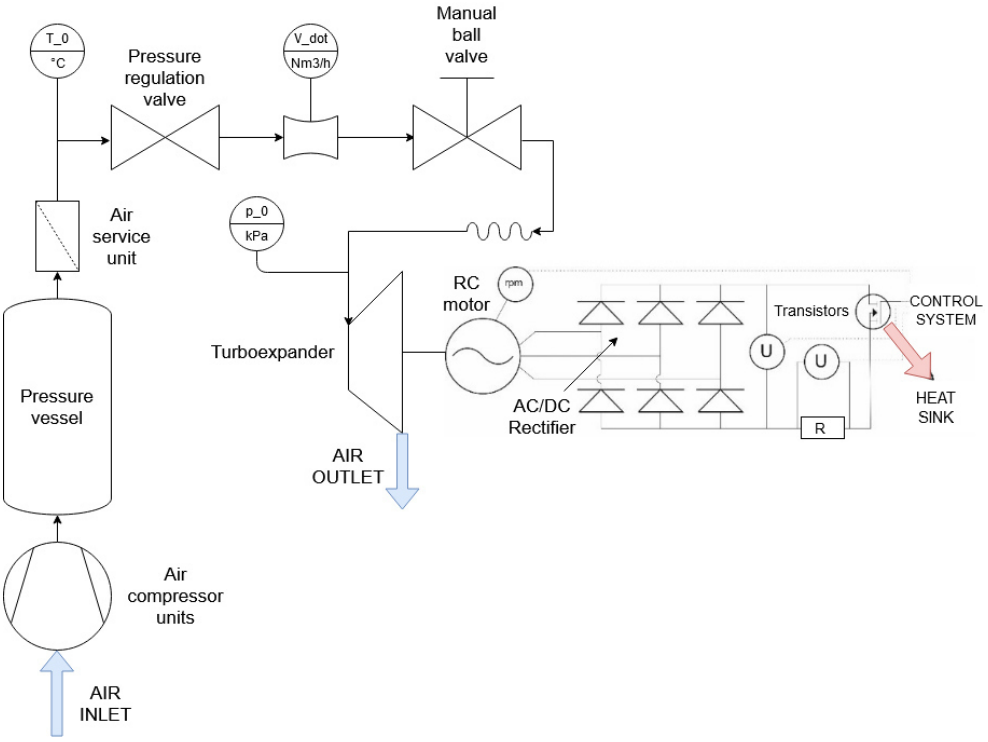

Figure 5.7: Schematics of the test rig configuration

struments was already present in the laboratory, which is fully equipped with instrumentation and piping for aerodynamic tests of turbomachines with compressed air.

Apart from the turboexpander itself, an electrical device which serves as an integrated instrumentation and control system but also as a variable load and a heat sink was developed. The main components of the electrical device are also shown in Figure 5.7. All the electrical components were fitted into a frame which is easily transportable and mobile. The rotor of the turboexpander is directly coupled to the BLDC motor operating in the generator regime. Three-phase alternating current is produced by the generator. It is then rectified, and the overall voltage is measured. A calibrated precise resistor is used for current measurement by measuring the voltage drop. The generator speed and electrical parameters are measured. The rotational speed is measured from the generated phase-voltage frequency, which is directly proportional to the generator rotational speed by fixed periods per revolution. The test rig is also equipped with a redundant optical sensor which measures the rotational speed of the generator and thus the turbine rotor wheel. Some troubles with the electronics occurred – overloading the transistors or distortion in the electronic signal – but were finally solved.

Temperature, pressure and the volumetric flow rate is logged into the lab-

Table 5.4: List of measurement devices used during the experiment

Sensor	Measured quantity	Signal	Range	Error
IFM PG 2453	Pressure	4-20 mA	-1 – 25 bar(g)	0.5 %
Thermocouple K KMQSS-125G-6 +USB-TC01	Temperature	4-20 mA	-100 - +1400°C	0.7°C
Postberg cp104s	Volumetric flow rate	0-10 V	2.26 - 462 $m_N^3 \cdot h^{-1}$	± 3 %
SIEMENS Sitrans PN150	Pressure difference	4-20 mA	0 - 60 mbar	0.2 %
Frequency of the alternating current	Rotational speed (el.)	-	Up to 500k rpm	2 rpm (at 10k rpm)
IR sensor TCRT5000	Rotational speed (opt.)	3.3-5 V	Up to 500k rpm	20 rpm (at 10k rpm)
Voltage divider +Arduino A/D	Voltage	0-60 V	0-60 V	2 % +0.03 V
Arduino A/D via U drop (1 block)	Current	0-15 A	0-15 A	2 % +0.02 A

oratory LabView system. Other parameters – rotational speed, voltage and current are gathered by Arduino, which then through USB connection sends the information into the PC. Ambient pressure was measured on a separate device and logged manually. The list of all the measurement devices and their parameters is shown in Table 5.4.

These data are then visualised in a single-purpose in-house developed software. This software allows, besides live visualization of the measured data, also to regulate and control either the rotational speed of the turbine (mode "Constant RPM" – see Fig. 5.10) or the load (mode "Constant Current"). It is also able to control the current through the transistors in their linear region and thus to control the load of the generator and therefore also the rotational speed of the turboexpander. There are in total four transistors, each with a separate heat sink in the form of a CPU cooler. While changing the rotational speed of the turboexpander in the "Constant RPM" mode, the generator is initially less loaded, and it increases the speed up to the desired level and exceeds it by an inevitable overshooting error. This error is then regulated by a PID regulator to avoid oscillation. The opposite direction, decreasing its rotational speed, the generator is more loaded, and the feedback comes from the electrical parameters, as soon as the rotational speed achieves the set parameter, it is again regulated to keep the rotational speed constant.

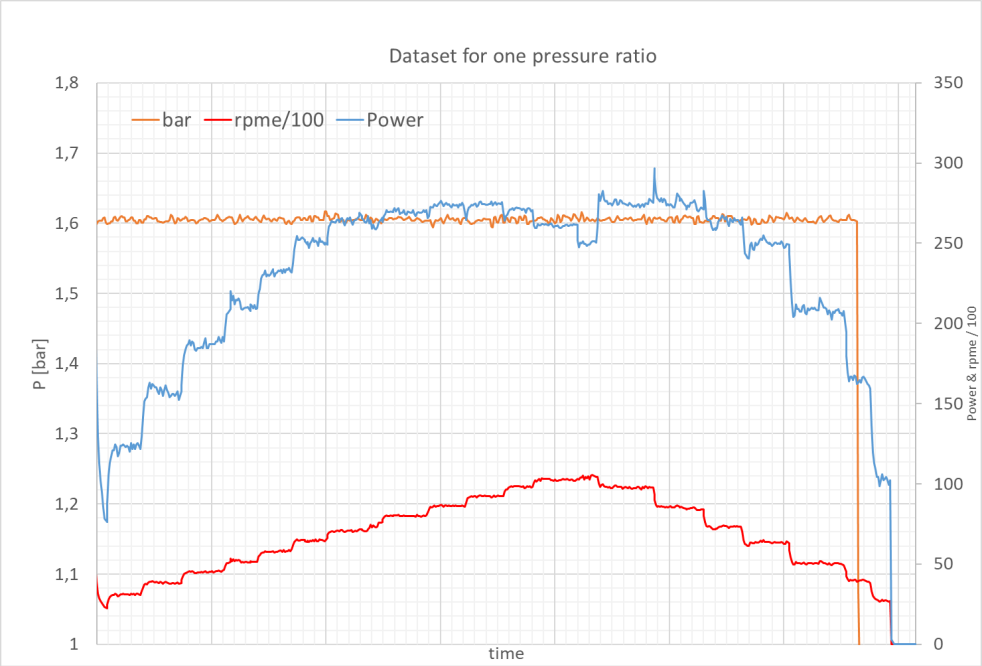

Figure 5.8: Raw dataset from the experimental campaign for one pressure ratio - RPM and electrical power output

5.3 Data evaluation

The raw dataset of power, rotational speed, voltage, current and inlet pressure obtained from the experimental campaign is displayed in Fig.5.8 and Fig.5.9. The steady states were manually chosen with the corresponding timestamps to average the quantities during the steady-state operation of the turbomachine. The averaged quantities are then evaluated with an objective to obtain the isentropic efficiency of the turbine at a given condition.

The raw data needs to be processed to evaluate the isentropic efficiency of each turbine assembly. First of all, steady states, i.e. constant RPM, are chosen, which was done manually. All the quantities are then averaged for the period of each steady-state, and the calculations below are performed for each of the averaged steady states, both ramping the rotational speed up and down. To obtain the isentropic power for the fluid isentropic expansion process, mass flow rate is evaluated from the volumetric flow rate which is calibrated for air at normal conditions as Eq.(5.1):

$$\dot{m}_{\text{air}} = \dot{V}_{\text{air}} \cdot \rho_{\text{norm}} \left[kg \cdot s^{-1} \right] \tag{5.1}$$

Enthalpy and entropy at the inlet (state 1) and respectively at the outlet

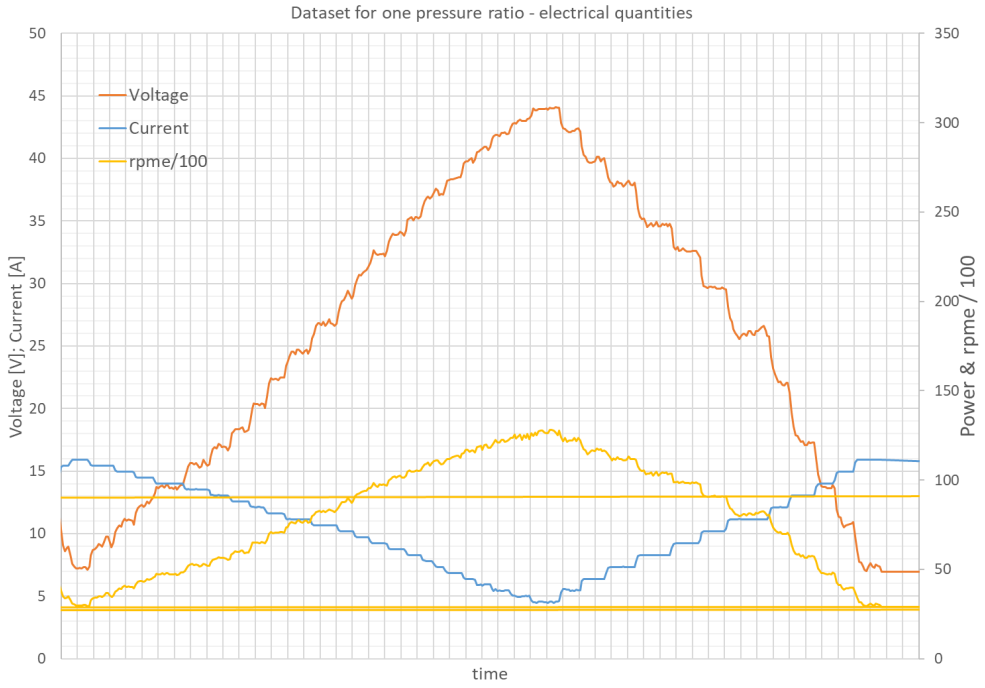

Figure 5.9: Raw dataset from the experimental campaign for one pressure ratio - RPM, current and voltage

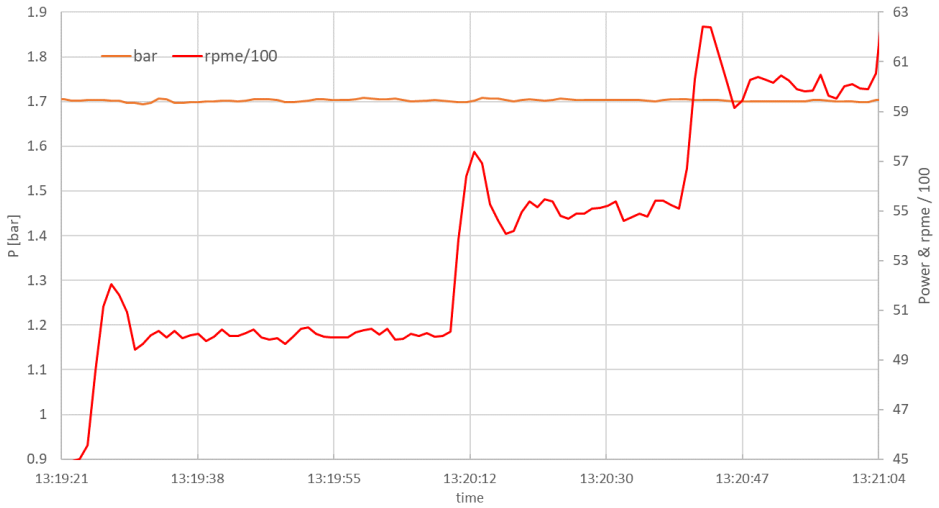

Figure 5.10: A detailed sample of the rpm signal - regulation for constant rpm

(state 3) are calculated using fluid properties database REFPROP Eq.(5.2,5.3,5.4).

$$h_1 = \text{Enthalpy}\,(p_1; T_1)\left[kJ \cdot kg^{-1}\right] \tag{5.2}$$

$$s_1 = \text{Enthalpy}\,(p_1; T_1)\left[kJ \cdot kg^{-1} \cdot K^{-1}\right] \tag{5.3}$$

$$h_{3_{is}} = \text{Enthalpy}\,(p_3; s_1)\left[kJ \cdot kg^{-1}\right] \tag{5.4}$$

Isentropic power is then Eq.(5.5:

$$P_{is} = \dot{m}_{air} \cdot \frac{(h_1 - h_{3is})}{1000}[W] \tag{5.5}$$

The measured power output is evaluated from the electrical current and voltage as Eq.(5.6).

$$P_{\text{el}_{meas}} = U \cdot I[W] \tag{5.6}$$

Power loss at the rectifier is added to that, assuming a constant voltage drop of 1,5 V over two low-drop diodes in a rectifier bridge - Eq.(5.7):

$$P_{\text{rect}} = dU_{\text{rect}} \cdot I[W] \tag{5.7}$$

From the electrical power and rotational speed, initial guess of the torque is calculated - Eq.(5.8):

$$T = \frac{(P_{\text{el}_{meas}} + P_{\text{rect}})}{\omega}[N \cdot m] \tag{5.8}$$

Electrical efficiency of the generator (Turnigy SK3-6364-245 for most of the experiments with the aluminium stator frame, Turnigy NTM PropDrive v2 5060-270 for the rest of the experiments with the plastic nylon frame) is calculated by the TorqueCalc tool at eCalc website. [145] for certain rotational speed and torque. These data have been obtained experimentally for each generator (BLDC motor) type. An assumption of equal efficiency in motor and generator regime is presumed for the same mechanical power output on the shaft. See Eq.(5.9).

$$\eta_g = f(n, T)[-] \mid \tag{5.9}$$

With the electrical efficiency (including also bearing friction losses), a new value of torque is calculated, and this process is repeated iteratively. As to do this process manually would be very tedious and exhaustive; this process was automated using VBA macros and GoalSeek function. The generator efficiency 2-D plot is shown in Figure 5.11. The automatic iteration loop then

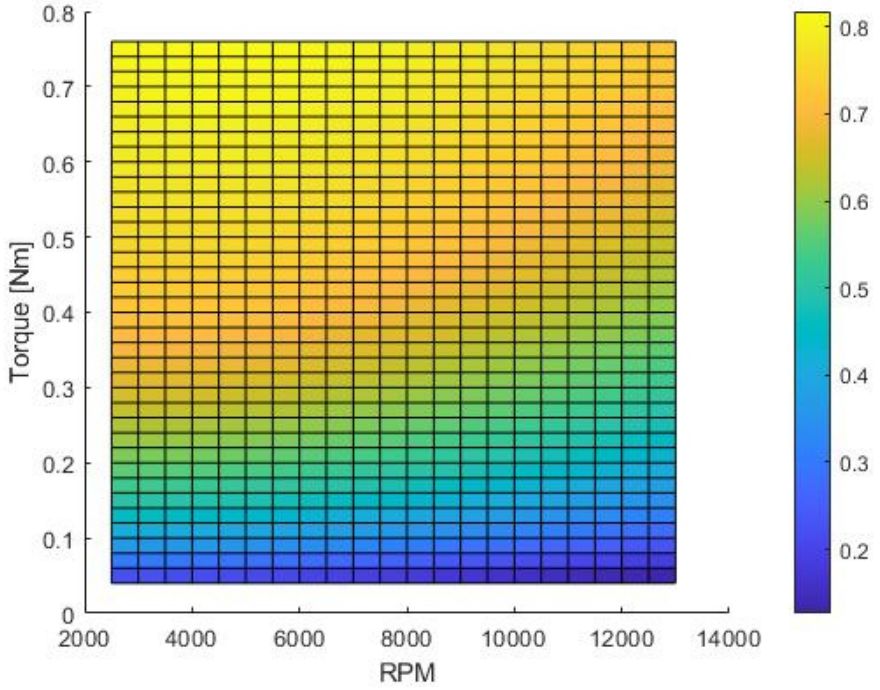

Figure 5.11: Electrical efficiency map of Turnigy SK3-6364-245 generator as a function of rpm and torque, source: [145]

uses this 2-D map for bilinear interpolation of the efficiency value according to the formula in Eq.(5.10).

$$\begin{aligned}\eta_g(n,T) \approx \frac{1}{\{(n_{\{2\}}-n_{\{1\}})(T_{\{2\}}-T)\}} \cdot (\eta_{g\{11\}} \cdot (n_{\{2\}}-n) \cdot (T_{\{2\}}-T) \\ +\eta_{g\{21\}} \cdot (n-n_{\{1\}}) \cdot (T_{\{2\}}-T) + \eta_{g\{12\}} \cdot (n_{\{2\}}-n) \cdot (T-T_{\{1\}}) \\ +\eta_{g\{22\}} \cdot (n-n_{\{1\}}) \cdot (T-T_{\{1\}}))[-]\end{aligned} \tag{5.10}$$

Mechanical power can be then calculated using the iterated electrical efficiency of the generator as in Eq.(5.11).

$$P_{\text{mech}} = \frac{(P_{\text{el}_{\text{meas}}} + P_{\text{rect}})}{\eta_g}[W] \tag{5.11}$$

Mechanical power divided by isentropic power gives the final and desired value of the *isentropic efficiency* at each steady state of each assembly at a given pressure ratio, as seen in Eq.(5.12). These values are then used to plot the efficiency charts as a function of the rotational speed at a certain

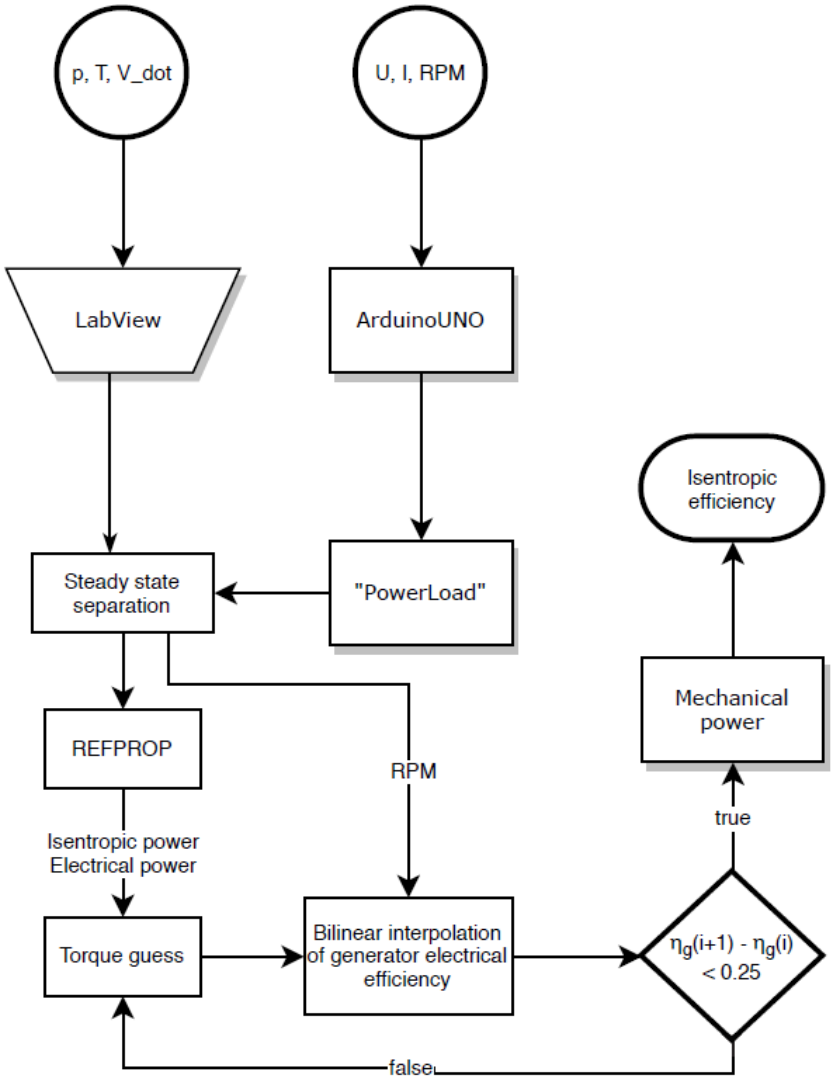

Figure 5.12: A flowchart describing the data acquisition and data evaluation methodology

pressure ratio. The mechanical losses in bearings are included in the generator efficiency.

$$\eta_{is} = \frac{P_{\text{mech}}}{P_{\text{is}}}[-] \tag{5.12}$$

To better illustrate the isentropic efficiency evaluation methodology, a simple flowchart was created - see Fig.5.12.

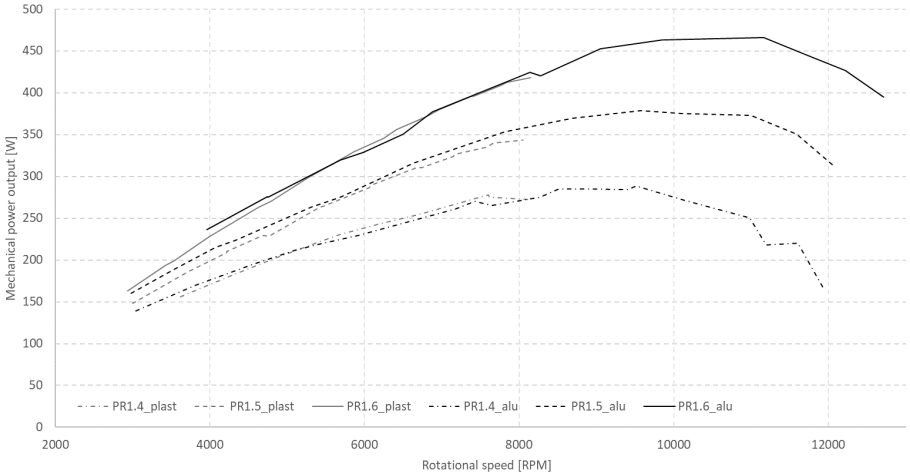

Figure 5.13: Validation of the evaluation methodology and replicability of the results - two different stator frames and generators; both wheels selective laser sintered (SLS) nylon powder (short chord)

5.4 Results and discussion

This subchapter presents the results from the experimental cold aerodynamic campaign of the first and second generation axial impulse micro turboexpanders. There were various tasks to be performed and phenomena to be studied and analysed from the experimental trials.

The first and the main goal was to build the test rig for pressurized air, which would enable to easily interchange the flow components and reliably and quickly evaluate the isentropic efficiency of the tested turbine configuration. With this goal in mind, a replicability analysis of the measured values of efficiency was performed. The same stator/rotor combination was tested in two different stator frames (one nylon, the other aluminium) mounted with two kinds of BLDC generators. The result was quite positive, as can be observed on the course of the matching mechanical power outputs in Figure 5.13. The limit of the rpm for the plastic frame was caused by vibrations and contact between stator and rotor beyond certain points.

In total, over twenty experimental campaigns were conducted at the test rig; each for four pressure ratios by varying the inlet pressure of the compressed air, ergo over 80 efficiency curves were measured in a region of 3000 to 12000 rpm with a step of more or less 500 rpm both ramping up the rotational speed and, on the way down, reducing the speed of the turbine. So ideally, two data points for the same rotational speed were obtained. For some of the turbine assemblies, this was however not possible, since the mechanical vibrations at the resonance speed were too high and could not have been overcome. The

highest reached value of isentropic efficiency for the design pressure was 40 % for an SLS long chord stator and an SLS rotor wheel with doubled partial admission arc out of the 1^{st} gen.

5.4.1 First generation results and discussion

For the first generation turboexpander experiments, eight combinations of rotor and stator wheels are presented. In the 1^{st} generation wheels, it is apparent, that there is a significant difference in between the assemblies depending not only on the manufacturing method, the material and the resulting surface roughness but also on the short or long chord version of the stator wheel. The maximum isentropic efficiencies for various 1^{st} gen configurations as a function of the pressure ratio are shown in Figure 5.14. Together with this chart, also the graph of the rotational speed for the maximum measured isentropic efficiency is presented - Fig.5.15. One conclusion from these measurements is that overall, the long chord versions of the stator wheels (thus low number of blades for stator) achieved the highest efficiencies. Also, as expected, the highest efficiency points usually laid very close to the design pressure ratio and incrementally decreased. For increasing pressure ratios, the rotational speed for maximum efficiency points moved towards higher numbers.

The 1^{st} gen DMLS steel turbine assemblies overall reached the lowest performance amongst the measured campaigns. This may have been caused by several effects. One of them could be that the leakages were higher due to worse sealing between the steel stator wheel and the steel stator frame. Other reason for that might be that the surface roughness of the flow components, especially the rotor, which had not been polished, was significantly higher than that of the plastic wheels. And also, since the rotor was substantially heavier, it rotated with greater inertia and its resonance frequency was much lower, close to 7500 rpm and could not have been exceeded due to extreme vibrations of the machine. The highest values of isentropic efficiency (40 %) were obtained for the combination of SLS long chord stator and SLS rotor with the doubled degree of admission of the stator nozzles, for higher rotational speeds, this experimental campaign was not conducted due to the concerns for the power electronics because of the high electrical power output. The lowest value of the maximum isentropic efficiency of around 10 % was reached with the DMLS assembly with the stator wheel with *functional supports* as will be discussed later on.

When the test rig was successfully proven to yield reliable values of isentropic efficiency and mechanical power output, the specific phenomena were analysed. Initially, the suitability of either long or short chord stator wheel was assessed. These two were designed to study the impact that the length of the chord and the number of blades, respectively the Reynolds number effect would yield in this microturbine design. This has been studied on the selective laser sintered flow components. The results of this analysis are shown in

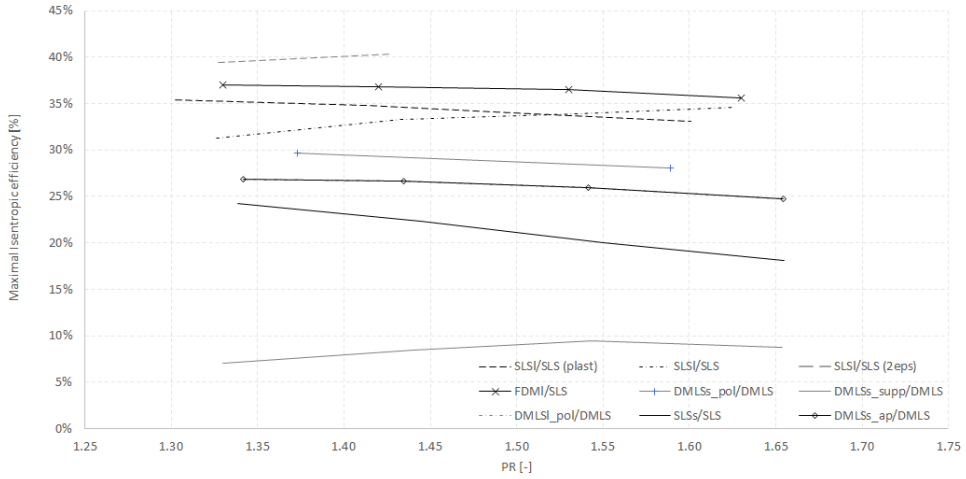

Figure 5.14: Experimental results of maximal isentropic efficiencies at chosen pressure ratios of all the 1^{st} generation turbine configurations

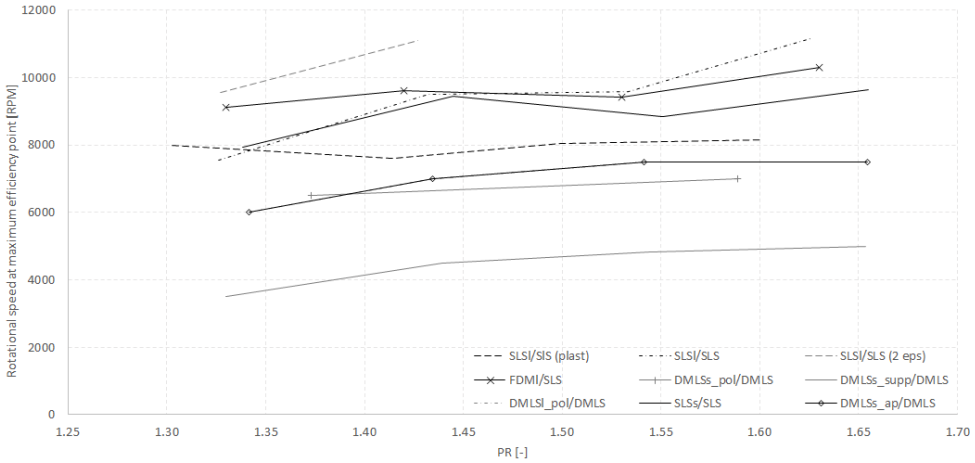

Figure 5.15: Rotational speed corresponding to the maximum isentropic efficiency point for 1^{st} generation turbine configurations

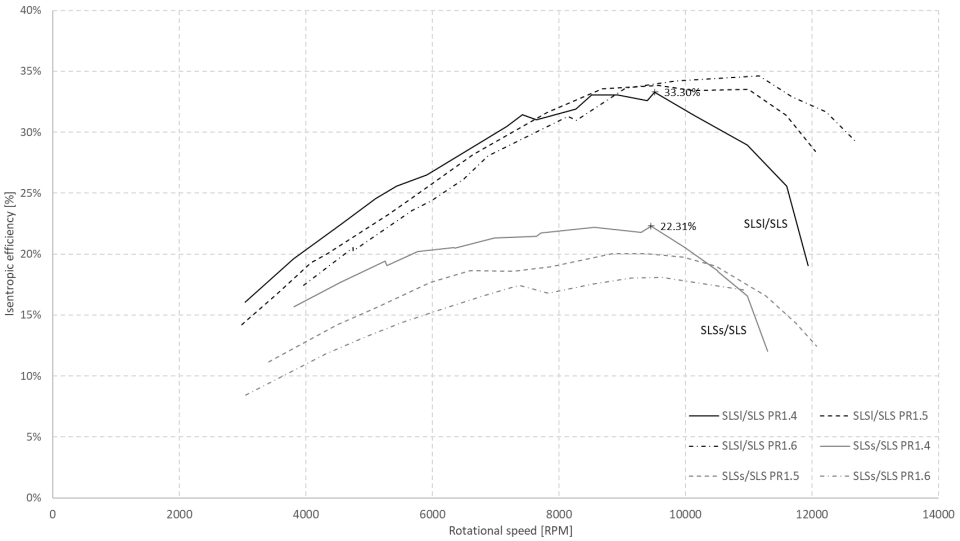

Figure 5.16: Experimental comparison of the long and short chord SLS stator wheel (rotor also SLS) at different PRs

Figure 5.16, and it is apparent, that the assembly with a stator wheel with a longer chord and lower number of blades was significantly better in performance at all pressure ratios compared to the stator wheel with a shorter chord. This has also been confirmed for other configurations with long chord stator wheels.

The author argues that it may be caused by several effects – one being that for the long chord stator, only one nozzle segment was admitted by the pressurized air but three nozzle segments for the short chord ones. Therefore, the profile losses caused by the surface roughness are higher and also since there is a finite width of the trailing edge of the blades, some mixing of the streams occurs at the outlet. Also, as the nozzle channel is longer for the long chord stators, the flow is fully attached to the nozzle geometry, and the shape of the nozzle directs the fluid flow at design outlet angle, which might not be the case for the rather short chord lengths. Finally, the geometrical precision and accuracy of the AM method for the small short chord blade, relatively to the chord length, is much higher and the blades may not be shaped precisely according to the design.

One of the other subtasks was to investigate the effect of the friction losses of the DMLS steel flow components with different finishing methods and to compare the impact that improving the surface roughness has on the overall isentropic efficiency of the turbomachine. In Fig.5.2, the as printed DMLS stator wheel, polished stator wheel and the stator wheel with *functional supports* as suggested by the manufacturer is shown. This effect is displayed in Fig.5.17, where the *functional supports* have proven to be maybe beneficial

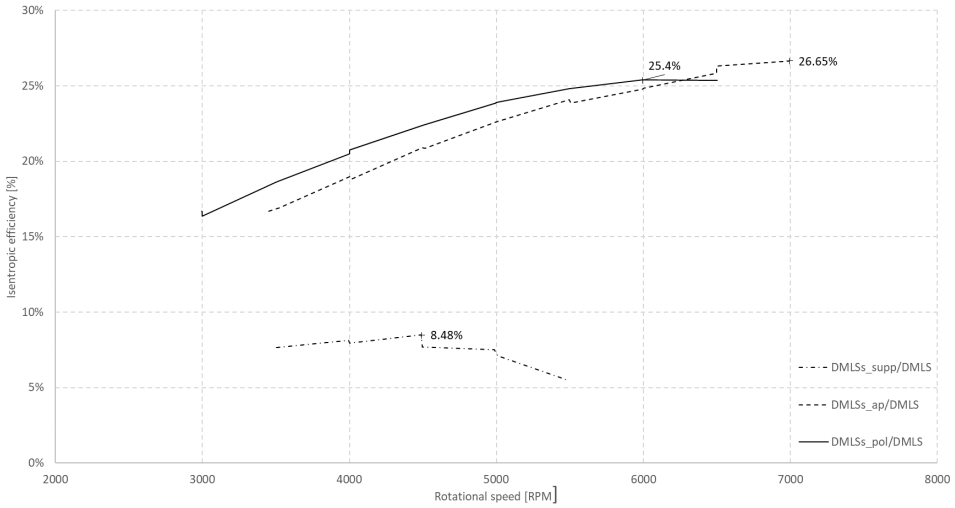

Figure 5.17: Effect of the surface roughness on the isentropic efficiency at PR 1.4; stator DMLSs with various postprocessing

from the manufacturing point of view, but as anticipated, completely unusable from the aerodynamical viewpoint. Also, it is apparent, that especially in the region of low rotational speed, the polished nozzle surface improves the isentropic efficiency by a significant margin, which diminishes with increasing RPM.

This on first sight appears illogical, since the Reynolds number during the low rotational speed is kept. At this low Re region, the increased surface roughness may act as a turbulator which interrupts the large laminar viscous sublayer near the blade surface, which improves the overall performance due to lower profile losses. As the turbine operating point moves towards higher rotational speed, the flow gets into a fully turbulent region in which the effect of the high surface roughness is adverse. Though it is this high rotational speed region, in which the as printed stator assembly is superior in performance when compared to the polished one. This goes against the anticipated logic and author suggests to conduct another experimental campaign with these two assemblies to verify this observation. The values of Reynolds number of the fluid flow for the first and second generation rotor wheels is shown in Table 5.5.

Next effect that was studied was the effect of the partial admission on the turbine performance and the validity of the correlation for the ventilation losses, which was discussed in Eq.(4.27). This has been experimentally verified by performing measurements first for a single partial admission segment (one nozzle) and then for double the arc (two nozzles). The ventilation loss model should reflect the twofold increase in partial admission and the experimental results would match the estimate from the 1-D model. The results can be

Table 5.5: Reynolds numbers for 1^{st} generation (short and long chord) and 2^{nd} generation designs according to Eq.(2.7); *low* values are for 3000 rpm and *high* values for 10 000 rpm

Parameter	$1^{st}gen_{short}$	$1^{st}gen_{long}$	$2^{nd}gen$	Units
C_{ax}	0.0098	0.0385	0.018	m
Re_{low}	12 032	47 267	22 100	-
Re_{high}	40 107	157 562	73 667	-

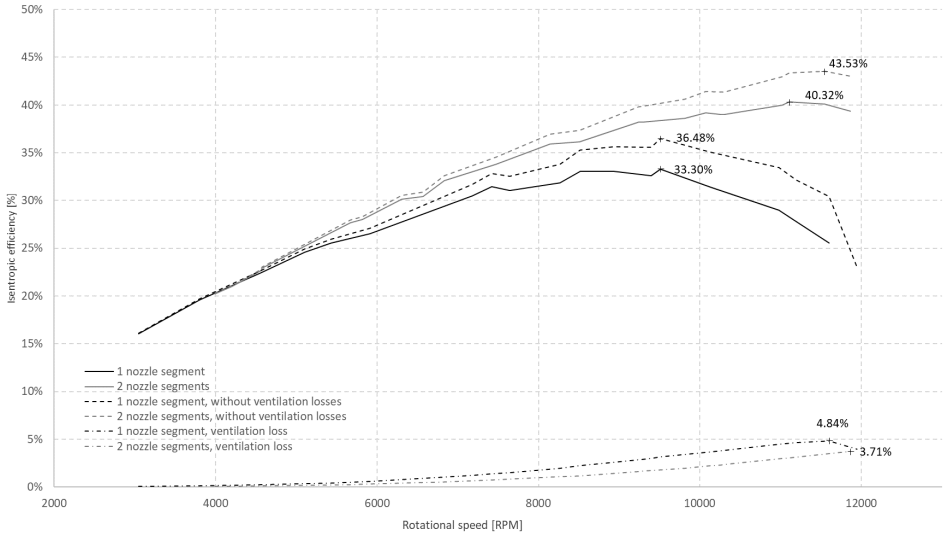

Figure 5.18: Effect of the partial admission on the ventilation loss correlation and turbine performance; both stator and rotor - selective laser sintered (SLS, long chord stator)

observed in Figure 5.18, and it is apparent that doubling the partial admission arc, the maximum efficiency point moves towards higher rotational speed and also increases by 7 % points, this is most likely caused by that the design degree of admission of the turbine was 34% and in other cases for the 1^{st} gen trials, the turbines were operated with only 6.7 % degree of admission. Doubling it then moves the turboexpander closer to its design point, and it goes in hand with an increase of isentropic efficiency.

Furthermore, the operation of the turbine and especially the rotational speed control was remarkably improved when adopting double partial arc admission. The author considers this to be a result of balancing a counterforce by adding an additional fluid stream since the double partial arc admission was realised by adding an additional admitted nozzle at 180° on the opposite to the other nozzle.

Since the results of isentropic efficiency without ventilation loss are quite

different to each other, at these small power and very low partial arc admission, it appears as not directly applicable, respectively another effect associated with partial admission arc extent is present or the nature of rough printed parts and extremely low partial admission does not allow to use the applied correlation.

Next on the list was the comparison of FDM and SLS stator wheels, especially the effect of different surface roughness and surface nature of each 3-D printing method. As can be seen in Fig.5.3, FDM components are distinguished by the specific layer-by-layer structure which is the result of the manufacturing procedure, and it increases the roughness of the surface especially in the direction perpendicular to the build direction.

In this case, the layer structure was indeed built perpendicularly to the flow path, so it was anticipated, that this FDM stator wheel would yield worse performance compared to the more uniform and less rough SLS stator wheel. However, the latter was the case, as one can observe in Fig.5.19, and perhaps as a result of the same effect as with the DMLS steel stators, the rougher the surface of the nozzles, the higher was the performance. Contradictory to the expected behaviour, despite having rougher surface by 40 % compared to the SLS, the turbine assembly with FDM stator wheel was superior in terms of isentropic efficiency for any measured pressure ratios.

In spite of being the most affordable and common 3-D printing technology, ultimately and quite surprisingly, the FDM manufacturing method turned out to achieve the best values of isentropic efficiencies amongst all of the measured 1^{st} gen turbine assemblies (excluding the double admission experiment). This conclusion, however, should not be adopted to other turboexpanders without at least preliminary assessment of the fluid flow regime.

Finally, the effects of surface treatment such as sanding, polishing, metal plating, or chemical treatment of the plastic 3-D printed parts have not been analyzed despite the potential it may bring to the turboexpander performance. This may be considered a potential for future work.

5.4.2 Second generation results and discussion

As the 2^{nd} gen turboexpander was designed to operate with hexamethyldisiloxane, and also the flow components were designed according to that, the goal was to identify how transferable are the cold aerodynamic tests for an ORC turbine design. Additionally, and similarly to the 1^{st} gen tests, various additive manufacturing technologies were used for the nozzle segments and rotor wheels. The effect of the resulting surface roughness on the isentropic efficiency and also the operational parameters of the turbines were investigated and compared amongst the AM methods. Some of the AM methods were also adopted for the 1^{st} gen wheel, such as SLS and DMLS, and some of them were new – SLA, MJF. In total, nine combinations of nozzle segments and rotor

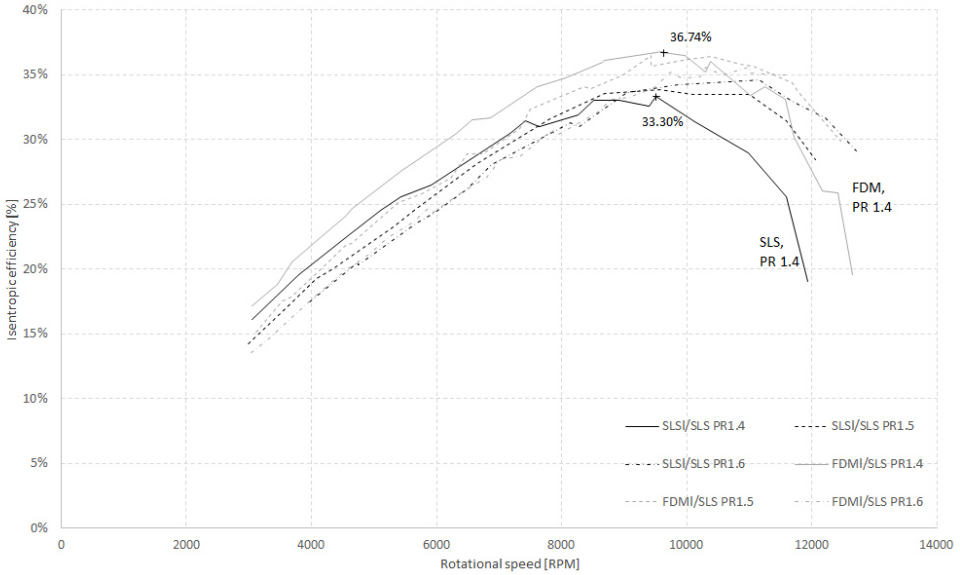

Figure 5.19: Comparison of FDM and SLS (long chord) stator wheels and the effect of 3-D printing methods on the isentropic efficiency; both with SLS rotor; measured at three different PRs

wheels were measured, differing only in the material and AM method, not in the number of blades or nozzle segments, nor the degree of admission.

Contrary to the 1^{st} gen experiments, very narrow band of isentropic efficiencies in between 25 and 30 % was obtained for different AM technologies. Moreover, the turboexpanders showed rather flat behaviours of their efficiency curves with increasing rotational speed and especially with an increasing pressure ratio. This can be observed in Fig.5.20 and Fig.5.21, respectively. The highest overall isentropic efficiency was measured for the pair of SLS nozzle segments and SLS rotor wheel, again despite having the highest surface roughness of the measured nozzle segments. This combination was superior at any measured pressure ratio but only by a small margin compared to the rest of the nozzle/rotor combinations. This can also be seen in the efficiency charts in Fig.5.22 for the given pressure ratios.

From the operational standpoint, it was also an overarching goal amongst all of the experiments to evaluate the effect of geometrical inaccuracies of the AM flow components on the assembly, fitting, sealing and safe operation of the turbines. In previous and commissioning tests, the sealing appeared as an important issue of the proposed modular configuration, as was used in [146], [147]. The above-reported results were after these issues satisfactorily handled, though precise sealing the potential leakage paths was still crucial to reproduce the measurement results.

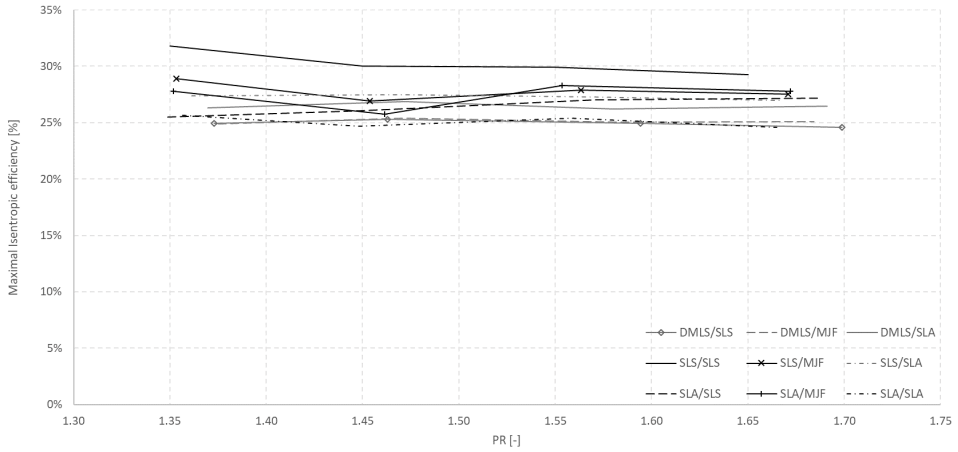

Figure 5.20: Maximal isentropic efficiencies at chosen pressure ratios of all the 2^{nd} generation turbine configurations

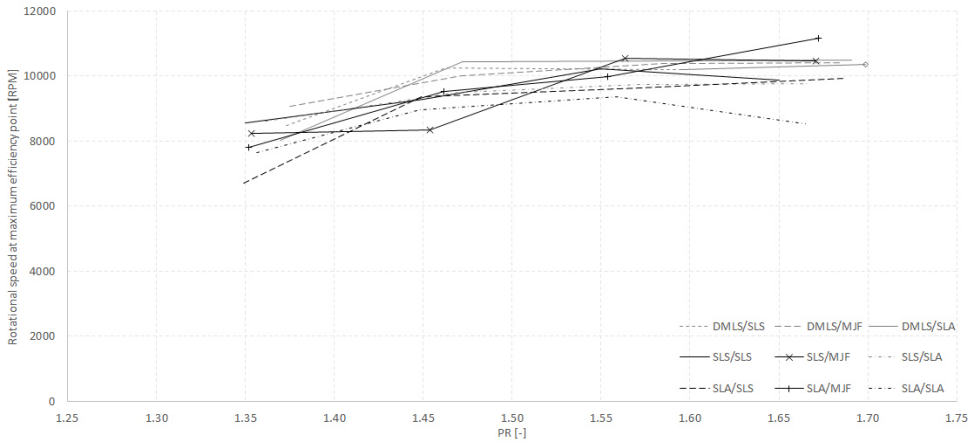

Figure 5.21: Rotational speed corresponding to the maximum isentropic efficiency point for 2^{nd} generation turbine configurations

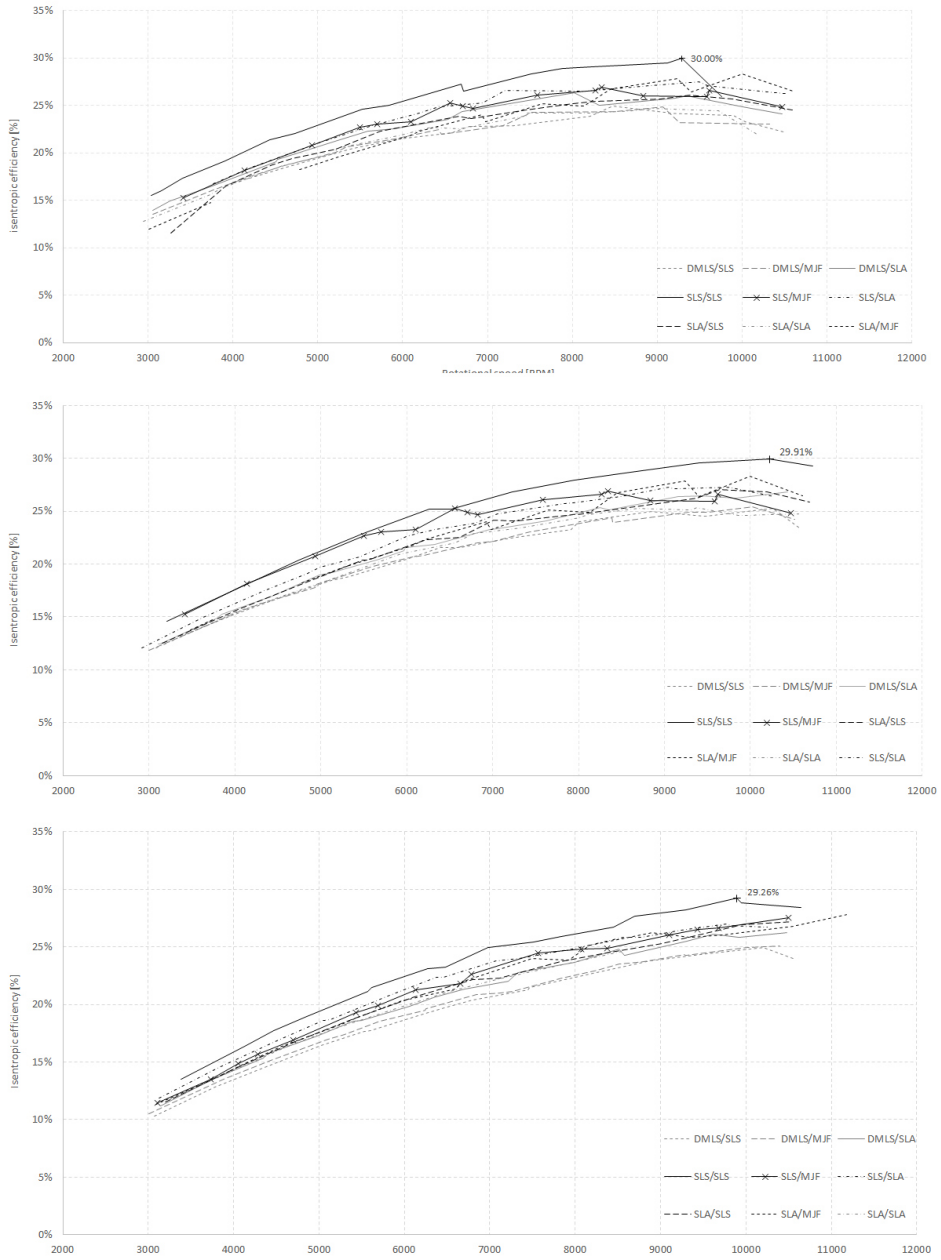

Figure 5.22: Second generation design, different AM methods stator/rotor; PRs top to bottom: 1.4, 1.5 and 1.6

Some mechanical issues were observed as well, mostly as a result of a dynamic runout of the rotor wheel caused by the inhomogeneity of the additive manufactured part and also by the *overhung rotor concept*, which resulted in further dynamic imbalance and finally bending the shaft. Even though the rotors were dynamically balanced, there were some incidents leading to the total destruction of the rotor, as shown in Figure 5.6.

Issues with an inaccuracy of some of the manufacturing methods were also observed, most apparent for the SLA manufacturing technology. The inaccuracies negatively affected the fitting and assembly of the parts. Also, some problems with different rate of thermal expansion of the plastic wheels and the aluminium stator frame occurred, which lead to troubles with exchanging the prototyped stator wheels.

Chapter 6

Conclusions and Future Work

This thesis follows the design evolution of an axial impulse single stage micro turboexpander from the proof-of-concept towards the experimental trials with cold air, and finally the design of the full-scale turboexpander for a micro CHP unit operating with ORC. Moreover, this thesis explored the possibilities of additive manufacturing for rapid prototyping of micro turboexpanders based on the performed experiments.

A review of the small-scale ORC micro turboexpanders and their architectures was conducted in the introduction of the thesis and it identified the suitable turbine architecture for the desired application. Based on the conclusions coming from the references, some peculiarities of designing an ORC turbomachinery with regards to the real gas effects on the flow components design were discussed. A separate chapter was dedicated for additive manufacturing with a focus on turbomachinery, discussing the potentials, advantages and drawbacks of each of the manufacturing method. There is a significant lack of references for applications of additive manufacturing technology for prototyping small scale turbines in the literature and this thesis hopes to bring some insight into this topic.

In Chapter 4, the reference scheme of the two previously designed generations of the micro turboexpanders is presented. A third generation ORC micro turboexpander is designed within the chapter using a developed 1-D meanline model using real gas properties adopting recommendations and design choices for ORC micro turbomachinery according to the literature. The main flow components of the turbine were designed from the fluid dynamics standpoint and a preliminary geometrical design of the nozzles and the rotor wheel was performed. The design point of the third generation axial impulse single stage turboexpander is at 69.2 % isentropic total to static efficiency and 10.8 kW of mechanical power output with a heat input to the cycle of 120 kW. This is a 30 % increase of mechanical power output compared to the state of the art solution with a volumetric expander of 8.2 kW shaft mechanical power. The turboexpander design was partially optimized for maximum efficiency, though

Table 6.1: Evaluation of the AM methods applicability potential for micro scale turbomachinery based on experience with cold air tests

Technology	FDM	SLS	SLA	DMLS	MJF
Accuracy & precision	-	+	–	+	++
Homogeneity	–	+	+	-	++
As printed surface roughness	-	+	++	–	+
Price per printed part	++	+	–	–	++
Mechanical properties	-	+	-	++	+
Durability	-	+	–	++	+
Measured efficiency	++	++	-	–	+
Overall performance	-	+	–	-	++

a more detailed optimization is needed before the experimental investigation.

The experimental investigation of the first two generations of the turboexpanders is reported in Chapter 5. Details concerning the experimental method – the design of the test rig, instrumentation and control system, data evaluation procedure and finally the results and discussion are presented. The conclusions regarding the achieved isentropic efficiencies and mechanical power output for each of the prototyped turbine assembly are discussed broadly within the chapter. The efficiency charts from the experimental campaign are presented and show large variations amongst the configurations. The highest values of isentropic efficiency obtained from the measurements were reaching 40 % and exceeding 500 W mechanical power output for the first generation designed specifically for such conditions. The 2^{nd} generation design for ORC conditions yielded around 30 % of isentropic efficiency, similarly across all the explored configurations. This expander was operating in completely off-design condition. Various aspects of additive manufacturing and their impacts on the overall turbine performance were analysed and studied experimentally. One of the main characteristics, that was investigated was the resulting surface roughness of the 3-D printed parts and its effect on the isentropic efficiency. Contrary to the expectation, that higher the surface roughness, the worse would be the performance of the turbine, the results are not that conclusive and reveal that the phenomenon is more complicated than that and such a simple theorem should not be applied without at least a preliminary analysis of the fluid flow.

With these lessons learnt from the cold aerodynamic testing, the following Table 6.1 intents to summarize the experience of the author with experimental investigation of additively manufactured turbine components. The evaluation criteria are very simple and do not aim at being objective and unbiased. The same weight for each criterium is considered.

The Multi Jet Fusion AM technology was identified as the most promising method for cold aerodynamic testing and rapid prototyping of turbine flow

components based on the author's experience.

What concludes this thesis does not conclude the author's research and development of small scale turboexpanders for distributed power systems. There is a plethora of future improvements and design steps to be done towards a successful – reliable, efficient and cost effective – industrial application of the ORC micro turboexpander. With this goal in mind, the author proposes the following steps in the development, which he will address in a dissertation thesis dedicated on this topic.

- Implementing other, ORC specific 1-D loss models such as the ones from Aungier, Da Lio, Agromayor [85], [87], [148] or others and comparing the results obtained
- Creating a throughflow model - As ORC turbines are highly nonconventional, the adoption of common blade profiles is questionable and a specific aerodynamic design is highly recommended. – a connection between low-fidelity and high-fidelity models.
- Calculation of the span-wise variation of the flow quantities.
- Creating an aerodynamic design of the turbine blades according to the spanwise changing velocity triangles and flow quantities.
- Optimization of the mean-line preliminary design by maximization of the fitness function by the means of a genetic algorithm
- Perform a CFD simulation of the ORC fluid flow through the turbine and iteratively change the previous design
- Create a reliable and manufacturable mechanical design of the whole turbine assembly – focus on bearings, sealing and especially the electrical power output – whole BLDC generator assembly needs to be designed and built together with the power electronics
- Manufacturing and assembling the designed turbine assembly and investigate its performance initially on a dedicated ORC test rig – to verify and tune the loss models
- Operate the turbine in the target ORC power system in both design and off-design condition
- Create a robust ORC microturbine design tool from the above-mentioned steps

The discussion and the results presented in this thesis suggest that, even micro ORC turbines can perform with high efficiency if designed properly. It is of upmost importance especially for emerging micro-ORC power systems to

design the expansion machine reliably, cost-efficiently at high efficiencies and not to spend a lot of resources designing and customizing it. Advanced specific ORC turboexpander design tools are and will even more be essential to make the micro ORC power systems viable for a large variety of applications and achieve a widespread on the market.

List of Figures

List of Tables

Bibliography

[1] E. Macchi and M. Astolfi, *Organic Rankine Cycle (ORC) Power Systems: Technologies and Applications*. Woodhead Publishing, 2016.

[2] J. Mascuch, V. Novotny, V. Vodicka, J. Spale, and Z. Zeleny, "Experimental development of a kilowatt-scale biomass fired micro CHP unit based on ORC with rotary vane expander," *Renewable Energy*, sep 2018.

[3] V. Novotny, V. Vodicka, J. Mascuch, and M. Kolovratnik, "Possibilities of water-lithium bromide absorption power cycles for low temperature, low power and combined power and cooling systems," *Energy Procedia*, vol. 129, pp. 818–825, 2017. [Online]. Available: http://dx.doi.org/10.1016/j.egypro.2017.09.104

[4] O. Dumont, "Experimental Investigation and Modelling of a 1.5 kW Axial Turbine for Waste Heat Recovery of a Gasoline Passenger Car through a Rankine Cycle," *SAE Technical Paper*, vol. 37, no. 0007, may 2018.

[5] O. Dumont, S. Quoilin, and V. Lemort, "Design, Modeling and Experimentation of a Reversible HP-ORC Prototype," in *Volume 3B: Oil and Gas Applications; Organic Rankine Cycle Power Systems; Supercritical CO2 Power Cycles; Wind Energy*. ASME, jun 2014, p. V03BT26A010.

[6] R. Dickes, "Solar-based ORC power systems," *ORC-PLUS Workshop*, 2016.

[7] P. Colonna, E. Casati, C. Trapp, T. Mathijssen, J. Larjola, T. Turunen-Saaresti, and A. Uusitalo, "Organic Rankine Cycle Power Systems: From the Concept to Current Technology, Applications, and an Outlook to the Future," *Journal of Engineering for Gas Turbines and Power*, vol. 137, no. 10, p. 100801, oct 2015. [Online]. Available: http://gasturbinespower.asmedigitalcollection.asme.org/article.aspx?doi=10.1115/1.4029884

[8] R. Padinger, S. Aigenbauer, and C. Schmidl, "Best practise report on decentralized biomass fired CHP plants and status of biomass fired small- and micro scale CHP technologies," *IEA Bioenergy*, vol. 32, no. February 2019, 2019.

[9] "GMK." [Online]. Available: www.gmk.info

[10] "Bosch KWK Systeme (former Köhler und Ziegler Anlagentechnik)." [Online]. Available: www.bosch-kwk.de

[11] "Ergion." [Online]. Available: www.ergion.de

[12] "WSK Energie und Umwelttechnik." [Online]. Available: www.wsk-group.com

[13] "Ormat." [Online]. Available: http://www.ormat.com

[14] "Infinity Turbine." [Online]. Available: http://www.infinityturbine.com/

[15] "LTi REEnergy." [Online]. Available: www.lti-reenergy.com

[16] "TRI-O-GEN." [Online]. Available: www.triogen.nl

[17] "Electratherm." [Online]. Available: www.electratherm.com

[18] "TransPacific Energy." [Online]. Available: http://www.transpacenergy.com

[19] "Caltenix." [Online]. Available: www.calnetix.com

[20] "DürrCyplan." [Online]. Available: http://www.durr-cyplan.com

[21] "Enerbasque." [Online]. Available: http://enerbasque.com

[22] "Enogia." [Online]. Available: www.enogia.com/

[23] "Kaishan." [Online]. Available: http://kaishantechnologies.com

[24] "Orcan." [Online]. Available: http://www.orcan-energy.com

[25] "Rank." [Online]. Available: http://www.rankweb.es/

[26] "Zuccato." [Online]. Available: http://www.zuccatoenergia.it

[27] "Freepower." [Online]. Available: http://www.freepower.co.uk/

[28] "POWER Engineering." [Online]. Available: www.pwr.cz

[29] G. Zywica, T. Z. Kaczmarczyk, and E. Ihnatowicz, "Application of a heat resistant plastic in a high-speed microturbine designed for the domestic ORC system," pp. 1–8, 2019.

[30] G. Qiu, Y. Shao, J. Li, H. Liu, and S. B. Riffat, "Experimental investigation of a biomass-fired ORC-based micro-CHP for domestic applications," *Fuel*, vol. 96, pp. 374–382, 2012. [Online]. Available: http://dx.doi.org/10.1016/j.fuel.2012.01.028

[31] J. Mascuch, V. Novotny, J. Spale, V. Vodicka, and Z. Zeleny, "Experience from set-up and pilot operation of an in-house developed biomass-fired ORC microcogeneration unit," *Renewable Energy*, vol. 165, pp. 251–260, mar 2021. [Online]. Available: https://linkinghub.elsevier.com/retrieve/pii/S0960148120317626

[32] M. Jradi and S. Riffat, "Experimental investigation of a biomass-fuelled micro-scale tri-generation system with an organic Rankine cycle and liquid desiccant cooling unit," *Energy*, vol. 71, pp. 80–93, jul 2014. [Online]. Available: https://linkinghub.elsevier.com/retrieve/pii/S0360544214004903

[33] G. Carraro, V. Bori, A. Lazzaretto, G. Toniato, and P. Danieli, "Experimental investigation of an innovative biomass- fi red micro-ORC system for cogeneration applications," *Renewable Energy*, vol. 161, pp. 1226–1243, 2020. [Online]. Available: https://doi.org/10.1016/j.renene.2020.07.012

[34] M. Imran, M. Usman, B.-S. Park, and D.-H. Lee, "Volumetric expanders for low grade heat and waste heat recovery applications," *Renewable and Sustainable Energy Reviews*, vol. 57, pp. 1090–1109, may 2016.

[35] S. Quoilin, M. V. D. Broek, S. Declaye, P. Dewallef, and V. Lemort, "Techno-economic survey of organic rankine cycle (ORC) systems," *Renewable and Sustainable Energy Reviews*, vol. 22, pp. 168–186, 2013.

[36] D. Fiaschi, G. Manfrida, and F. Maraschiello, "Thermo-fluid dynamics preliminary design of turbo-expanders for ORC cycles," *Applied Energy*, vol. 97, pp. 601–608, sep 2012.

[37] S. H. Kang, "Design and experimental study of ORC (organic Rankine cycle) and radial turbine using R245fa working fluid," *Energy*, vol. 41, no. 1, pp. 514–524, 2012. [Online]. Available: http://dx.doi.org/10.1016/j.energy.2012.02.035

[38] M. Pini, C. De Servi, M. Burigana, S. Bahamonde, A. Rubino, S. Vitale, and P. Colonna, "Fluid-dynamic design and characterization of a mini-ORC turbine for laboratory experiments," *Energy Procedia*, vol. 129, pp. 1141–1148, 2017. [Online]. Available: http://dx.doi.org/10.1016/j.egypro.2017.09.186

[39] D. Fiaschi, G. Manfrida, and F. Maraschiello, "Design and performance prediction of radial ORC turboexpanders," *Applied Energy*, vol. 138, pp. 517–532, 2015. [Online]. Available: http://dx.doi.org/10.1016/j.apenergy.2014.10.052

[40] F. Alshammari, A. Karvountzis-Kontakiotis, A. Pesiridis, and T. Minton, "Radial Expander Design for an Engine Organic Rankine Cycle Waste Heat Recovery System," *Energy Procedia*, vol. 129, pp. 285–292, sep 2017.

[41] S. Dixon and C. Hall, *Fluid Mechanics and Thermodynamics of Turbomachinery*. Elsevier, 2014. [Online]. Available: https://linkinghub.elsevier.com/retrieve/pii/C20110050597

[42] P. Gaetani, "Similitude in turbomachinery," *Politecnico di Milano*, vol. Turbomachinery A course, 2018.

[43] O. E. Baljé and R. L. Binsley, "Axial turbine performance evaluation. Part B-optimization with and without constraints," *Journal of Engineering for Gas Turbines and Power*, vol. 90, no. 4, pp. 349–359, 1962.

[44] O. A. Balje, "A Study on Design Criteria and Matching of Turbomachines; Part A - Similarity Relatives and Design Criteria of Turbines, year = 1962," *ASME Series A*.

[45] P. Colonna, A. Guardone, and N. R. Nannan, "Siloxanes: A new class of candidate Bethe-Zel'dovich-Thompson fluids," *Physics of Fluids*, vol. 19, no. 8, 2007.

[46] A. P. Weiß, "Volumetric expander versus turbine - which is the better choice for small ORC plants," in *3rd ASME ORC Conference, Brussels (Belgium)*, 2015, pp. 1–10.

[47] A. P. Weiß, T. Popp, J. Müller, J. Hauer, D. Brüggemann, and M. Preißinger, "Experimental characterization and comparison of an axial and a cantilever micro-turbine for small-scale Organic Rankine Cycle," *Applied Thermal Engineering*, vol. 140, no. January, pp. 235–244, 2018. [Online]. Available: https://doi.org/10.1016/j.applthermaleng.2018.05.033

[48] F. Ljungström, "The Development of the Ljungström Steam Turbine and Air Preheater," *Proceedings of the Institution of Mechanical Engineers*, vol. 160, no. 1, pp. 211–223, jun 1949. [Online]. Available: http://journals.sagepub.com/doi/10.1243/PIME{_}PROC{_}1949{_}160{_}023{_}02

[49] M. C. R. Claudio Spadacini, Lorenzo Centemeri, Luca G. Xodo, Marco Astolfi, "Exergy: a New Configuration for Organic Rankine Cycle Power Systems," 2011.

[50] G. Persico, M. Pini, V. Dossena, and P. Gaetani, "Aerodynamics of Centrifugal Turbine Cascades," *Journal of Engineering for Gas Turbines and Power*, vol. 137, no. 11, nov 2015. [Online]. Available: https://asmedigitalcollection.asme.org/gasturbinespower/article/doi/10.1115/1.4030261/373910/Aerodynamics-of-Centrifugal-Turbine-Cascades

[51] C. Spadacini, L. Centemeri, D. Rizzi, M. Sanvito, and A. Serafino, "Fluid-Dynamics of the Orc Radial Outflow Turbine," *Proceedings of the 3rd International Seminar on ORC Power Systems. ASME ORC 2015*, no. 1, pp. 1–10, 2015.

[52] T. Tartière and M. Astolfi, "A World Overview of the Organic Rankine Cycle Market," *Energy Procedia*, vol. 129, pp. 2–9, 2017. [Online]. Available: http://dx.doi.org/10.1016/j.egypro.2017.09.159

[53] E. Macchi and A. Perdichizzi, "Efficiency Prediction for Axial-Flow Turbines Operating with Nonconventional Fluids," *Journal of Engineering for Power*, vol. 103, no. 4, pp. 718–724, oct 1981. [Online]. Available: https://asmedigitalcollection.asme.org/gasturbinespower/article/103/4/718/405029/Efficiency-Prediction-for-AxialFlow-Turbines

[54] P. Colonna, N. R. Nannan, A. Guardone, and E. W. Lemmon, "Multiparameter equations of state for selected siloxanes," *Fluid Phase Equilibria*, vol. 244, no. 2, pp. 193–211, 2006.

[55] G. Cammi, C. C. Conti, A. Spinelii, F. Cozzi, and A. Guardone, "Experimental Characterization of Nozzle Flow Expansions of Siloxane MM for ORC Turbines Applications," *ORC 2019 Proceedings*, no. 2008, pp. 1–11, 2019.

[56] P. Colonna and P. Silva, "Dense Gas Thermodynamic Properties of Single and Multicomponent Fluids for Fluid Dynamics Simulations," *Journal of Fluids Engineering*, vol. 125, no. 3, pp. 414–427, may 2003. [Online]. Available: https://asmedigitalcollection.asme.org/fluidsengineering/article/125/3/414/463240/Dense-Gas-Thermodynamic-Properties-of-Single-and

[57] B. P. Brown and B. M. Argrow, "Application of Bethe-Zel'dovich-Thompson Fluids in Organic Rankine Cycle Engines," *Journal of Propulsion and Power*, vol. 16, no. 6, pp. 1118–1124, nov 2000. [Online]. Available: https://arc.aiaa.org/doi/10.2514/2.5686

[58] J. F. MONACO, M. S. CRAMER, and L. T. WATSON, "Supersonic flows of dense gases in cascade configurations," *Journal of Fluid Mechanics*, vol. 330, pp. 31–59, jan 1997. [Online]. Available: https://www.cambridge.org/core/product/identifier/S0022112096003564/type/journal{_}article

[59] T. Z. Kaczmarczyk, G. Żywica, and E. Ihnatowicz, "Experimental Investigation of a Radial Microturbine in ORGANIC RANKINE CYCLE SYSTEM WITH HFE7100 AS WORKING FLUID," *Proceedings of the 3rd International Seminar on ORC Power Systems*, pp. 1–10, 2015.

[60] G. Żywica, T. Kaczmarczyk, E. Ihnatowicz, P. Bagiński, and A. Andrearczyk, "Design and manufacturing of micro-turbomachinery components with application of heat resistant plastics," *Mechanics and Mechanical Engineering*, vol. Vol. 22, no. nr 2, 2018.

[61] G. Żywica, T. Z. Kaczmarczyk, Ł. Breńkacz, M. Bogulicz, A. Andrearczyk, and P. Bagiński, "Investigation of dynamic properties of the microturbine with a maximum rotational speed of 120 krpm â€“ predictions and experimental tests," *Journal of Vibroengineering*, vol. 22, no. 2, pp. 298–312, 2020. [Online]. Available: https://www.jvejournals.com/article/20816

[62] S. Riffat and X. Zhao, "A novel hybrid heat-pipe solar collector/CHP systemâ€"Part II: theoretical and experimental investigations," *Renewable Energy*, vol. 29, no. 12, pp. 1965–1990, oct 2004. [Online]. Available: https://linkinghub.elsevier.com/retrieve/pii/S0960148104001521

[63] I. Hernandez-Carrillo, C. Wood, and H. Liu, "Development of a 1000 W organic Rankine cycle micro-turbine-generator using polymeric structural materials and its performance test with compressed air," *Energy Conversion and Management*, vol. 190, pp. 105–120, jun 2019. [Online]. Available: https://linkinghub.elsevier.com/retrieve/pii/S0196890419303978

[64] W. Pu, C. Yue, D. Han, W. He, X. Liu, Q. Zhang, and Y. Chen, "Experimental study on Organic Rankine cycle for low grade thermal energy recovery," *Applied Thermal Engineering*, vol. 94, pp. 221–227, feb 2016. [Online]. Available: https://linkinghub.elsevier.com/retrieve/pii/S1359431115010662

[65] M. Li, J. Wang, W. He, L. Gao, B. Wang, S. Ma, and Y. Dai, "Construction and preliminary test of a low-temperature regenerative Organic Rankine Cycle (ORC) using R123," *Renewable Energy*, vol. 57, pp. 216–222, 2013. [Online]. Available: http://dx.doi.org/10.1016/j.renene.2013.01.042

[66] G. Pei, J. Li, Y. Li, D. Wang, and J. Ji, "Construction and dynamic test of a small-scale organic rankine cycle," *Energy*, vol. 36, no. 5, pp. 3215–3223, may 2011. [Online]. Available: https://linkinghub.elsevier.com/retrieve/pii/S0360544211001666

[67] V. Nguyen, P. Doherty, and S. Riffat, "Development of a prototype low-temperature Rankine cycle electricity generation system," *Applied Thermal Engineering*, vol. 21, no. 2, pp. 169–181, jan 2001. [Online]. Available: https://linkinghub.elsevier.com/retrieve/pii/S1359431100000521

[68] W. Yagoub, P. Doherty, and S. Riffat, "Solar energy-gas driven micro-CHP system for an office building," *Applied Thermal Engineering*, vol. 26, no. 14-15, pp. 1604–1610, oct 2006. [Online]. Available: https://linkinghub.elsevier.com/retrieve/pii/S135943110500414X

[69] P. Klonowicz, F. Heberle, M. Preißinger, and D. Brüggemann, "Significance of loss correlations in performance prediction of small scale, highly loaded turbine stages working in Organic Rankine Cycles," *Energy*, vol. 72, pp. 322–330, aug 2014.

[70] L. Shao, J. Zhu, X. Meng, X. Wei, and X. Ma, "Experimental study of an organic Rankine cycle system with radial inflow turbine and R123," *Applied Thermal Engineering*, vol. 124, pp. 940–947, sep 2017. [Online]. Available: https://linkinghub.elsevier.com/retrieve/pii/S1359431117339200

[71] J. R. Seume, M. Peters, and H. Kunte, "Design and test of a 10kW ORC supersonic turbine generator," *Journal of Physics: Conference Series*, vol. 821, p. 012023, mar 2017. [Online]. Available: http://stacks.iop.org/1742-6596/821/i=1/a=012023?key=crossref.72d8a5757d05901f6c137e81d16e2423

[72] K. Kosowski, M. Piwowarski, R. Stępień, and W. Włodarski, "Design and investigations of the ethanol microturbine," *Archives of Thermodynamics*, vol. 39, no. 2, pp. 41–54, 2018.

[73] C. Gazet, A. Leroux, B. Paillette, and A. Pauchet, "OPERATIONAL EXPERIENCE ON ORC USE FOR WASTE HEAT VALORIZATION IN BIOGAS POWER PLANT," *Proceedings of the 3rd International Seminar on ORC Power Systems*, pp. 1–7, 2015.

[74] C. Yue, Y. Huang, and Y. Wu, "Experimental Study of Low-temperature Organic Rankine Cycle with Axial Flow Turbine," *Energy Procedia*, vol. 75, pp. 1583–1589, aug 2015. [Online]. Available: https://linkinghub.elsevier.com/retrieve/pii/S1876610215011315

[75] L. Guillaume, A. Legros, A. Desideri, and V. Lemort, "Performance of a radial-inflow turbine integrated in an ORC system and designed for a WHR on truck application: An experimental comparison between R245fa and R1233zd," *Applied Energy*, vol. 186, pp. 408–422, jan 2017. [Online]. Available: https://linkinghub.elsevier.com/retrieve/pii/S0306261916303233

[76] J. Demierre, D. Favrat, J. Schiffmann, and J. Wegele, "Experimental investigation of a Thermally Driven Heat Pump based on a double Organic Rankine Cycle and an oil-free Compressor-Turbine Unit," *International Journal of Refrigeration*, vol. 44, pp. 91–100, aug 2014. [Online]. Available: https://linkinghub.elsevier.com/retrieve/pii/S0140700714001005

[77] S.-Y. Cho, C.-H. Cho, and S.-K. Choi, "Experiment and cycle analysis on a partially admitted axial-type turbine used in the organic Rankine cycle," *Energy*, vol. 90, pp. 643–651, oct 2015. [Online]. Available: https://linkinghub.elsevier.com/retrieve/pii/S0360544215009871

[78] A. M. Jubori, F. N. Al-Mousawi, K. Rahbar, and R. Al-Dadah, "Design and manufacturing a small-scale radial-inflow turbine for clean organic rankine power system," *Journal of Cleaner Production*, p. 120488, 2020. [Online]. Available: https://doi.org/10.1016/j.jclepro.2020.120488

[79] A. Meroni, A. La Seta, J. Andreasen, L. Pierobon, G. Persico, and F. Haglind, "Combined Turbine and Cycle Optimization for Organic Rankine Cycle Power Systems - Part A: Turbine Model," *Energies*, vol. 9, no. 5, p. 313, apr 2016. [Online]. Available: http://www.mdpi.com/1996-1073/9/5/313

[80] A. Meroni, M. Robertson, R. Martinez-Botas, and F. Haglind, "A methodology for the preliminary design and performance prediction of high-pressure ratio radial-inflow turbines," *Energy*, vol. 164, pp. 1062–1078, 2018. [Online]. Available: https://doi.org/10.1016/j.energy.2018.09.045

[81] R. Agromayor and L. Nord, "AxialOpt: a meanline model for the design and optimization of axial turbines," 2019.

[82] A. Weiß, V. Novotný, T. Popp, G. Zinn, and M. Kolovratnik, "Customized Small-scale ORC Turbogenerators - Combining a 1D-design Tool, a Micro-turbine-generator construction Kit and Potentials of 3D-printing," in *Proceedings of ORC2019*, Athens, 2019.

[83] E. W. Lemmon, M. L. Huber, and M. O. McLinden, "NIST Standard Reference Database 23: Reference Fluid Thermodynamic and Transport Properties-REFPROP, Version 9.1, National Institute

of Standards and Technology," 2013. [Online]. Available: https://www.nist.gov/srd/refprop

[84] L. Da Lio, G. Manente, and A. Lazzaretto, "Predicting the optimum design of single stage axial expanders in ORC systems: Is there a single efficiency map for different working fluids?" *Applied Energy*, vol. 167, pp. 44–58, 2016. [Online]. Available: http://dx.doi.org/10.1016/j.apenergy.2016.01.020

[85] L. Da Lio, G. Manente, and A. Lazzaretto, "New efficiency charts for the optimum design of axial flow turbines for organic Rankine cycles," *Energy*, vol. 77, pp. 447–459, 2014.

[86] H. R. M. Craig and H. J. A. Cox, "Performance Estimation of Axial Flow Turbines," *Proceedings of the Institution of Mechanical Engineers*, vol. 185, no. 1, pp. 407–424, jun 1970. [Online]. Available: http://journals.sagepub.com/doi/10.1243/PIME{_}PROC{_}1970{_}185{_}048{_}02

[87] R. Aungier, "Turbine Aerodynamics," *ASME Press*, 2006.

[88] M. H. Vavra, "Axial flow turbines," *Von Karman Institute for Fluid dynamics*, vol. Lecture se, 1969.

[89] J. Dunham and P. M. Came, "Improvements to the Ainley-Mathieson Method of Turbine Performance Prediction," *Journal of Engineering for Power*, vol. 92, no. 3, pp. 252–256, jul 1970. [Online]. Available: https://asmedigitalcollection.asme.org/gasturbinespower/article/92/3/252/404009/Improvements-to-the-AinleyMathieson-Method-of

[90] D. G. Ainley, "An Examination of the Flow and Pressure Loss in Blade Rows of Axial-Flow Turbines, Aeronautical Research Council," *R&M*, vol. 2891, no. 2891, 1955.

[91] B. Lakshminarayana, *Fluid Dynamics and Heat Transfer of Turbomachinery*. Hoboken, NJ, USA: John Wiley & Sons, Inc., dec 1995. [Online]. Available: http://doi.wiley.com/10.1002/9780470172629

[92] R. Beer, "Aerodynamic Design and Estimated Performance of a Two-stage Curtis Turbine for the Liquid Oxygen Turbopump of the M-1 Engine," 1965.

[93] T. Reynolds, "Aerodynamic Design Model II Turbine M-1 Fuel Turbopump Assembly," 1966.

[94] V. Novotny, J. Spale, M. Vitvarova, M. Kolovratnik, and P. Zikmund, "3D Printing in Turbomachinery - Overview of Technologies, Applications and Possibilities for Industry 4.0," *ASME Press*, pp. 1–9, 2019.

[95] J. R. Tumbleston, D. Shirvanyants, N. Ermoshkin, R. Janusziewicz, A. R. Johnson, D. Kelly, K. Chen, R. Pinschmidt, J. P. Rolland, A. Ermoshkin, E. T. Samulski, and J. M. DeSimone, "Continuous liquid interface production of 3D objects," *Science*, vol. 347, no. 6228, pp. 1349–1352, mar 2015. [Online]. Available: http://www.sciencemag.org/cgi/doi/10.1126/science.aaa2397

[96] R. Janusziewicz, J. R. Tumbleston, A. L. Quintanilla, S. J. Mecham, and J. M. DeSimone, "Layerless fabrication with continuous liquid interface production." *Proceedings of the National Academy of Sciences of the United States of America*, vol. 113, no. 42, pp. 11 703–11 708, oct 2016.

[97] K. Rahbar, S. Mahmoud, R. K. Al-Dadah, N. Moazami, and S. A. Mirhadizadeh, "Development and experimental study of a small-scale compressed air radial inflow turbine for distributed power generation," *Applied Thermal Engineering*, vol. 116, pp. 549–583, 2017. [Online]. Available: http://dx.doi.org/10.1016/j.applthermaleng.2017.01.100

[98] M. Meier, W. Gooding, J. Fabian, and N. L. Key, "Considerations for Using Additive Manufacturing Technology in Centrifugal Compressor Research," *Journal of Engineering for Gas Turbines and Power*, pp. 1–10, 2019.

[99] I. Hernandez-Carrillo, C. Wood, and H. Liu, "Development of a 1000 W organic Rankine cycle micro-turbine-generator using polymeric structural materials and its performance test with compressed air," *Energy Conversion and Management*, vol. 190, no. December 2018, pp. 105–120, 2019. [Online]. Available: https://doi.org/10.1016/j.enconman.2019.03.092

[100] I. Hernandez-Carrillo, C. J. Wood, and H. Liu, "Advanced materials for the impeller in an ORC radial microturbine," *Energy Procedia*, vol. 129, pp. 1047–1054, 2017. [Online]. Available: http://dx.doi.org/10.1016/j.egypro.2017.09.241

[101] I. Hernandez, H. Liu, and C. Wood, "Advanced Materials for the Impeller in an ORC radial micro-turbine (presentation)," in *ORC 2017*, Milano, 2017.

[102] J. E. Grady, W. J. Haller, P. E. Poinsatte, M. C. Halbig, S. L. Schnulo, D. Weir, N. Wali, M. Vinup, M. G. Jones, C. Patterson, T. Santelle, and J. Mehl, "A Fully Nonmetallic Gas Turbine Engine Enabled by Additive Manufacturing Part I : System Analysis , Component Identifi cation , Additive Manufacturing , and Testing of Polymer Composites," no. May, 2015.

[103] K. C. Chuang, J. E. Grady, S. M. Arnold, R. D. Draper, E. Shin, C. Patterson, T. Santelle, R. Prototyping+manufacturing, C. Lao, M. Rhein, and J. Mehl, "A Fully Nonmetallic Gas Turbine Engine Enabled by Additive Manufacturing Part II: Additive Manufacturing and Characterization of Polymer Composites," 2015.

[104] M. Arifin, B. Wahono, E. Junianto, and A. D. Pasek, "Process manufacture rotor radial turbo-expander for small scale organic Rankine cycles using selective laser melting machine," *Energy Procedia*, vol. 68, pp. 305–310, 2015. [Online]. Available: http://dx.doi.org/10.1016/j.egypro.2015.03.260

[105] Y. Zhang, T. Duda, J. A. Scobie, C. M. Sangan, C. D. Copeland, and A. Redwood, "Design of an Air-Cooled Radial Turbine: Part 1 - Computational Modelling," in *Volume 8: Microturbines, Turbochargers, and Small Turbomachines; Steam Turbines*. ASME, jun 2018, p. V008T26A013. [Online]. Available: http://proceedings.asmedigitalcollection.asme.org/proceeding.aspx?doi=10.1115/GT2018-76378

[106] ——, "Design of an Air-Cooled Radial Turbine: Part 2 - Experimental Measurements of Heat Transfer," in *Volume 8: Microturbines, Turbochargers, and Small Turbomachines; Steam Turbines*. ASME, jun 2018, p. V008T26A014.

[107] P. ASTM International, West Conshohocken, "Standard for Additive Manufacturing â€“ Post Processing Methods â€“ Standard Specification for Thermal Post-Processing Metal Parts Made Via Powder Bed Fusion," *ASTM F3301-18a*, 2018. [Online]. Available: www.astm.org

[108] M. H. Bocanegra-Bernal, "Hot Isostatic Pressing (HIP) technology and its applications to metals and ceramics," *Journal of Materials Science*, vol. 39, no. 21, pp. 6399–6420, nov 2004. [Online]. Available: http://link.springer.com/10.1023/B:JMSC.0000044878.11441.90

[109] B. Chmiela, B. Koscielniak, and J. Cwajna, "Effect of hot isostatic pressing on the microstructure of turbine blade airfoil made of nickel-base superalloy," *Archives of Metallurgy and Materials*, vol. 62, no. 1, pp. 241–245, 2017.

[110] Quintus Technologies, "Hot Isostatic Pressing Supporting Additive Manufacturing Industry," pp. 1–4.

[111] L. Hackel, J. R. Rankin, A. Rubenchik, W. E. King, and M. Matthews, "Laser peening: A tool for additive manufacturing post-processing," *Additive Manufacturing*, vol. 24, no. May, pp. 67–75, 2018. [Online]. Available: https://doi.org/10.1016/j.addma.2018.09.013

[112] Additive Manufacturing Standardization Collaborative, "Standardization Roadmap for Additive Manufacturing, version 2," no. June, p. 269, 2018. [Online]. Available: https://share.ansi.org/SharedDocuments/StandardsActivities/AMSC/AMSC{_}Roadmap{_}June{_}2018.pdf

[113] Y. Fu, X. Wang, H. Gao, H. Wei, and S. Li, "Blade surface uniformity of blisk finished by abrasive flow machining," *The International Journal of Advanced Manufacturing Technology*, vol. 84, no. 5-8, pp. 1725–1735, jan 2016.

[114] Extrude Hone, "AFM: High-Quality Finishing for Industrial 3D Printing - Extrude Hone," 2016.

[115] VDMA, "Technische Fachübersetzungen in alle Weltsprachen (GER)," 2018. [Online]. Available: https://goo.gl/xBv1hz

[116] C. Yang, X. Tian, D. Li, Y. Cao, F. Zhao, and C. Shi, "Influence of thermal processing conditions in 3D printing on the crystallinity and mechanical properties of PEEK material," *Journal of Materials Processing Technology*, vol. 248, pp. 1–7, oct 2017.

[117] W. Jo, O.-C. Kwon, and M.-W. Moon, "Investigation of influence of heat treatment on mechanical strength of FDM printed 3D objects," *Rapid Prototyping Journal*, vol. 24, no. 3, pp. 637–644, apr 2018.

[118] V. Slavković, N. Grujović, A. Disic, A. Dišić, and A. Radovanović, "Influence of Annealing and Printing Directions on Mechanical Properties of PLA Shape Memory Polymer Produced by Fused Deposition Modeling," in *6th International Congress of Serbian Society of Mechanics*, Mountain Tara, 2017.

[119] P. Parandoush and D. Lin, "A review on additive manufacturing of polymer-fiber composites," *Composite Structures*, vol. 182, pp. 36–53, dec 2017. [Online]. Available: https://linkinghub.elsevier.com/retrieve/pii/S0263822316329063

[120] A. Kamil, "Post Processing for Nylon 12 Laser Sintered Components," Dissertation thesis, Newcastle University, 2016.

[121] A. Garg, A. Bhattacharya, and A. Batish, "On Surface Finish and Dimensional Accuracy of FDM Parts after Cold Vapor Treatment," *Materials and Manufacturing Processes*, vol. 31, no. 4, pp. 522–529, mar 2016.

[122] V. Novotny, M. Vitvarova, M. Kolovratnik, B. B. Stunova, V. Vodicka, J. Spale, P. Zikmund, M. Drasnar, and E. Schastlivtseva, "Design and Manufacturing of a Metal 3D Printed kW Scale Axial Turboexpander." ASME International, jun 2019.

[123] V. Navrotsky, "Using AM for gas turbine repair," *Metal Powder Report*, vol. 69, no. 6, pp. 36–37, nov 2014. [Online]. Available: https://linkinghub.elsevier.com/retrieve/pii/S0026065714702784

[124] A. P. Charles and C. A. Gonzalez Taylor, "Development of a Method to Repair Gas Turbine Blades using Electron Beam Melting Additive Manufacturing Technology," 2017. [Online]. Available: http://www.diva-portal.org/smash/record.jsf?pid=diva2{%}3A1076149{&}dswid=-8584

[125] P. Zelinski, "Using Hybrid AM, GE Leverages Turbine Blade Repair into Efficiency Improvement," 2017. [Online]. Available: https://www.additivemanufacturing.media/blog/post/using-hybrid-am-ge-leverages-turbine-blade-repair-into-efficiency-improvement

[126] M. Astolfi and E. Macchi, "Efficiency Correlations for Axial Flow Turbines Working With Non-Conventional Fluids," *Asme Orc 2015*, pp. 1–12, 2015.

[127] L. Keulen, S. Gallarini, C. Landolina, A. Spinelli, P. Iora, C. Invernizzi, L. Lietti, and A. Guardone, "Thermal stability of hexamethyldisiloxane and octamethyltrisiloxane," *Energy*, vol. 165, pp. 868–876, 2018. [Online]. Available: https://doi.org/10.1016/j.energy.2018.08.057

[128] T. G. Erhart, J. Gölz, U. Eicker, and M. Van Den Broek, "Working fluid stability in large-scale organic rankine cycle-units using siloxanes - Long-term experiences and fluid recycling," *Energies*, vol. 9, no. 6, pp. 1–16, 2016.

[129] W. Traupel, *Thermische Turbomaschinen*. Springer Singapore Pte. Limited, 2001.

[130] S. C. Kacker and U. Okapuu, "A Mean Line Prediction Method for Axial Flow Turbine Efficiency," *Journal of Engineering for Power*, vol. 104, no. 1, p. 111, jan 1982.

[131] A. P. Weiß, V. Novotný, T. Popp, P. Streit, J. Špale, G. Zinn, and M. Kolovratník, "Customized ORC micro turbo-expanders - From 1D design to modular construction kit and prospects of additive manufacturing," *Energy*, p. 118407, jul 2020.

[132] T. Mathijssen, M. Gallo, E. Casati, N. R. Nannan, C. Zamfirescu, A. Guardone, and P. Colonna, "The flexible asymmetric shock tube (FAST): a Ludwieg tube facility for wave propagation measurements in high-temperature vapours of organic fluids," *Experiments in Fluids*, vol. 56, no. 10, p. 195, oct 2015. [Online]. Available: http://link.springer.com/10.1007/s00348-015-2060-1

[133] A. J. Head, C. De Servi, E. Casati, M. Pini, and P. Colonna, "Preliminary Design of the ORCHID: A Facility for Studying Non-Ideal Compressible Fluid Dynamics and Testing ORC Expanders," in *Volume 3: Coal, Biomass and Alternative Fuels; Cycle Innovations; Electric Power; Industrial and Cogeneration; Organic Rankine Cycle Power Systems*. American Society of Mechanical Engineers, jun 2016. [Online]. Available: https://asmedigitalcollection.asme.org/GT/proceedings/GT2016/49743/Seoul,SouthKorea/239399

[134] F. Reinker, E. Y. Kenig, M. Passmann, and S. aus der Wiesche, "Closed Loop Organic Wind Tunnel (CLOWT): Design, Components and Control System," *Energy Procedia*, vol. 129, pp. 200–207, sep 2017. [Online]. Available: https://linkinghub.elsevier.com/retrieve/pii/S1876610217340274

[135] A. Spinelli, M. Pini, V. Dossena, P. Gaetani, and F. Casella, "Design, Simulation, and Construction of a Test Rig for Organic Vapors," *Journal of Engineering for Gas Turbines and Power*, vol. 135, no. 4, apr 2013. [Online]. Available: https://asmedigitalcollection.asme.org/gasturbinespower/article/doi/10.1115/1.4023114/367050/Design-Simulation-and-Construction-of-a-Test-Rig

[136] R. Watzlawick, "Untersuchung der wesentlichen Einflussfaktoren auf die Sekundärverluste in Verdichter-und Turbinengittern bei Variation des Schaufelseitenverhältnisses," Ph.D. dissertation, 1991.

[137] C. Pfleiderer and H. Petermann, *Strömungsmaschinen*. Springer-Verlag, 7. Auflage, 2004.

[138] R. Newlands, "The Thrust Optimised Parabolic nozzle," *Aspire space, Purdue University*, pp. 1–6, 2017.

[139] G. V. R. RAO, "Exhaust Nozzle Contour for Optimum Thrust," *Journal of Jet Propulsion*, vol. 28, no. 6, pp. 377–382, jun 1958. [Online]. Available: https://arc.aiaa.org/doi/10.2514/8.7324

[140] M. Deich, "Investigation and Design of Axial Turbine Stages (in Russian)," *Mashinostroenie*, 1964.

[141] O. Zweifel, "The Spacing of Turbo-Machine Blading, Especially with Large Angular Deflection," *Brown Boveri Review*, 1945.

[142] J. Hauer, "Analytische Studie zur optimierten Turbinenauslegung," Ph.D. dissertation, Hochschule Amberg â€“ Weiden, 2011.

[143] R. H. Aungier, *Turbine Aerodynamics*, 2006.

[144] P. Gaetani, "Stator-Rotor Interaction in Axial Turbine: Flow Physics and Design Perspective," in *Aircraft Technology*. InTech, sep 2018. [Online]. Available: http://www.intechopen.com/books/aircraft-technology/stator-rotor-interaction-in-axial-turbine-flow-physics-and-design-perspective

[145] M. Müller, "TorqueCalc." [Online]. Available: https://www.ecalc.ch/torquecalc.php

[146] V. Novotny, M. Vitvarova, P. Zikmund, V. Vodicka, J. Spale, and M. Kolovratník, "3D Printing for Low-Cost Low-Parameters and Rapidly Developed Turboexpanders for Decentralized Micro-Power Systems," in *ASME Turboexpo 2018 (poster)*, Oslo, 2018.

[147] V. Vodicka, V. Novotny, Z. Zeleny, J. Mascuch, and C. Republic, "Rotary vane expander - Analysis and prediction of delayed chamber closure," *ORC2019*, no. 5, pp. 1–10, 2019.

[148] R. Agromayor and L. O. Nord, "Preliminary Design and Optimization of Axial Turbines Accounting for Diffuser Performance," *International Journal of Turbomachinery, Propulsion and Power*, vol. 4, no. 3, p. 32, sep 2019. [Online]. Available: https://www.mdpi.com/2504-186X/4/3/32

Appendix **A**

List of symbols

A area $[mm^2]$

a speed of sound $[m \cdot s^{-1}]$

b channel width $[mm]$

C chord length $[mm]$

c absolute velocity, specific heat capacity $[m \cdot s^{-1}]$ or $[kJ \cdot kg^{-1} \cdot K^{-1}]$

d diameter $[mm]$

e partial admission [%]

H enthalpy head $[kJ \cdot kg^{-1}]$

h blade height, specific enthalpy $[mm]$ or $[kJ \cdot kg^{-1}]$

I rothalpy, current $[kJ \cdot kg^{-1}]$ or $[A]$

i number of segments, [-]

l length $[mm]$

Ma Mach number [-]

$\dot{m}$ mass flow rate $[kg^{-1} \cdot s^{-1}]$

n number [-]

P power $[W]$

p pressure $[kPa]$

R degree of reaction [-]

Re Reynolds number [-]

r radius $[mm]$

s blade pitch, specific entropy $[mm]$ or $[kJ \cdot kg^{-1} \cdot K^{-1}]$

T torque, temperature $[Nm]$ or $[°C]$

t thickness, time $[mm]$ or $[s]$

U voltage $[V]$

u peripheral blade speed $[m \cdot s^{-1}]$

$\dot{V}$ volumetric flow rate $[m^3 \cdot s^{-1}]$

v specific volume $[m^3 \cdot kg^{-1}]$

w relative velocity $[m \cdot s^{-1}]$

z number of blades [-]

α absolute flow angle [°]

β relative flow angle [°]

ϵ flow deflection [°]

γ isentropic expansion coefficient, blade stagger angle [-] or [°]

η efficiency [%]

θ blade camber angle [°]

μ dynamic viscosity $[Pa \cdot s]$

ρ density $[kg \cdot m^{-3}]$

σ solidity [-]

ϕ flow coefficient, profile loss coefficient [-]

ψ stage loading coefficient [-]

ω angular velocity $[s^{-1}]$

Γ fundamental derivative in gas dynamics [-]

Appendix B

Subscripts

el electrical

th thermal

u tangential

ax axial

mech mechanical

meas measured

is isentropic

sh superheated

g generator

rect rectifier

norm normal

m meridional

r relative

s specific

h hydraulic

Bl blade

No nozzle

Rot rotor

in inlet

out outlet

V ventilation

fr frictional

st stage

p at constant pressure

opt optimal

id ideal

it iterated

turb turbine

corr corrected

Appendix C

Acronyms

AM Additive manufacturing

AM Aspect ratio

CHP Combined heat and power

ORC Organic Rankine cycle

MM Hexamethyldisiloxane

RPM Rotational speed

SLS Selective laser sintering

SLA Stereolitography

DMLS Direct metal laser sintering

FDM Fused deposition modelling

FFE Fused filament extrusion

LPBF Laser powder bed fusion

ABS Acrylonitrile butadiene styrene

VBA Visual Basic for Applications

AC Alternating current

DC Direct current

BLDC Brushless direct current

ASU Air service unit

PR Pressure ratio

PID Piping and instrumentation diagram

PFD Process flow diagram

CAD Computer aided design

HIP Hot isostatic pressing

ASTM American Society for Testing and Materials

WEDM Wire electrical discharge machining

ECM Electrochemical machining

AFM Abrasive flow machining

PEEK Polyether-ether-ketone

CLIP Continuous liquid interface

MJF Multi jet fusion

DOD Drop-on-demand

BJ Binder jetting

MJ Material jetting

EBM Electron beam melting

SLM Selective laser melting

EoS Equation of state

ROT Radial outflow turbine

IFR Inflow radial (turbomachine)

OFR Outflow radial (turbomachine)

(V)IGV (variable) Inlet guide vane

BL Boundary layer

CFD Computational fluid dynamics

WHR Waste heat recovery

Appendix D

Selected full-sized charts

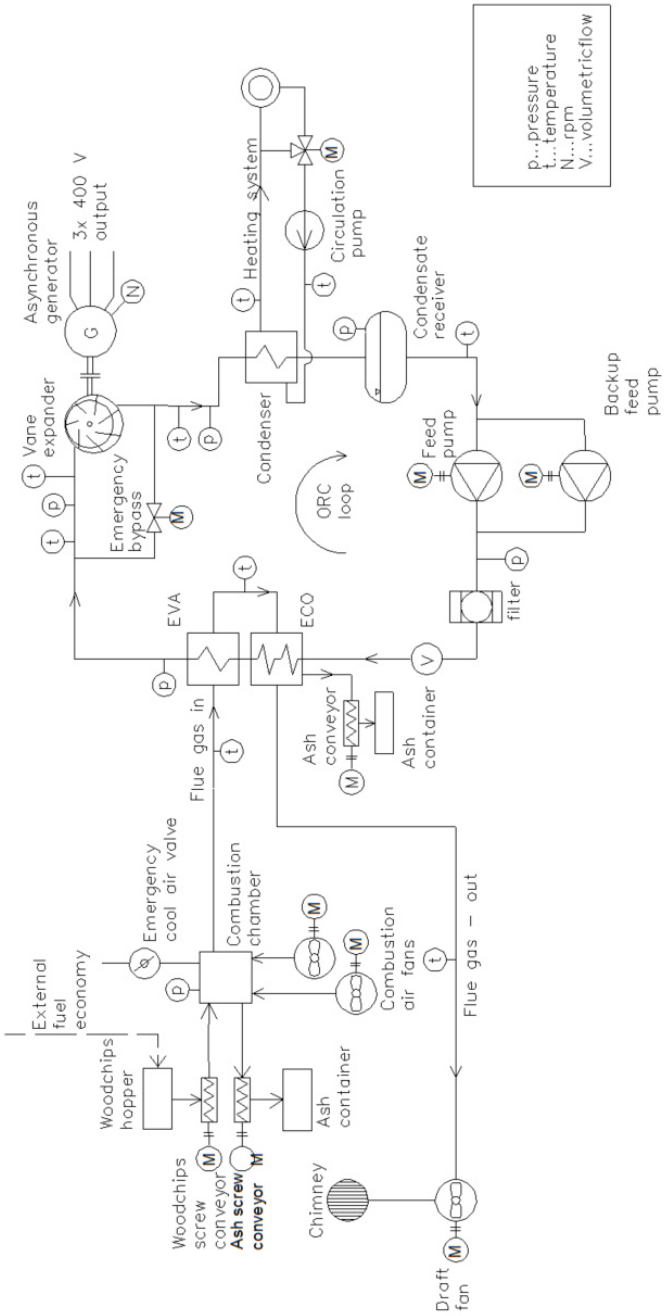

Figure D.1: Process flow diagram of the μCHP ORC unit Wave120

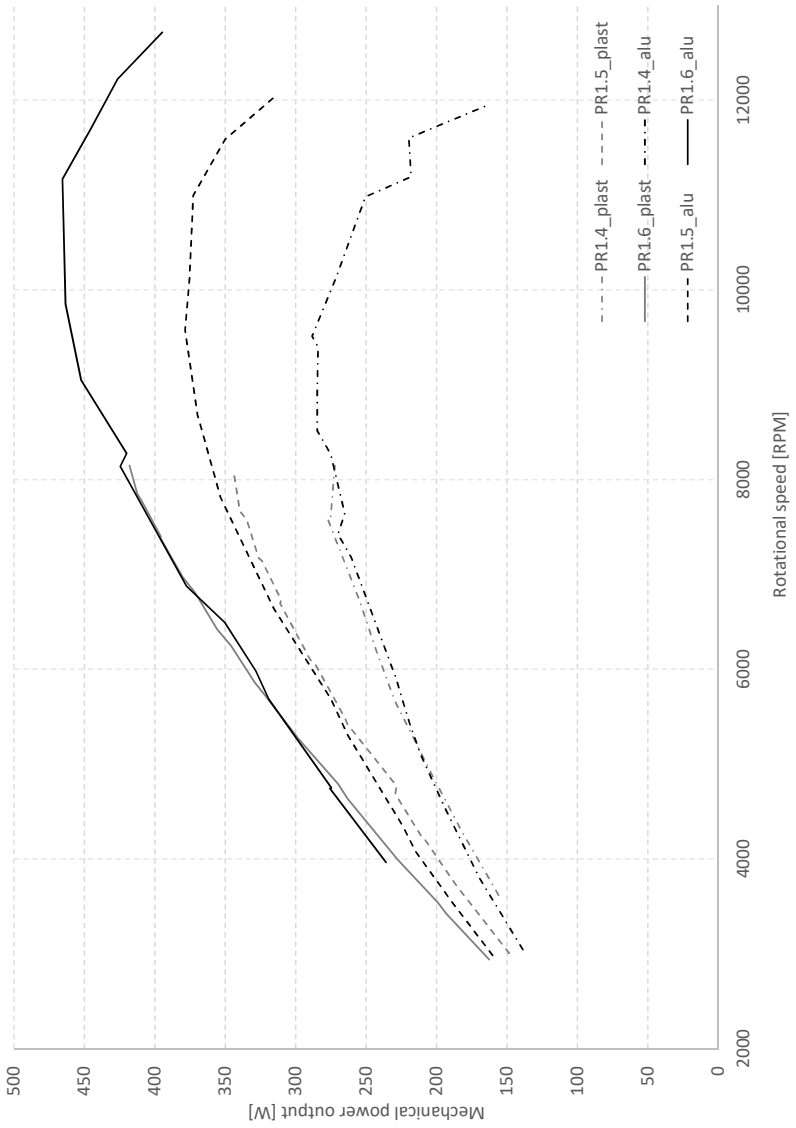

Figure D.2: Validation of the evaluation methodology and replicability of the results - two different stator frames and generators; both wheels selective laser sintered (SLS) nylon powder (short chord) - full scale

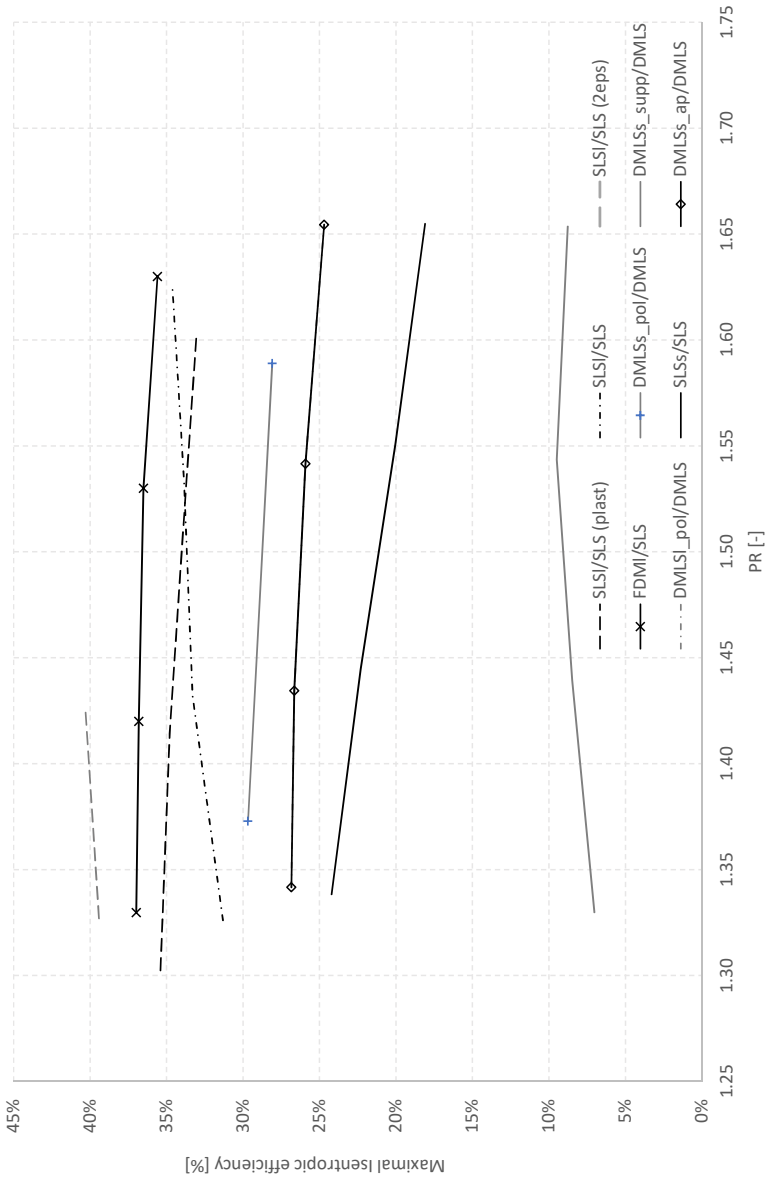

Figure D.3: Experimental results of maximal isentropic efficiencies at chosen pressure ratios of all the 1^{st} generation turbine configurations - full scale

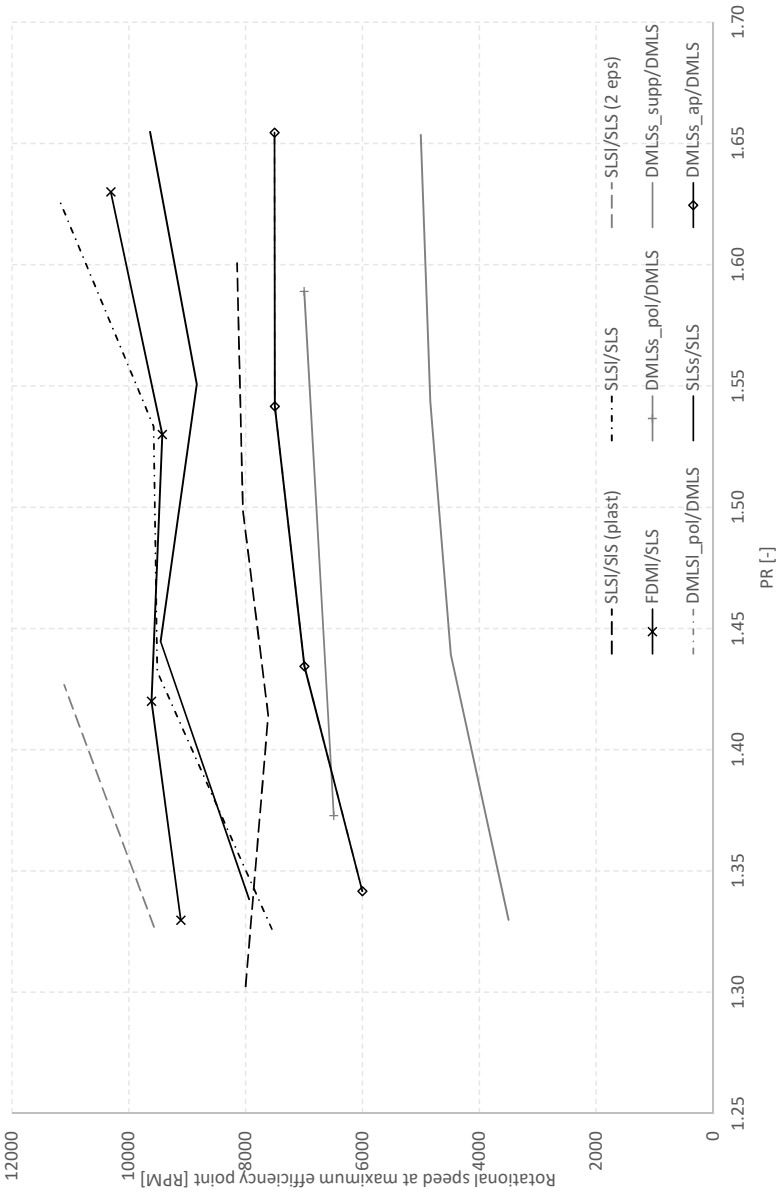

Figure D.4: Rotational speed corresponding to the maximum isentropic efficiency point for 1^{st} generation turbine configurations - full scale

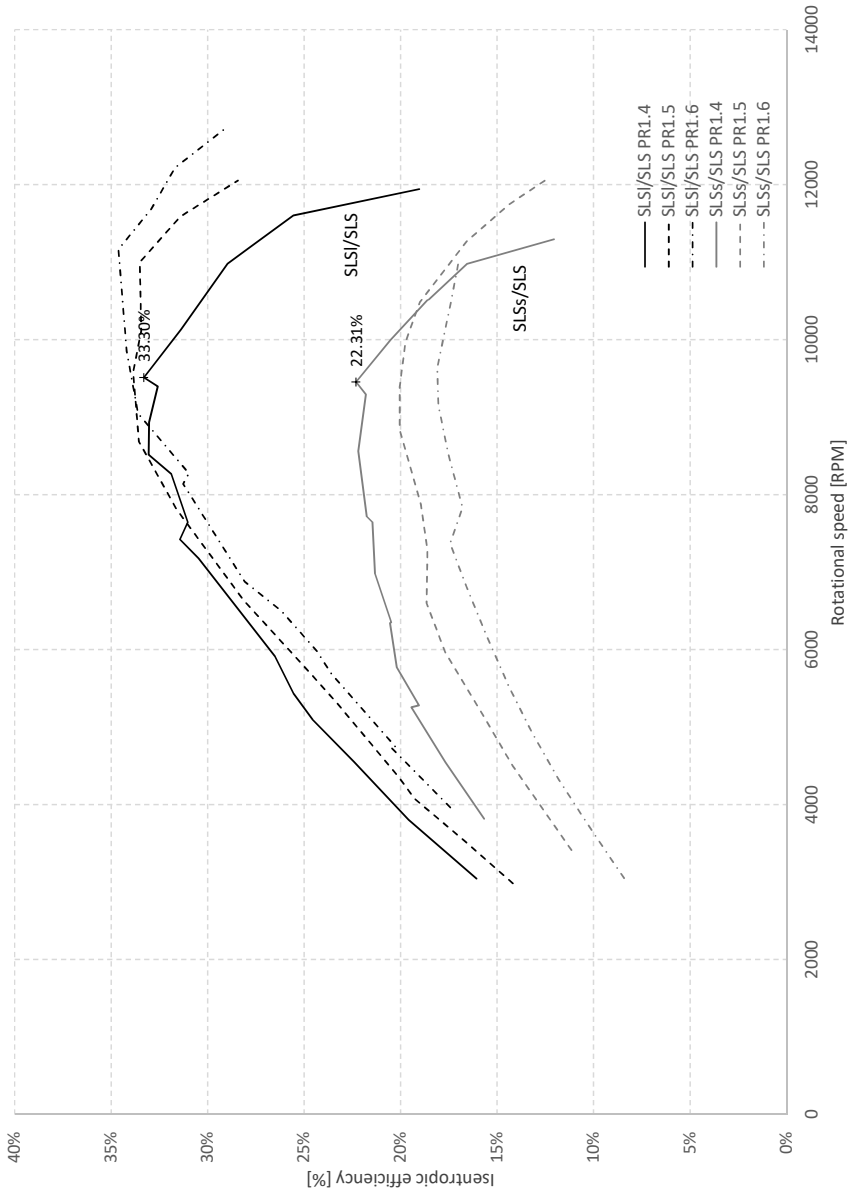

Figure D.5: Experimental comparison of the long and short chord SLS stator wheel (rotor also SLS) at different PRs - full scale

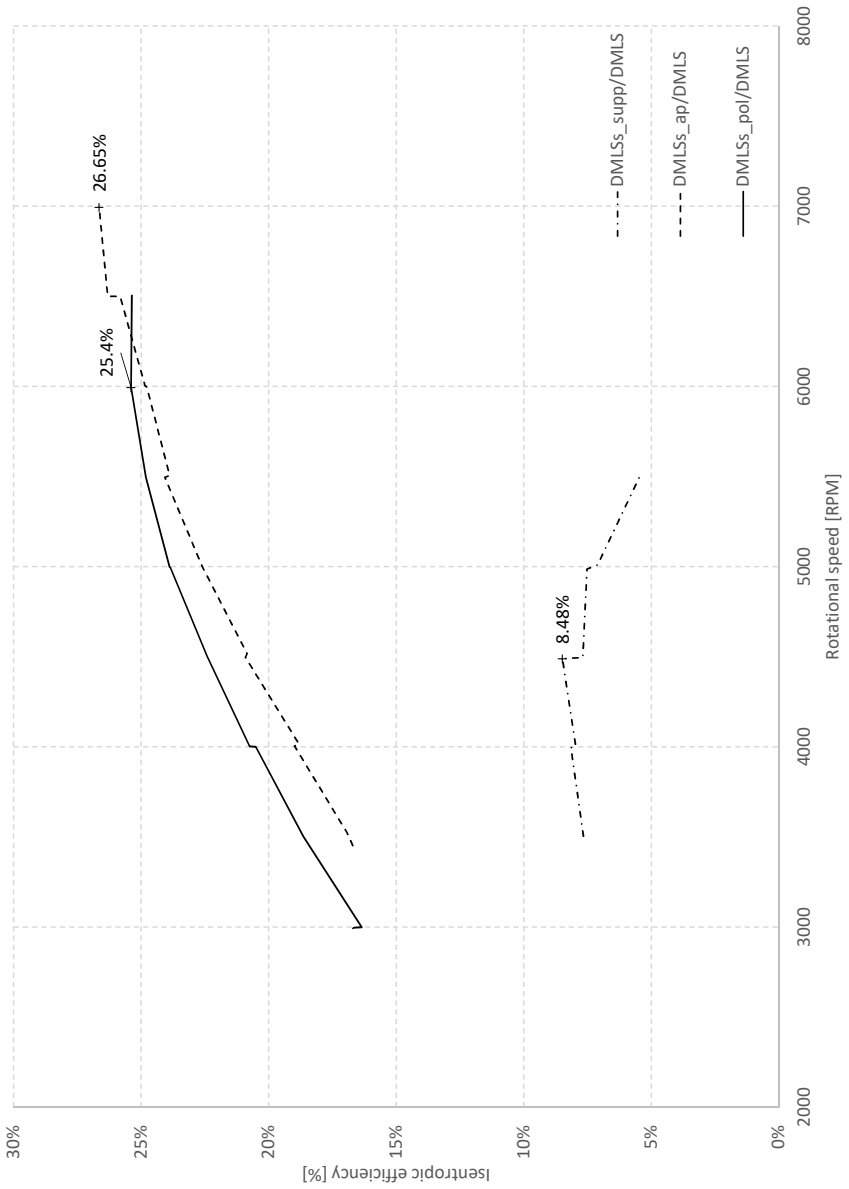

Figure D.6: Effect of the surface roughness on the isentropic efficiency at PR 1.4; stator DMLSs with various postprocessing - full scale

Figure D.7: Effect of the partial admission on the ventilation loss correlation and turbine performance; both stator and rotor - selective laser sintered (SLS, long chord stator) - full scale

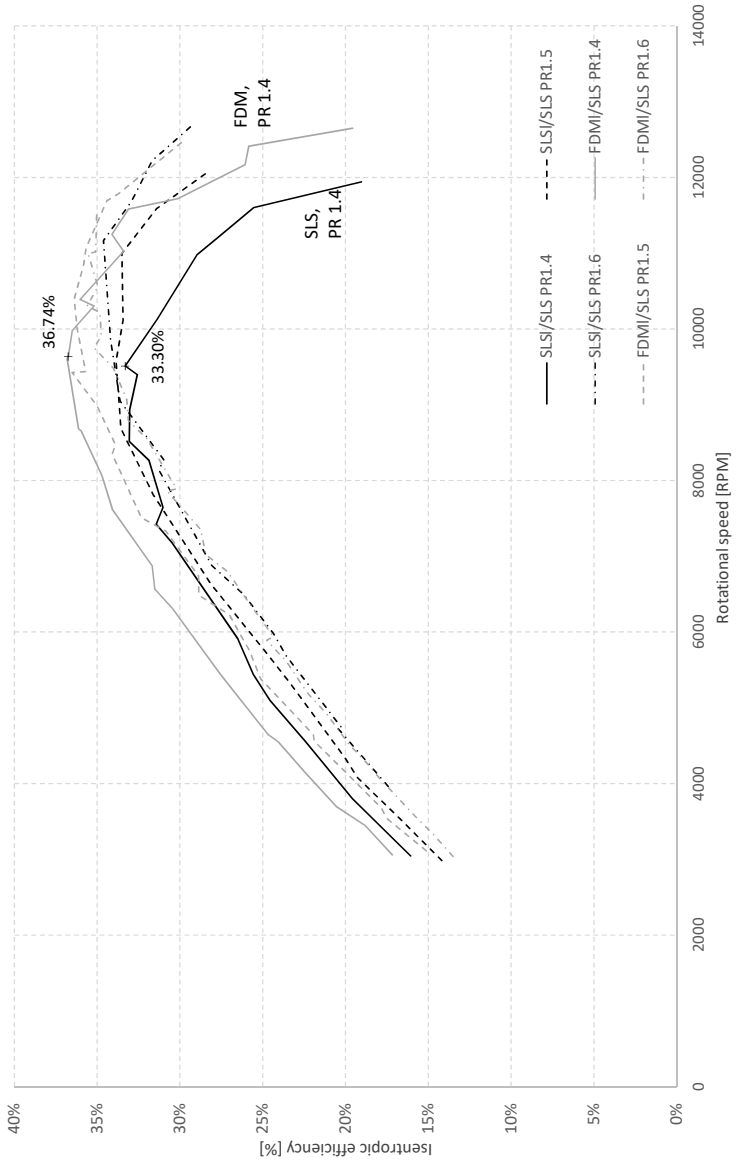

Figure D.8: Comparison of FDM and SLS (long chord) stator wheels and the effect of 3-D printing methods on the isentropic efficiency; both with SLS rotor; measured at three different PRs - full scale

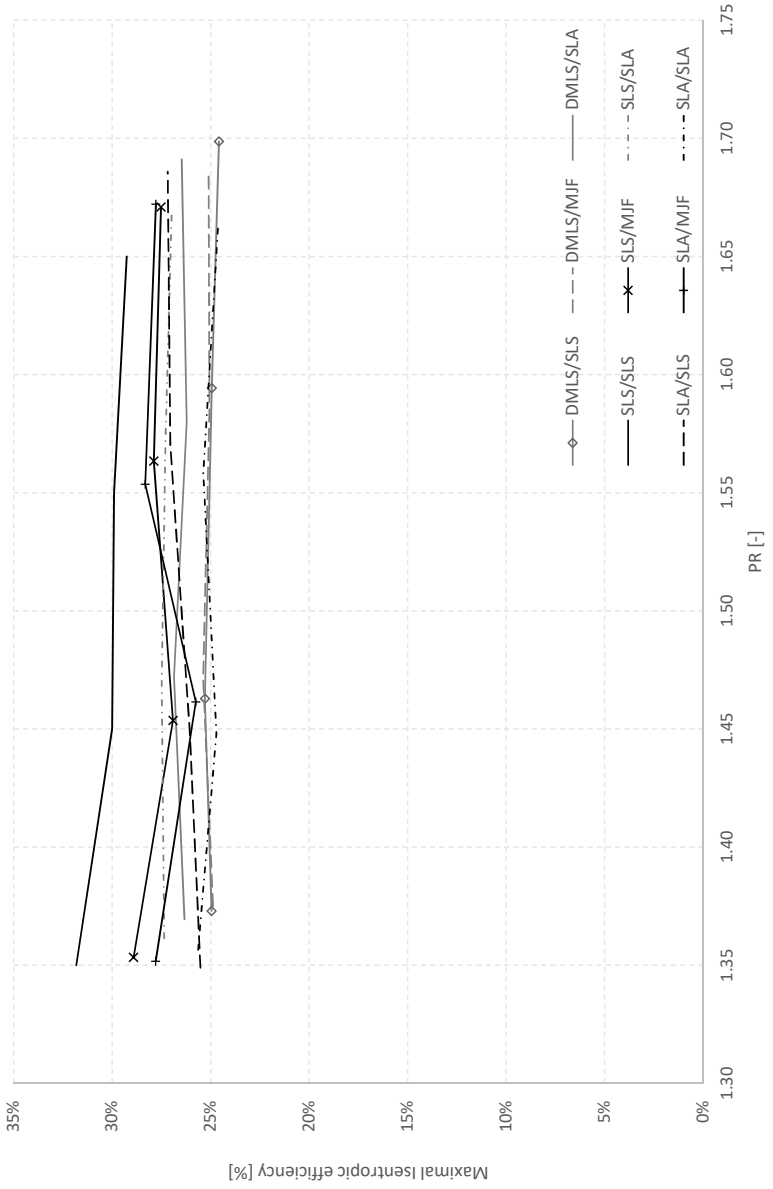

Figure D.9: Maximal isentropic efficiencies at chosen pressure ratios of all the 2^{nd} generation turbine configurations - full scale

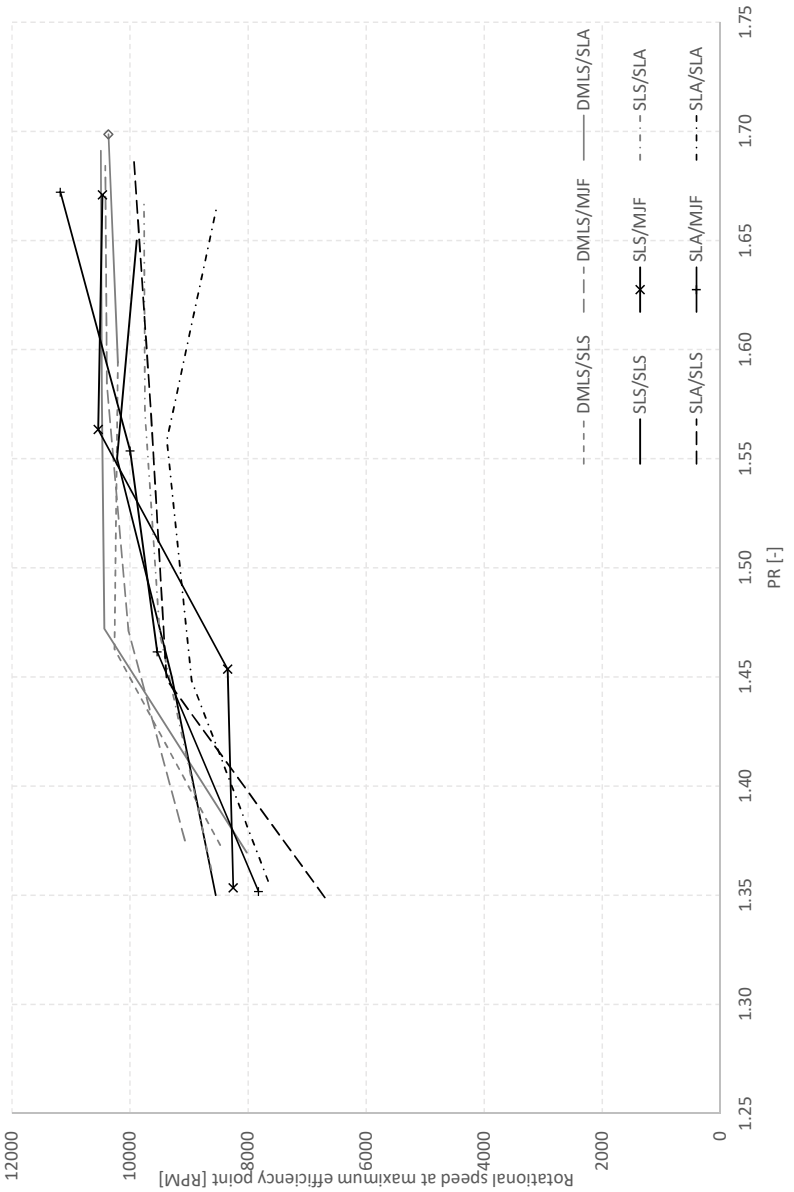

Figure D.10: Rotational speed corresponding to the maximum isentropic efficiency point for 2^{nd} generation turbine configurations - full scale

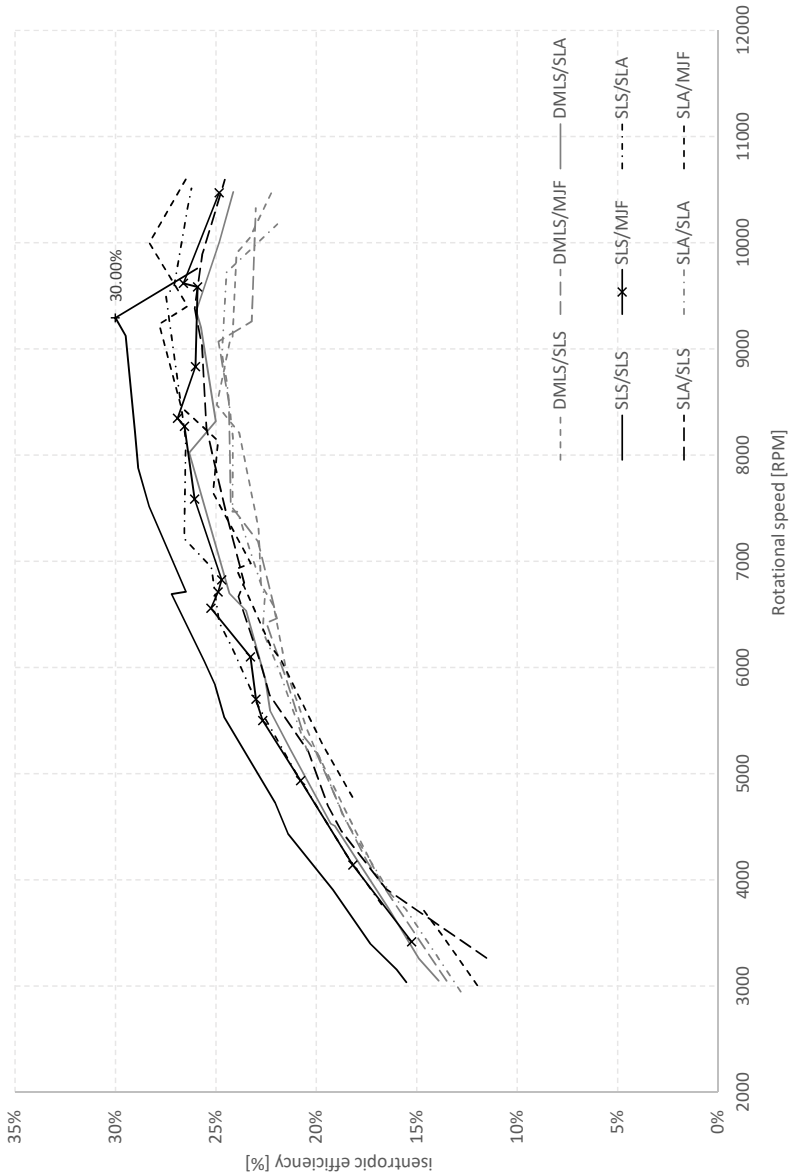

Figure D.11: Second generation design, different AM methods stator/rotor; PR 1.4- full scale

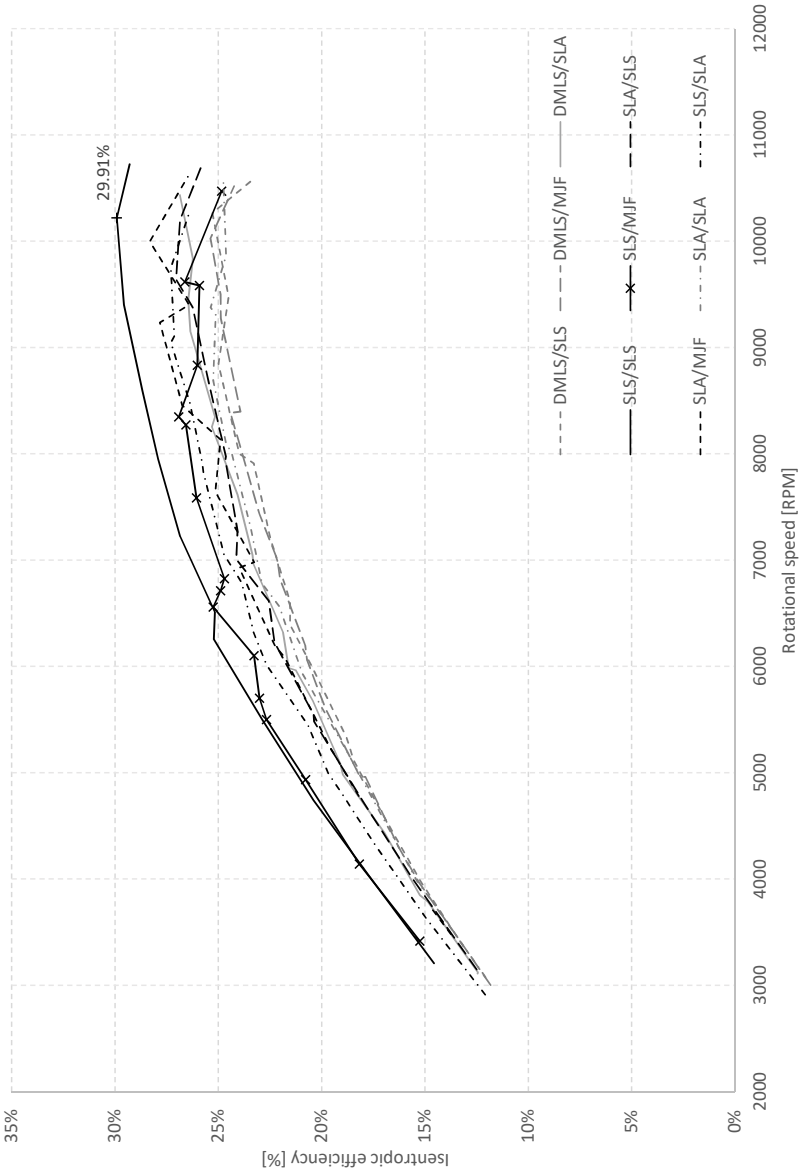

Figure D.12: Second generation design, different AM methods stator/rotor; PR 1.5 - full scale

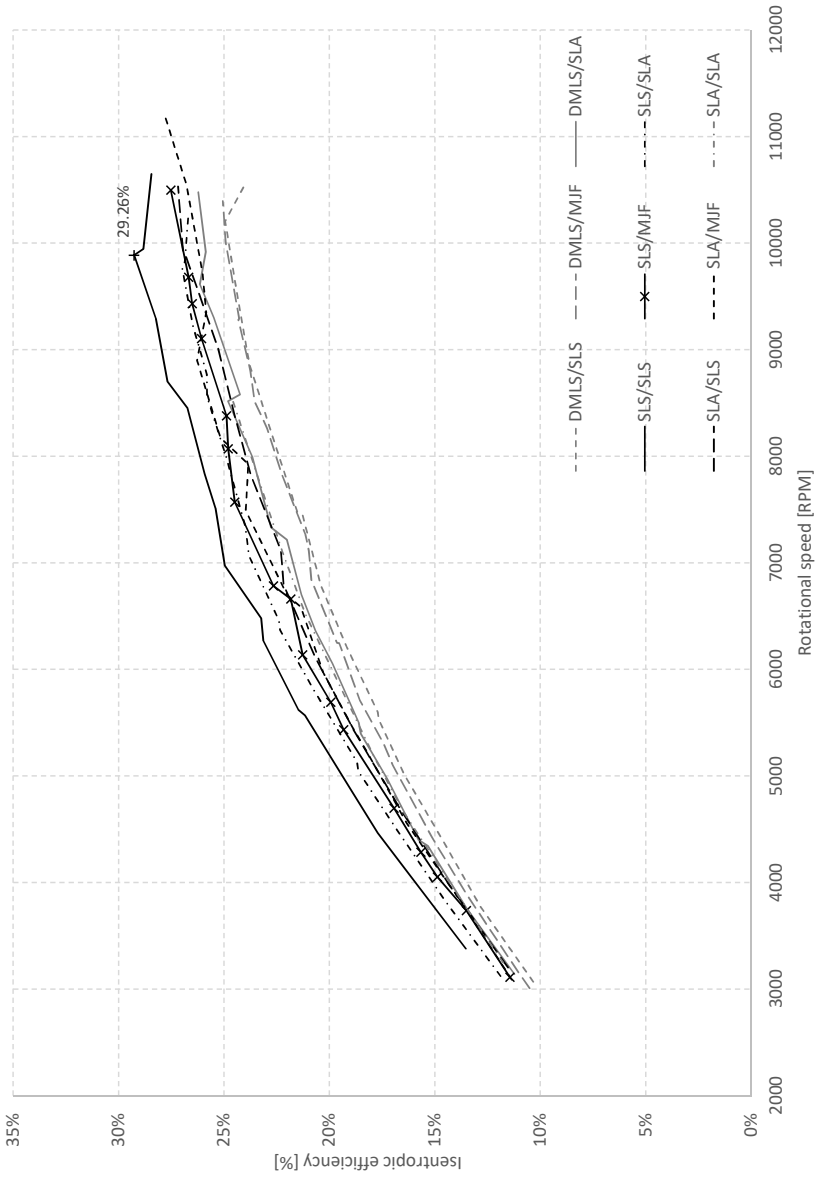

Figure D.13: Second generation design, different AM methods stator/rotor; PR 1.6 - full scale

Appendix E

Contents of enclosed CD

- `readme.txt` ..... the file with CD contents description
- `src` ..... the directory of source codes
  - `thesis` ..... the directory of LaTeX source codes of the thesis
- `text` ..... the thesis text directory
  - `thesis.pdf` ..... the thesis text in PDF format